UNIVERSITY OF LONDON

IMPERIAL COLLEGE OF SCIENCE AND TECHNOLOGY

(PHYSICS DEPARTMENT)

A NEW SCANNING METHOD FOR THE DETERMINATION OF OPTICAL TRANSFER FUNCTIONS

by

MICHAEL D. WATERWORTH

Thesis submitted for the

Degree of Doctor of Philosophy

December 1965

ABSTRACT

Of the different criteria of performance of optical systems which have so far been proposed, the optical transfer function has rapidly become accepted as the preferred criterion. This has required the application of Fourier techniques to the theory of optical image forming processes, a theory which may be applied to compound lens systems, even in the presence of aberrations. This has given rise to the need for the development of instruments for the measurement of optical transfer functions.

There are two kinds of method of measuring transfer functions, namely interferometric methods, and those based on the Fourier analysis of the image of a line source (the spread function) using scanning methods. Both these methods are discussed.

A new and simple method of scanning the line spread function has been devised, permitting measurements of optical transfer functions which are repetitive with an accuracy of better than 2%. Both a reference signal and the test signal are derived from the one light source, and both are fed into the one photodetector and amplifier. This eliminates any errors due to fluctuations in light intensity, photodetector sensitivity and amplifier gain. A null-setting is employed to determine both the modulus and phase of the transfer function. The test lens is mounted on a nodal slide, so that measurements in any off-axis

position may be made. The lens may also be tested in any azimuth.

The measured values of modulus and phase of the transfer functions have been correlated with theoretical values for several lens systems. At low apertures, the agreement is very good, but at higher apertures the agreement is poorer. This has been shown to be due to the presence of on-axis coma, arising from the decentring of one or more of the lens components. Measurements in white light have also been made, and these compared with those obtained with monochromatic light.

CONTENTS

Abstract

Chapter I : A Survey of Methods for Assessing Image Quality.

(1) Introduction ... ... Page 1

(2) Criteria for Image Quality in Optical Systems ... ... Page 2

(3) Conclusion ... ... Page 8

(4) References ... ... Page 10

Chapter II : The Theory of the Optical Transfer Function.

(1) Introduction ... ... Page 11

(2) Basic Postulates and General Theory ... ... Page 11

(3) The Calculation of the Optical Transfer Function based on Diffraction Theory ... ... Page 17

(4) References ... ... Page 26

Chapter III : A Survey of Methods for Measuring Optical Transfer Functions

(1) Introduction ... ... Page 27

(2) Direct Scanning Methods ... Page 27

(3) Scanning with Periodic Screens ... ... Page 27
(4) Interferometric Methods . Page 28
(5) Conclusion .. .. Page 29
(6) References ... ... Page 30

Chapter IV : A General Description of the Optical Transfer Function Test Bench.
(1) Introduction . ... Page 31
(2) A Method for Determining Optical Transfer Functions Page 31
(3) A General Description of the Apparatus ... ... Page 36

Chapter V : Theory of the Method of Instrument Operation.
(1) Introduction ... ... Page 39
(2) Theoretical Analysis of Scanning Technique ... Page 39
(3) Optimisation of Parameters for Signal to Noise Ratio Page 47
(4) Influence of Variation in Intensity in Spread Function ... ... Page 56

(5) Influence of Decollimator and Magnifying System Aberrations on Spread Function ... ... Page 59

(6) Aberrations Introduced by Image Rotating Prisms .. Page 61

(7) Effect of Non-Parallel Light Striking Parallel Plate Micrometer . ... Page 62

(8) Effect of Position and Shape of Scanning Grating ... Page 64

(9) Influence of Circular Slit on Reference Signal ... Page 65

(10) Tolerance on Calibration of Density Wedges ... ... Page 67

(11) Actual Signals fed to Photomultiplier .. ... Page 68

(12) References ... . Page 70

Chapter VI : A Detailed Description of the Apparatus Construction.

(1) Introduction . ... Page 71

(2) General Remarks .. ... Page 71

(3) Illuminating System ... Page 73

(4) Test Lens and Nodal Slide Page 78

(5) Decollimator ... ... Page 79

(6) Magnifying System ... ... Page 80

(7) Image Rotating Prism .. ... Page 81

(8) Parallel Plate Micrometer ... Page 82

(9) Scanning and Reference Slits Page 84

(10) Scanning Drum and Grating ... Page 86

(11) Post Drum Optics ... ... Page 88

(12) Photomultiplier Detector ... Page 92

(13) Frequency Selective Amplifier Page 93

(14) Main Power Amplifier .. ... Page 94

(15) Detector and Output Control . Page 94

(16) Method of Operation ... ... Page 95

Chapter VII : Setting Up and Alignment of the Apparatus.

(1) Introduction Page 97

(2) Mounting of Components on a Base-Plate ... ... Page 97

(3) Determination of the Optical Axis ... ... Page 100

(4) Determination of the Final Image Plane ... ... Page 102

(5) Positioning of the Base-Plate Page 102

(6) Magnification Through the System ... ... Page 104

(7) Positioning of the Test-Lens ... ... Page 105

(8) Determination of the Nodal Point of the Test-Lens . Page 106

(9) Positioning of the Photomultiplier Tube ... Page 106

Chapter VIII : The Measurement of Optical Transfer Functions.

(1) Introduction ... ... Page 107

(2) Measurements on the 20" Lens ... ... Page 107

(3) Measurements on the Plano-Convex Lens ... ... Page 128

(4) Measurements on the 8" Pentac Lens ... ... Page 133

Conclusions Page 141

Appendix I : Theory of Image Rotating Prism

Appendix II : Theory of Parallel Plate Micrometer

Appendix III : Design of Magnifying System

Acknowledgements

FIGURES.

Figure 1	Point scan and slit scan.
Figure 2(a)	Edge Image and Line Spread Function Summation.
Figure 2(b)	Acutance Curve and Definition of Acutance.
Figure 3	Equivalent Bandwidth of Transfer Function.
Figure 4	Illustrating the Image of an Extended Object as the Superposition of Spread Functions.
Figure 5	Intensity Distributions in the Image of a Sine-Wave Test Object.
Figure 6	Coordinates for the Calculation of Diffraction Images in the Focal Plane.
Figure 7	The Region of Integration in the Transfer Function Integral.
Figure 8	Principle of the Transfer Function Measuring Interferometer.
Figure 9	(a) Method of Fourier Analysing Spread Function. (b) Circular and Rectangular slits (c) Explanation of spatial frequency variation.
Figure 10	Block Diagram of Instrument.
Figure 11	Post Drum Optics.
Figure 12	Black Box Representation of Instrument.
Figure 13(a)	Image Space Coordinates and Scanning Slit
Figure 13(b)	Image Space with Scanning Grating included.

Figure 14(a)	Variation of (d/p) with ϕ.
Figure 14(b)	Variation of Signal to noise ratio for a fixed value of ϕ.
Figure 15	Significance of M.S. ratio on scanning grating.
Figure 16	Variation of g(s) and g'(s) with s.
Figure 17	Image Rotating Prism.
Figure 18(a)	Initial Layout of Components.
Figure 18(b)	Resolution Limits as a Function of Lens Aperture.
Figure 19	Illumination System.
Figure 20	Characteristics of Wratten filters Nos. 77 and 77A.
Figure 21	Calibration of Parallel Plate Micrometers.
Figure 22	Calibration Curves for Parallel Plate Micrometers.
Figure 23	Bearing for Image Plane Graticule.
Figure 25	Post Drum Optics.
Figure 25	Calibration of Density Wedges.
Figure 26(a)	Photomultiplier Sensitivity.
Figure 26(b)	Resistor Chain for Photomultiplier.
Figure 27	Frequency-Selective Amplifier.
Figure 28(a)	T-Filter.
Figure 28(b)	Characteristic Curve of Frequency Selective Amplifier.

Figure 29 Main Power Amplifier.

Figure 30 Detector and Measuring Circuit.

Figure 31 Response for Defocussing at a Fixed Spatial Frequency.

Figure 32 Transfer Function for 20" Lens at F/40 with defocussing.

Figure 33 Phase of Response for 20" Lens at F/40 with defocussing.

Figure 34 Transfer Function for 20" Lens at F/20 with defocussing.

Figure 35 Transfer Function for 20" Lens at F/10 with defocussing.

Figure 36 Transfer Function for 20" Lens at F/5.6 with defocussing.

Figure 37 Ratio of measured transfer functions to predicted transfer functions at F/10 and F/5.6.

Figure 38 Transfer Function for 20" Lens at F/20 for best focus at 40 lines /mm.

Figure 39 Comparison of 20" at F/10 for paraxial focus and best focus at 40 lines /mm.

Figure 40 Transfer Functions of Plano Convex Lens on-axis.

Figure 41 Transfer Functions of Plano Convex Lens 5° off-axis.

Figure 42 Transfer Functions of Plano Convex Lens with tilt on-axis.

Figure 43 Ratio of D(s) with and without tilt.

Figure 44 Transfer Function of 8" Pentac on-axis at F/8.

CHAPTER 1

A Survey of Methods for Assessing Image Quality.

(1) Introduction:-

Due to diffraction at the finite apertures of each component, it is not possible to obtain an optically perfect system. Hence this effect, as well as the effect of aberrations, on image quality must be examined.

The quality criteria used in past years, and indeed today still, have depended on the type of instrument and the use for which it is intended. For example, a telescope used for astronomical purposes is often required to be able to resolve clearly adjacent point objects. Again, a terrestrial telescope is required to produce a sharp image of an edge. Arising from the use of a particular type of instrument, there has been associated with the instrument a particular test for image quality. These quality criteria will be mentioned briefly in the next section.

Recently it has been recognised that, by the use of Fourier analysis, any object may be considered as the superposition of a number of sine wave objects, each having a fixed period (or spatial frequency). That is, any object may be considered as a number of sinusoidal gratings of different frequencies superposed in different azimuths. These gratings have a distinct advantage as test objects over others in that the image formed by an optical system of a

sine wave grating is of the same form. In addition, with this form of image the contrast may be determined from the design data, even in the presence of large amounts of aberration. Imaging gratings of different frequencies can then give complete information on the imaging properties of a lens system. This information, however, does not immediately allow the decision to be made that one lens is better than another, as further knowledge of the detecting system, and indeed of the type of object is required. Only then can the most suitable lens for a particular purpose be chosen.

The distinct advantages in using sine wave objects, that is using the transfer function of the system, are in its generality, and in providing an analytical description of the image forming properties of the given system.

(2) Criteria for Image Quality in Optical Systems:-

For an ideal optical system there would be a one-to-one correspondence between the object and the image. This can never occur in practice due to diffraction effects, but in designing a lens system one attempts to arrive as close as possible to the "perfect image". The imaging quality of an optical system may thus be measured in terms of the departure from the image that would be obtained if the system were diffraction limited.

A point source may be considered as the basic element to be imaged by an optical system. If the system is diffraction limited, the distribution of intensity in the image plane is given by

$$G = \left\{ \frac{2 J_1(2\pi p)}{2\pi p} \right\}^2$$

where $p = \frac{n \sin \alpha}{\lambda} \rho$, $n \sin \alpha$ is the numerical aperture, λ is the wavelength, and ρ is a radial coordinate in the image. In the presence of aberrations, this expression does not hold, and the image may assume a complicated structure. It is thus not always possible to apply successfully any criterion of performance, based on point-source images, to a system. Also, due to the small size of the scanning aperture required to make measurements on a point-source image, very little energy is available. This may be overcome to some extent by scanning the point image with a slit. This measures the line spread function which is related to the point spread function by the expression

$$G(u') = \int_{-\infty}^{\infty} G(u',v')\, dv'$$

where $G(u',v')$ is the intensity distribution in the image of a point. The line spread function so measured is identical if the point source is replaced by a line source

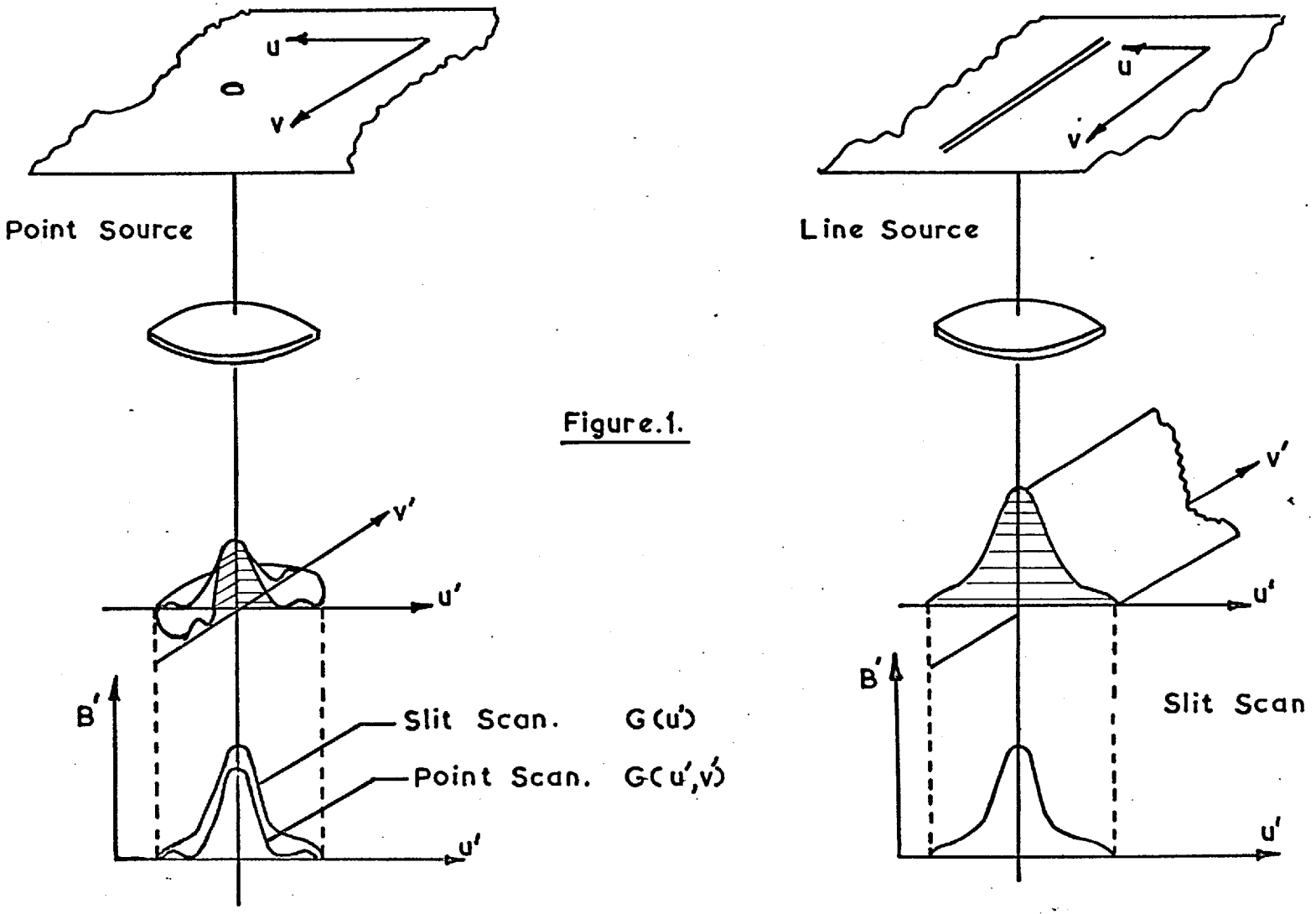

u
O
v
Point Source
v'
u'
B'
Slit Scan. G(u')
Point Scan. G(u',v')
u'
u
v
Line Source
v'
u'
B'
Slit Scan
u'

Figure.1.

parallel to the scanning slit.

Edge Gradient Criterion:-

The ideal image of an edge would be a step function. However, even in a diffraction limited system this is not so as the intensity distribution in the image follows a monotonically decreasing curve of finite slope. The slope at one half the maximum intensity is called the "edge gradient", and one finds that this slope decreases as the aberration present in the system increases. Both the image of an edge and the edge gradient are simply related to the line spread function. (See Figure 2(a)) The illuminated region on one side of the edge may be considered as composed of an infinite number of line sources, and it is the summation of the spread functions corresponding to these sources that is the edge-image distribution.

The practical measurement of the edge gradient, and its relation to the imaging of extended objects, present several difficulties. Firstly, the magnification of the system under test must be known, as this will alter the gradient in the same way as aberration. Secondly, the exact focal plane used in imaging extended objects must be known. Thirdly, the receptor used in assessing the image of an extended object may suffer from non-linearities, as compared with the receptor used for the

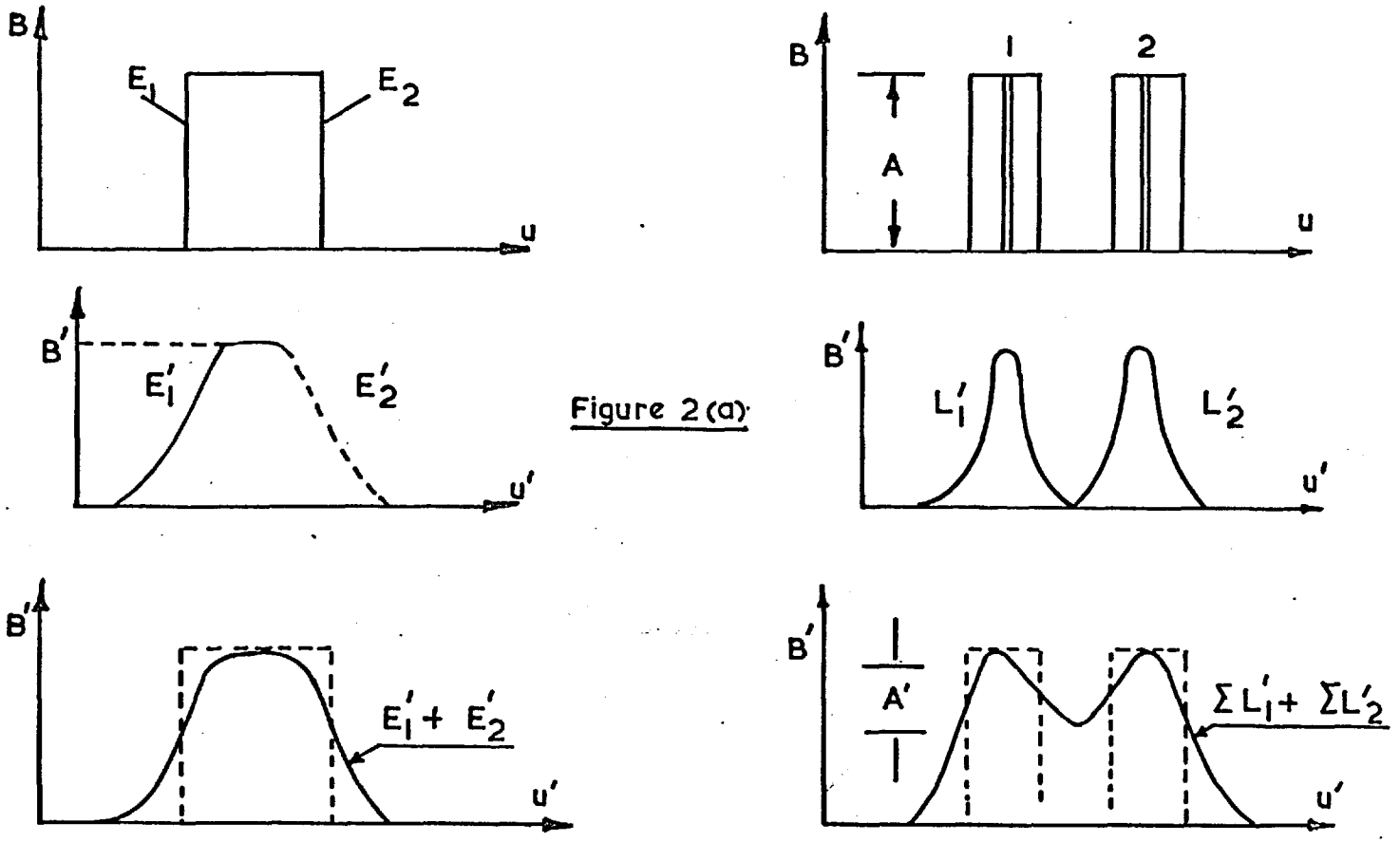


Figure 2 (a)

Edge Image Summation.

Line Spread Function Summation.

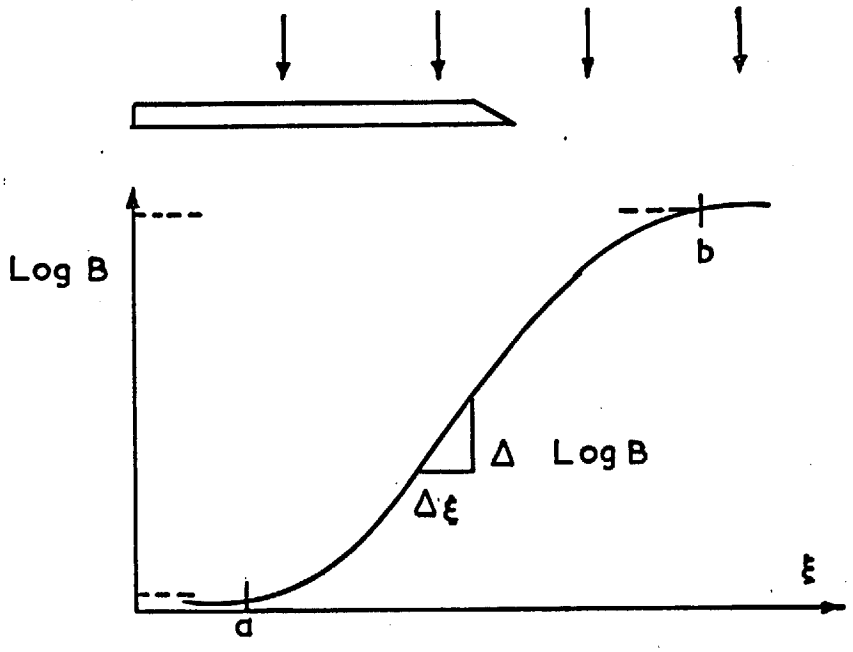


Figure 2(b)

measurement of the edge gradient. A criterion of image quality, taking this into account, and using the edge gradient as a starting point, is the acutance.

In Figure 2(b), the edge image distribution is plotted against the logarithm of intensity (this is approximately the intensity response of the eye). The curve is then split up into N segments, and the slope of each, $\frac{\Delta \log B}{\Delta \xi}$, is measured. The mean square gradient is then

$$\overline{m_\xi^2} = \sum_{n=1}^{N} \left(\frac{\Delta \log B}{\Delta \xi} \right)^2 \Big/ N$$

To take account of the sweep in the toe and shoulder of the curve, arbitrary limits a and b are introduced, the acutance then being defined as

$$\text{Acutance} = \overline{m_\xi^2} \Big/ (D_a - D_b)$$

$(D_a - D_b)$ being the density difference between the limits a and b.

As the edge gradient may be obtained from the line spread function, so may the acutance. Hence the acutance may be calculated for various states of correction of the optical system.

Resolution Limits:-

According to Rayleigh, the images, formed by an aberration-free system, of two equally bright objects can

be resolved when the first dark ring of one diffraction pattern coincides with the central maximum of the other. When this is so, the intensity of the central dip in the image is 81% of that of the two maxima. This has proved a useful rule, but it is not free from a certain arbitrariness in the criterion "resolved or not".

In some fields it has been useful to define the resolution limit of a system as the half width of the line spread function.

The resolution limit is determined by the closest spacing of the object for which its individual components are still detectable in the image. Various charts have been designed for determining this limit, some consisting of two-line objects of different spacings, and some containing more than two lines. Again, since detectors have widely varying sensitivities, it is advisable for test measurements of this kind to use the detector intended for use with the optical system in practice.

To use either the edge gradient or the resolution limit as a quality criterion for an optical system may be quite misleading. The average extended object to be photographed or examined contains both coarse and fine detail. The edge gradient or acutance criterion is predominantly concerned with coarser detail, that is low spatial frequencies, whereas the resolution limit criterion

is concerned with finer detail or high spatial frequencies. A system may thus have a low acutance but a high resolution, or vice versa. If a system has a high resolution limit, this does not necessarily mean that objects having coarse detail will be imaged with good quality. It is this information that is often required.

Sine Wave Contrast Transfer Function:-

The image of an object having a sinusoidal distribution of intensity has itself a sinusoidal intensity distribution but with reduced contrast. If sinusoidal objects, of different spatial frequencies, are imaged by a system, the images corresponding to each frequency will have different contrast values. The relation between the image contrast and the object contrast is known as the contrast transfer function of the system, and the value of this function varies with the spatial frequency of the object. In addition, there may be a lateral shift of the image relative to the geometrical image. Becuase of the fact that the image of a sinusoidal object is of the same form, it is a simple matter to specify the object-image relationship by means of a factor representing both the reduction in contrast and the lateral shift. This latter term may be measured as a phase shift and included with the contrast transfer factor to form a single complex number. This is called the optical transfer function (or frequency

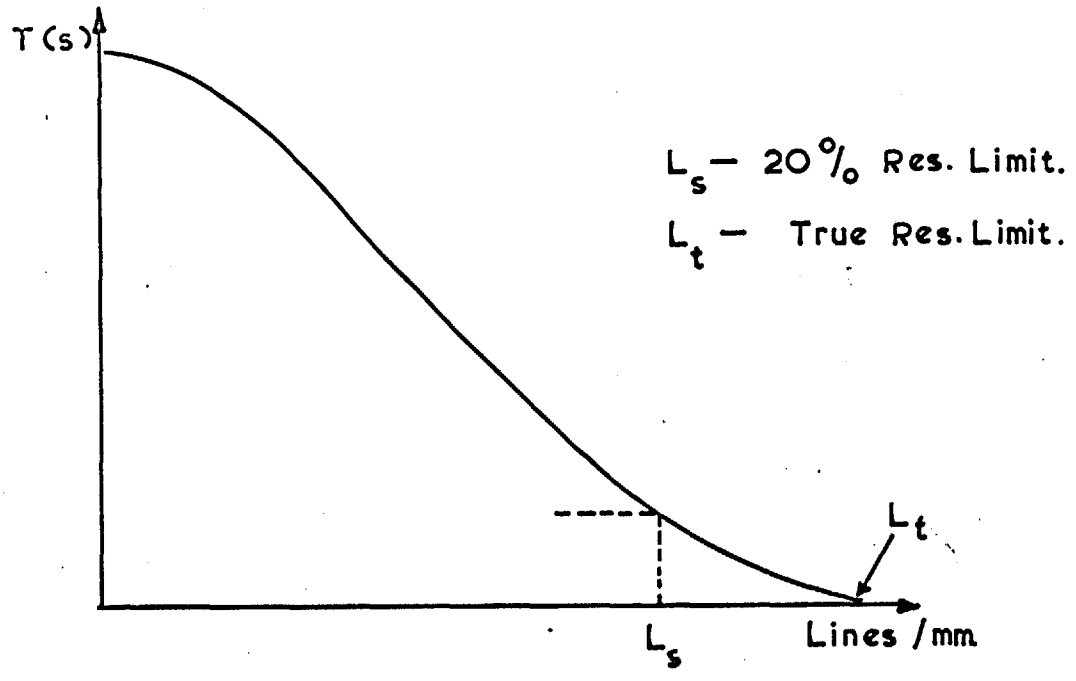
response) of the system.

It should be noted that the optical transfer function may be evaluated directly, and more simply, from the wave aberration of the optical system without first calculating the line spread function.

Attempts have frequently been made to assign a single number as an index of performance from the optical transfer function. One such method is to specify the equivalent bandwidth ΔB as indicated in Figure 3. This criterion suffers from the disadvantage that it does not specify the shape of the optical transfer function curve, so that the value of ΔB could be misleading.

(3) Conclusion:-

In 1959, Dixon showed that neither the resolution limit nor the edge gradient criteria give sufficient information about an optical system's performance. These tests describe only the performance under specified conditions, and depend on the detector employed. If, however, the optical transfer function is known, it is possible to find from it both the resolution limit and the edge gradient. Thus it is clear that the optical transfer function gives sufficient information to be able to assess the performance of any system for the conditions under which it is to operate. An exception might be made in the case of the image of a star field, where the object consists


T (s)
L_s — 20% Res. Limit.
L_t — True Res. Limit.
L_t
L_s
Lines / mm

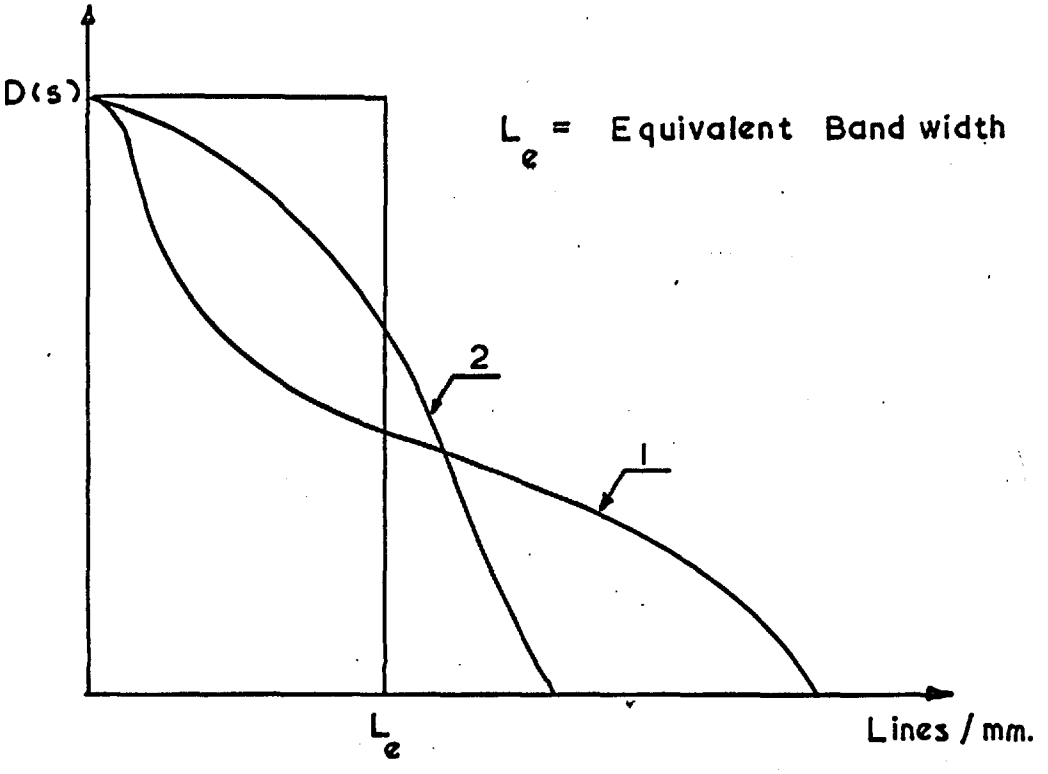

D(s)
L_e = Equivalent Band width
2
1
L_e
Lines / mm.

Figure 3

of isolated point sources. This corresponds to the case of a pulse circuit in electronics, where pulse-testing techniques are preferable to a detailed knowledge of the frequency response. For a lens system of course, the "impulse response" is simply the spread function, that is the intensity distribution in the image of a point source, in the two-dimensional case, or of a line source in the one-dimensional case.

References

Rayleigh, Lord	1888	Encyclopedia Brittanica (Wave Theory)
Dixon, F.	1959	The Influence of Aberration on Optical Images - Technical Optics Department, Imperial College.
Rayleigh, Lord	1879	Collected Works 1, 415-453 Phil.Mag. and Phil.Mag., 8, 266
Airy, G.B.	1834	Trans.Cambr.Phil.Soc., 5, 283
Cobb, P.W.	1915	Amer.J.Physiol. 36, 335

CHAPTER II

The Theory of the Optical Transfer Function:-

(1) Introduction

As mentioned in the previous chapter, the optical transfer function is derived from the fact that the image of a sinusoidal (or cosinusoidal) object has itself a sinusoidal (or cosinusoidal) distribution of intensity. This distribution may be reduced in contrast, and also may suffer a lateral shift from the geometrical image position.

The optical transfer function is the normalised inverse Fourier transform of the spread function, this latter being determined by the distribution of complex amplitude over the exit pupil of the optical system. This complex amplitude distribution is known as the pupil function, and is dependent on the wavefront aberration present in the system.

(2) Basic Postulates and General Theory:-

There are two basic postulates which must be satisfied in order that the theory of optical transfer functions is valid. These are the postulates of

(i) Superposition

(ii) Stationarity or Space Invariance.

If (i) and (ii) are satisfied, image formation may be considered as a passive linear process.

Let $B_1(u,v)$, $B_1'(u',v')$ be any two-dimensional intensity distributions in the object and image planes respectively of an optical system. Then, the postulate of superposition requires that

$$B_1(u,v) + B_2(u,v) \rightarrow B_1'(u',v') + B_2'(u',v') \qquad (1)$$

for any B_1 and B_2. This is satisfied if different object points are mutually incoherent so that intensities are additive in the image plane. A self-luminous object is an example of this.

The stationarity postulate requires that the image intensity distribution remains unchanged for a lateral shift in the object plane. That is

$$B_1\{(u-u_o),(v-v_o)\} \rightarrow B_1'\{(u'-u_o'),(v'-v_o')\} \qquad (2)$$

This will only be valid for small displacements (u_o,v_o). (2) requires that the image of a point source be the same for all points in the object. In practice, a small region of the image plane is considered, and it is assumed in the theoretical treatment that the aberration for the whole image is the same as the aberration for the central point of the region of the image considered. This is justifiable if the aberration of a system remains constant over a region of the image plane which just exceeds the region within which

the intensity in the image of a point source differs from zero. This is the condition of isoplanatism, and it appears to be well satisfied in the case of corrected optical systems. If this condition were not satisfied, disagreement between theoretical and experimental values of the transfer function would necessarily occur. This in turn would require a non-linear theory of optical systems to be investigated. Fortunately, good agreement is obtained between theory and experiment, so that the isoplanatic condition may be assumed to hold.

Now any two dimensional distribution $B(u,v)$ may be represented by a Fourier integral of the form

$$B(u_o,v_o) = k \iint_{-\infty}^{\infty} \beta(s_o,t_o)\cos[2\pi(u_o s_o + v_o t_o) + \theta(s_o,t_o)]ds_o dt_o$$

where k is constant and (s_o,t_o) are spatial frequencies. Each frequency pair (s_o,t_o) in the integrand represents, as a function of (u_o,v_o), a cosine distribution of intensity along the direction given by

$$\tan \phi = t_o/s_o$$

and has lines of constant intensity perpendicular to this direction. If new axes (u,v) are now chosen, with the v axis along the direction ϕ, the terms in equation (3) for which

$$t_o/s_o = \tan \phi = \text{constant},$$

will give an intensity distribution varying along the direction

u, but constant along the direction v. Thus any two-dimensional distribution, such as (3), is the sum over all azimuths ϕ of the above one dimensional objects.

This result implies that the imaging properties of an optical system may be described by means of curves of a single spatial frequency variable for a number of azimuths. Also, for experimental purposes, slits and gratings in varying azimuths may be used to determine the imaging properties of a system.

Let G(u') be the line spread function of an optical system. Practically, this means the intensity distribution in the image of an infinitely narrow, incoherently illuminated, slit lying along the v axis at u=o. Alternatively, G(u') may be considered as the output for a unit impulse at u=o. Any object distribution B(u) may be regarded as a spatial distribution of impulses of strengths B(u), and for a linear system the output will be

$$B'(u') = \int_{-\infty}^{\infty} B(u)\, G(u'-u)\, du \qquad (4)$$

This implies that the distribution of intensity in the image is given by the convolution of the intensity distribution in the object with the spread function. This is shown in Figure 4. The Fourier spectra of the functions in (4) are related by

$$b'(s) = b(s).g(s) \qquad (5)$$

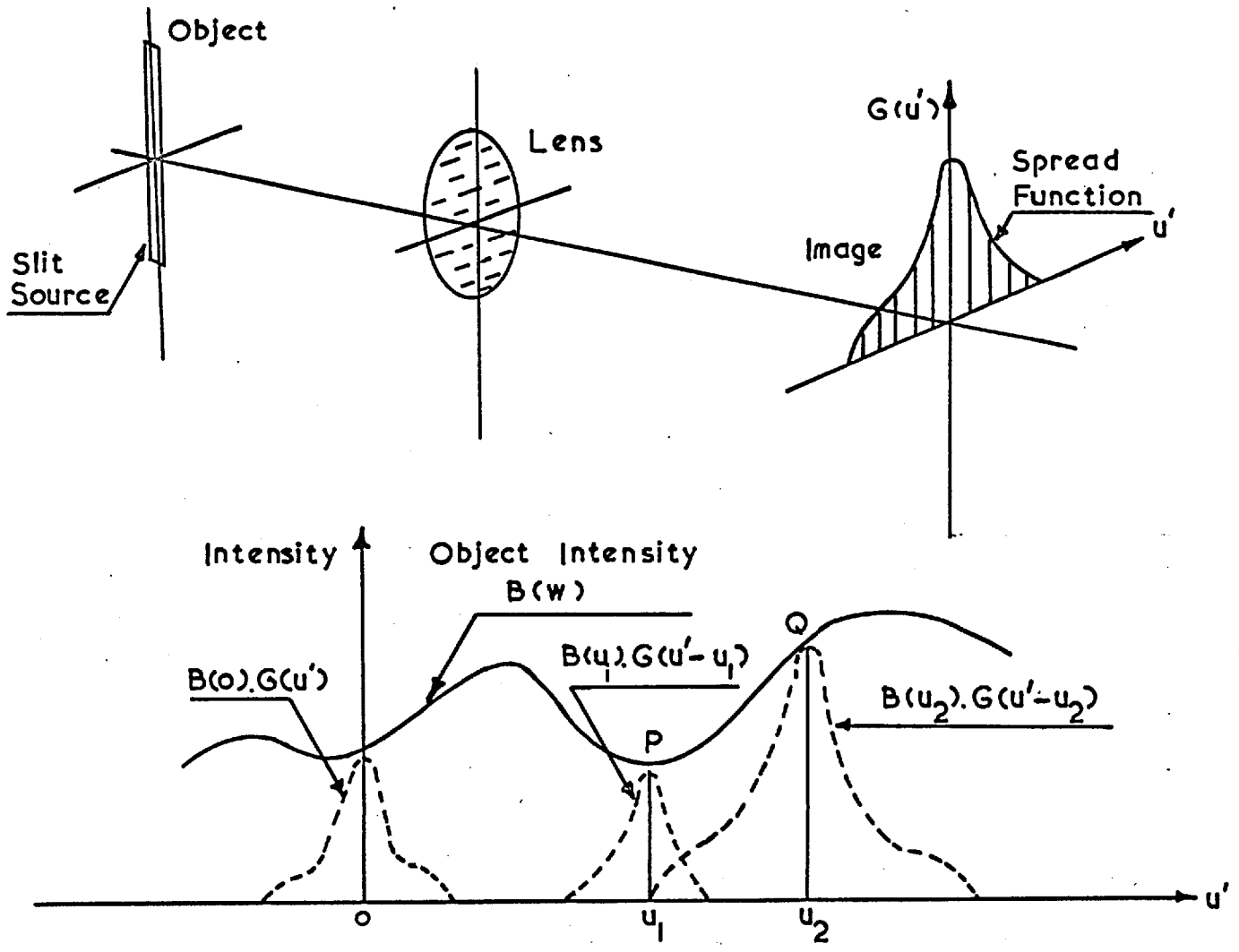


Figure 4 :— Illustrating the Image of an Extended Object as the Superposition of Spread Functions (Impulse Responses.)

where $g(s) = \int_{-\infty}^{\infty} G(u')\exp(-i2\pi u's)du'$ etc.

The significance of the relation (5) is that a cosine grating of the form

$$B(u) = \alpha + \beta\cos 2\pi us \tag{6}$$

will always have an image of the form

$$B'(u') = \alpha + T(s)\beta\cos\{2\pi u's + \theta(s)\} \tag{7}$$

In these equations, u and u' are defined by

$$u = \frac{n\sin\alpha}{\lambda}\xi\,, \quad u' = \frac{n'\sin\alpha'}{\lambda}\xi'$$

where $n\sin\alpha$, $n'\sin\alpha'$ are numerical apertures in the object and image spaces respectively, ξ and ξ' are spatial coordinates and λ in the wavelength. Note that

$$u' = u, \quad v' = v$$

give the position of the geometrical image of the point (u,v). Also, intensity units are chosen such that a uniform object distribution of unit intensity gives an image also having unit intensity.

The quantities T(s) and $\theta(s)$ are then related to g(s) by

$$T(s)\exp\{i\theta(s)\} = D(s) = \frac{g(s)}{g(o)} \tag{8}$$

T(s) is the contrast transfer function and is the ratio of the contrast in the image to that in the object. $\theta(s)$ is the spatial phase shift, and shifts the component of the image of frequency s by an amount

$$\delta u' = - \theta(s) / 2\pi s$$

relative to the geometrical image. If $\theta(s)$ is a linear function of s, there results a bodily shift of the image. Any non-linear part of $\theta(s)$ results in different frequency components being shifted by different amounts, giving phase distortion.

D(s) is the optical transfer function, and if specified for different aximuths completely describes the imaging properties of an optical system. It is important to note that only the postulates of superposition and stationarity have been used to obtain the relation (8).

If an optical system were ideal, there would be a 1:1 correspondence between points in the object and image planes. Then D(s) would take the value unity, that is the image would appear with unreduced contrast and zero phase shift. However, because of diffraction, light from any object point will spread, resulting in a reduction of contrast. The image of a diffraction limited system will have a transfer function decreasing with increasing spatial frequency. The presence of aberrations causes a further decrease in contrast, and may also cause a spatial phase

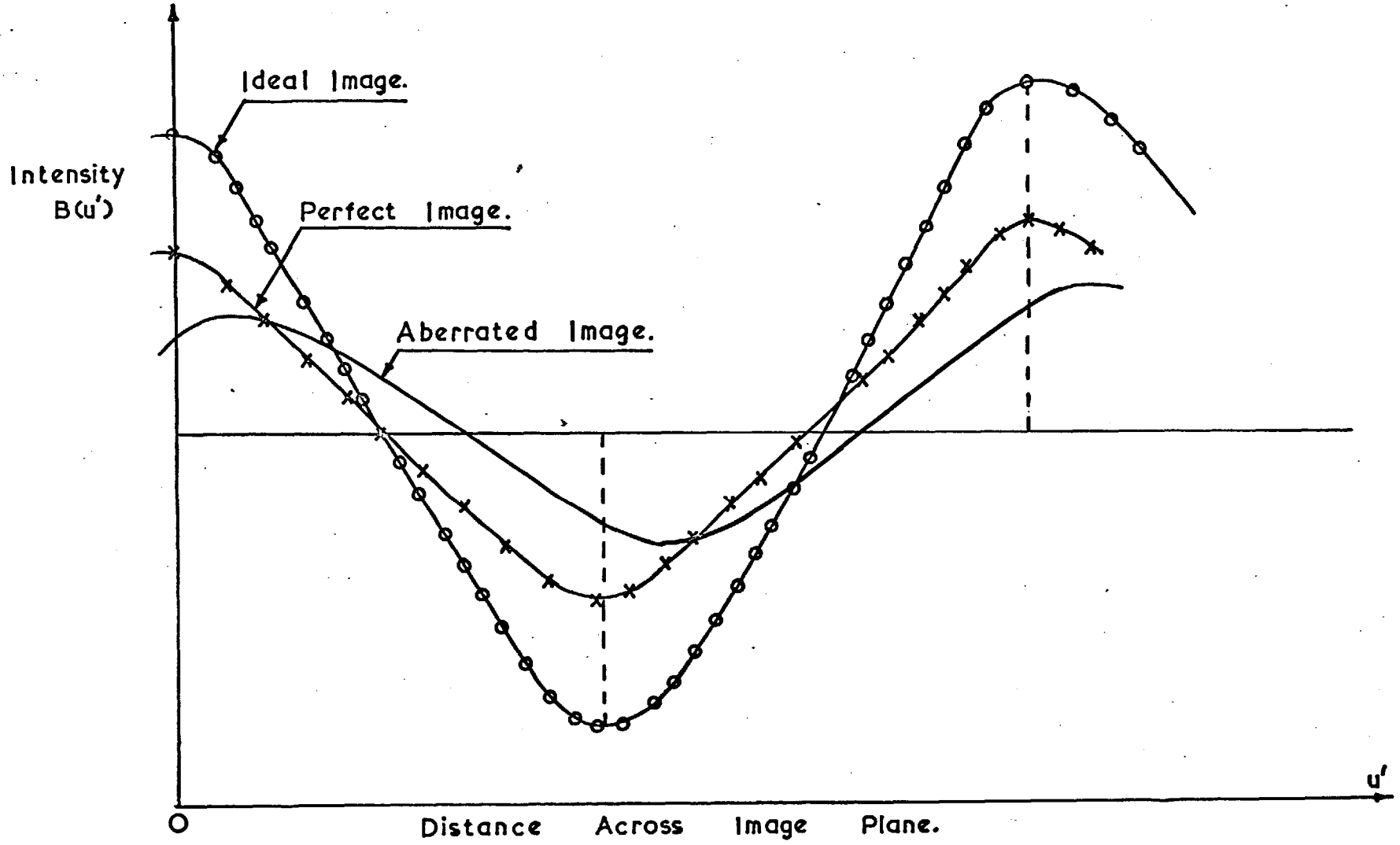


Figure 5:— Intensity Distribution in the Image of a Sine—Wave Test Object.

shift. These properties are illustrated in Figure 5.

(3) Calculation of the Optical Transfer Function from Diffraction Theory :-

One of the principal advantages of the above theory is the possibility of calculating the transfer function from the design parameters of an optical system. Tracing rays through a system enables the wavefront aberration $W(x,y)$ to be expressed in terms of the relative coordinates (x,y) of the points where rays intersect a reference sphere centred at Q' - Figure 6- in the image plane, and passing through the exit pupil at E'. For an extra-axial region of the image the aperture angle α' is here taken to be the angle subtended at the image point Q' by a point situated on the reference sphere and in the sagittal section at a distance h_s from the pupil ray $E'Q'$ (h_s is the sagittal incidence height along this ray at the plane through E'). Relative coordinates (x,y) are then defined by

$$x = \frac{X}{h_s} \quad , \quad y = \frac{Y}{h_s}$$

The reduced coordinates in the image plane are

$$u' = \frac{n' \sin\alpha' \, \xi'}{\lambda} \quad , \quad v' = \frac{n' \sin\alpha' \, \eta'}{\lambda}$$

and have their origin $\xi' = \eta' = o$ at Q'. In terms of these coordinates, the complex amplitude at the point $P'(u',v')$ in

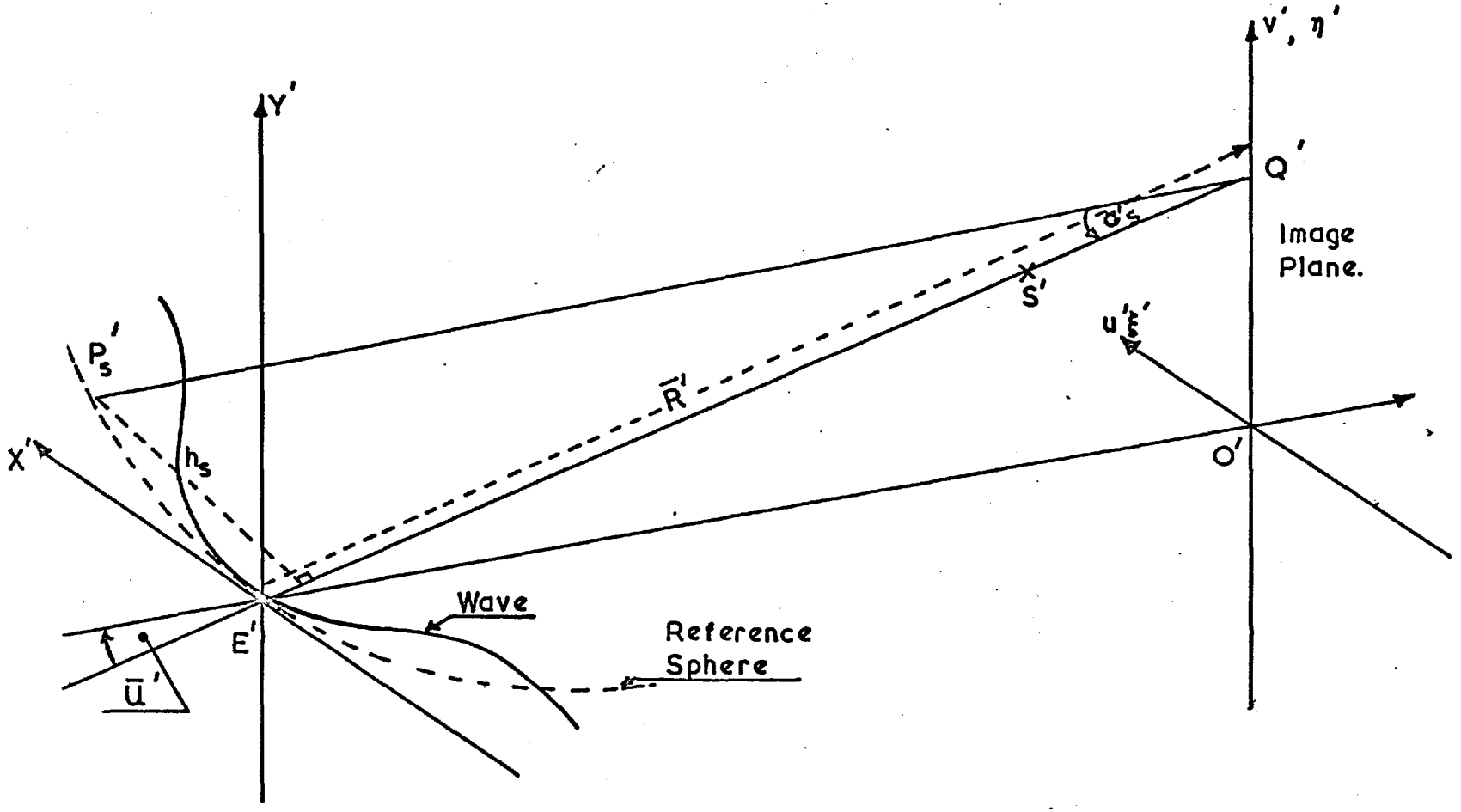


Figure 6 :— Co ordinates for the Calculation of Diffraction Images in the Focal Plane

the image plane is, apart from a constant factor

$$U_{P'} = \exp(i\delta)\iint_A \alpha(x,y)\exp[ikW(x,y)] \cdot \exp[i2\pi(u'x+v'y)]dxdy \qquad (9)$$

where $k = \frac{2\pi}{\lambda}$, and δ = constant $(u'^2 + v'^2)$. $W(x,y)$ is the wavefront aberration, and $\alpha(x,y)$ is the real amplitude over the reference sphere. The region of integration A corresponds to the aperture of the system.

To develop the theory further, the pupil function, defined by

$$f(x,y) = \begin{cases} \alpha(x,y)\exp[ikW(x,y)] & \text{in } A \\ 0 & \text{outside } A \end{cases}$$

is introduced. In an aberration free system with uniform transmission over the aperture, $W(x,y)$ is zero and $\alpha(x,y)$ has unit value, so that $f(x,y)$ has the value unity in A. In the case of incoherent objects it is only the intensity in the point source image that is required. For this case, equation (9) may be written

$$F(u',v') = \int_{-\infty}^{\infty}\int f(x,y)\exp[i2\pi(u'x+v'y)]\,dxdy$$

omitting the phase factor $\exp(i\delta)$ which disappears on taking the squared modulus of $F(u',v')$. The complex amplitude at P' is thus exactly the Fourier transform of the pupil function. The point spread function is given by

$$G(u',v') = |F(u',v')|^2$$

Now suppose the axes (u',v') and (x',y') are chosen so that v' and y' lie in the azimuth for which the optical transfer function is to be determined. The distribution of intensity in the image of an incoherent line source will then be given by

$$G(u') = \int_{-\infty}^{\infty} G(u',v')\, dv',$$

and the inverse Fourier transform of this line spread function is

$$g(s) = \int_{-\infty}^{\infty} \left\{ \int_{-\infty}^{\infty} G(u',v')dv' \right\} \exp(-i2\pi u's)\, du' \qquad (10a)$$

Also, the inverse Fourier transform of G(u',v') is given by

$$g(s,t) = \iint_{-\infty}^{\infty} G(u',v')\exp\{-i2\pi(u's+v't)\}du'dv' \qquad (10b)$$

A comparison of (10a) and (10b) shows that

$$g(s) = g(s,o)$$

which gives the inverse transform of the line spread function in terms of the inverse transform of the point spread function.

Equation (10b) may be written

$$g(s,t) = \iint_{-\infty}^{\infty} |F(u',v')|^2 \exp\{-i2\pi(u's+v't)\}du'dv'$$

or

$$g(s,t) = \iint_{-\infty}^{\infty} f(x + \tfrac{s}{2}, y + \tfrac{t}{2}).f^{x}(x - \tfrac{s}{2}, y - \tfrac{t}{2})\, dxdy \qquad (11)$$

Putting t=o in equation (11) gives for the optical transfer function

$$D(s) = \frac{1}{A} \iint_{-\infty}^{\infty} f(x+\tfrac{s}{2},y).f^{x}(x-\tfrac{s}{2},y)\,dxdy \qquad (12)$$

where $A = g(o) = g(o,o) = \iint_{-\infty}^{\infty} |f(x,y)|^2 dxdy$

Since the influence on diffraction of the non-uniformity of amplitude over the wave is generally negligible compared with the phase errors associated with aberration, it is usually permissible to write

$$\alpha(x,y) = 1$$

Then equation (12) becomes

$$D(s) = \frac{1}{A} \iint_{S} \exp\{ik[W(x+\tfrac{s}{2},y) - W(x-\tfrac{s}{2},y)]\}\,dxdy \qquad (13)$$

where S is the region common to two pupils centred on the points $(\frac{s}{2}, o)$, $(-\frac{s}{2},o)$ respectively. The pupil domain A, and the displaced pupils A_1 and A_2, and the region of integration S are illustrated in Figure 7.

If a system is free from aberration, $W(x,y) = o$ and then

$$D(s) \rightarrow D_o(s) = \frac{S}{A}$$

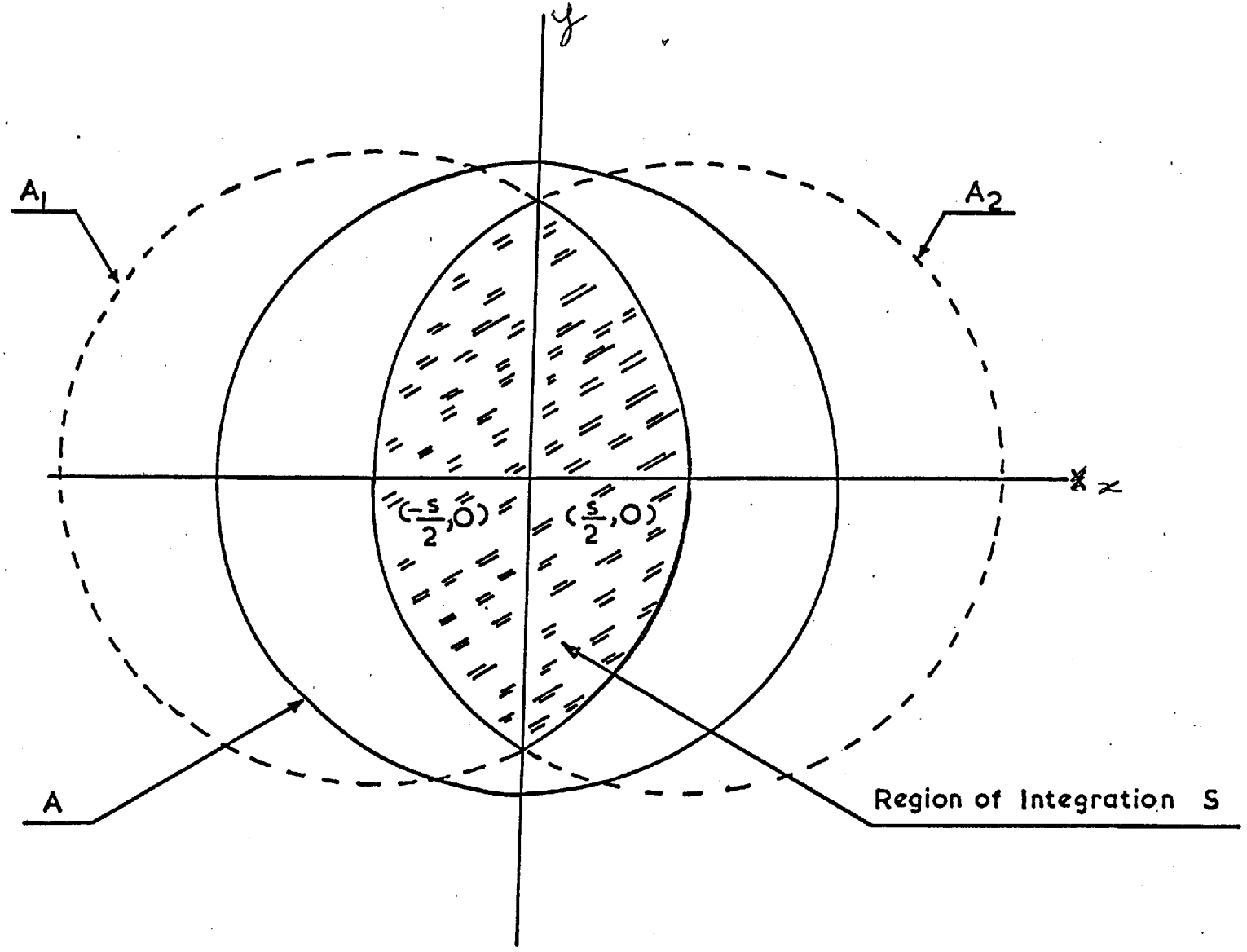


Figure 7 :— Region of Integration in the Transfer Function Integral.

When s is greater than or equal to 2, there is no area S in common, and so

$$D(s) = o$$

This is the limit of resolution, and from the equation

$$u' = \frac{n' \sin\alpha'}{\lambda} \quad \xi \quad = \frac{1}{2}$$

we obtain

$$\xi' = \frac{0.5\lambda}{n' \sin\alpha'}$$

This is simply the classical resolution limit

Returning to equation (13), we may write

$$V(x,y,s) = \frac{1}{s}\left\{W(x+\frac{s}{2},y) - W(x-\frac{s}{2},y)\right\}$$

$$= W_x^I(x,y) + \frac{1}{3!}(\frac{s}{2})^2 W_x^{III}(x,y) + \frac{1}{5!}(\frac{s}{2})^4 W_x^V(x,y) + \ldots$$

so that

$$D(s) = \frac{1}{A}\iint_S \exp\{iksV(x,y,s)\}\, dxdy \qquad (14)$$

From (14), several properties of the transfer function may be derived. Firstly, we have

$$T(s) = |D(s)|$$
$$\leqslant \frac{1}{A}\iint_S dxdy$$

$$\therefore T(s) \leqslant T_o(s)$$

That is, for a system with aberration, the contrast is less than that for an aberration-free system for all spatial frequencies other than s=o and s=2. These correspond to zero frequency and the resolution limit respectively.

Secondly, it is easy to show that the slope of the curve of T(s) at s=o is independent of the aberration present in the system. That is

$$\left\{ \frac{\partial\, T(s)}{\partial s} \right\}_{s=o} = \left\{ \frac{\partial T_o(s)}{\partial s} \right\}_{s=o}$$

This result explains why coarse structure in an object is discerned, even in poorly corrected systems.

Thirdly, it may be seen that for a large amount of aberration present in the system, the transfer function will be small except for the smaller values of s.

It is evident then, that the smaller the aberration present in a system, the finer the detail that may be resolved with good contrast in the image.

It has been shown that for a geometrical approximation, equation (14) becomes

$$D_G(s) = \frac{1}{A} \iint_{\Lambda} \exp \{iks.W_x^I(x,y)\}\, dxdy$$

the region of integration being the whole pupil. It is clear that this approximation will hold only in the low frequency region Since the transfer function has significance in this region only

when the aberrations are large, it is to be expected that geometrical optics will hold for larger aberrations.

For a circular pupil, calculations of the transfer functions for aberration-free defocussed systems, and for systems with astigmatism, were first made in 1955 by Hopkins and De. These curves showed a rapid collapse of the response for spatial frequencies above about $s = 0.20$. In 1958, Goodbody calculated the transfer functions in the presence of spherical aberration and coma. More recently Hindley has, using computer facilities, obtained transfer functions in the presence of any aberration, whether this be a single aberration such as coma or a combination of aberrations.

It should be noted here that when the pupil A is symmetrical and $W(x,y)$ is an even function of the aperture, the optical transfer function given by (14) is real. This means that the phase term $\theta(s)$ is either zero or π, the latter corresponding to the reversal of contrast in the image.

The above formulation of the theory makes possible the derivation of a criterion for image quality. It is possible to find a value of spatial frequency s sufficiently small so as to make the modulus of the transfer function differ from that obtained in a diffraction limited system by as small an amount as desired. This is true even when large aberrations are present. The ratio of the moduli of the transfer functions, with and without aberration,

is given by

$$M(s) = \left| \frac{D(s)}{D_o(s)} \right| = \left| \frac{1}{S} \iint_S \exp \{iks\ V(x,y,s)\}\ dxdy \right|$$

and the condition

$$M(s) \geqslant 0.80$$

provides a useful criterion for image quality. This leads to the following expression (Hopkins 1957)

$$M(s) \geqslant 1 - \frac{2\pi^2 s^2}{\lambda^2} K(s) \qquad (15)$$

where

$$K(s) = \frac{1}{S} \iint_S \{V(x,y,s)\}^2 dxdy - \left\{ \frac{1}{S} \iint_S V(x,y,s) dxdy \right\}^2$$

K(s) is the variance of V(x,y,s).

The relation (15) is valid provided the right hand side exceeds zero; when the right hand side exceeds about 0.70, the inequality may be replaced by an equal sign with good approximation. Since K(s) is a positive quadratic function of the aberration coefficients, it may be minimised with respect to any aberration coefficient ${}_iW_{jk}$ by satisfying the relation

$$\frac{\partial K(s)}{\partial\, {}_iW_{jk}} = 0$$

It is found that the above tolerance theory is valid for any frequency range, provided that M(s) exceeds 0.70. If the frequency range includes values of $s \geqslant 0.20$, the results of this treatment agree closely with those found using Marechal's formulation of the Strehl tolerance theory. This latter is simpler to apply practically, and is therefore preferred for cases with spatial frequency bandwidths exceeding 0.20. It is only in the range $s \leqslant 0.20$ that the tolerance based on transfer function theory is of greatest practical value.

REFERENCES

Born, M. and Wolfe, E., 1959, Principles of Optics (Oxford; Pergamon Press)

De, M., 1955 Dissertation Imperial College, Proc. Roy. Soc. A, 233, 91

Dixon, F., 1960 Dissertation Imperial College Proc. Phys. Soc, 75, 713

Goodbody, A., 1958 Thesis Imperial College Proc. Phys. Soc. 72, 411

1960 Proc. Phys. Soc., 75, 677

Hopkins H.H. 1949, Proc. Phys. Soc., B, 62, 22

1950, Wave Theory of Aberrations (Oxford; Clarendon Press)

1951, Proc. Roy. Soc., A, 208, 263
1953, Proc. Roy. Soc., A, 217, 408
1955, Proc. Roy. Soc., A, 231, 91
1955, Optica Acta, 2, No.1, 23
1956, Proc. Phys. Soc., B, 69, 562
1957, Proc. Phys. Soc., B, 70,1162
1957, Proc. Phys. Soc., B, 70, 449
1957, Proc. Phys. Soc., B, 70,1002
1962, Proc. Phys. Soc. Vol.79, Part 5 No:511 p.p 889-919

Hindley, J., 1963 Private communication.

CHAPTER III

A Survey of Methods for Measuring Optical Transfer Functions

(1) Introduction

Various methods of determining the optical transfer function practically have been devised. In this chapter, each method will be discussed briefly, the emphasis being placed on more recent methods.

(2) Direct Scanning Methods:-

It is sufficient to determine the distribution of intensity in the image of a point or line source for the evaluation of the transfer function. Authors, such as Naish, R.E. Hopkins, Herriot, Kwabara, and others, have devised various techniques for doing this. The direct scanning method has, however, a serious drawback in that any fluctuations in light intensity will lead to incorrect values. Recently, K.G. Birch has been able to obtain spread functions with reproducible intensity distributions, using a highly stabilised light source. To obtain the inverse Fourier transform of this intensity distribution, considerable calculation is needed; a large fraction of this may be avoided if the inverse Fourier transform can be determined directly.

(3) Scanning with Periodic Screens:-

If the spread function is scanned with a periodic screen, the inverse Fourier transform may be obtained

directly. Alternatively, one may use a periodic screen in the object plane, and scan the image with a slit. Schade, Lindberg, and Inglestam et al have used such methods, employing periodic screens of varying frequencies. Both modulus and phase measurements have been obtainable, but difficulties, both mechanical and optical, have been encountered, thus producing errors; in some cases it has been necessary to move the periodic screens at constant speed across the spread function. Also, it is difficult to make a series of accurate screens having sinusoidal transparency of different frequencies. A method of determining the inverse Fourier transform using a screen of single frequency would therefore be advantageous. Born, Firth and Pringle devised such a method in which a slit rotates relative to a moving grating, the image of a line source being arranged perpendicular to this slit for all rotations. K.G. Birch has also employed this method.

With these scanning methods, the light is converted into electrical signals by means of a photo-detector, the output being related directly to the optical transfer function.

A number of modifications of the above methods have been adopted by various authors, but these need not be described here.

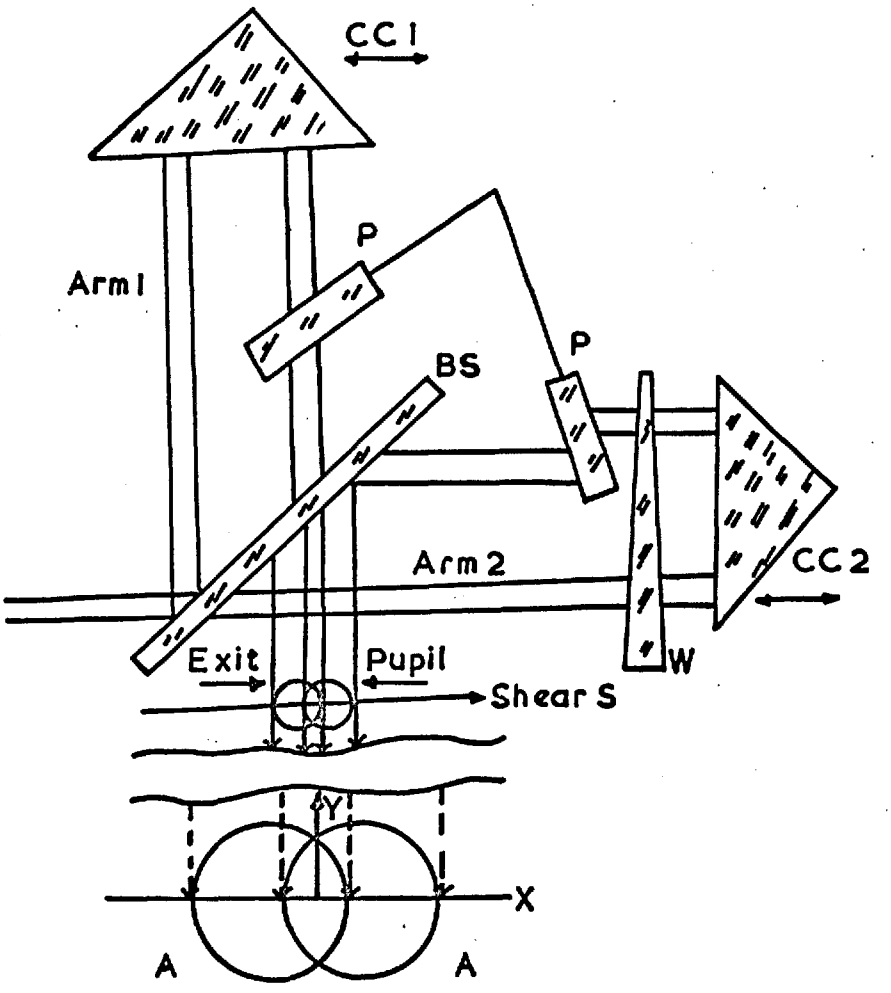
(4) Interferometric Methods:-

It was shown by Hopkins (1955) that the optical transfer function could be determined by measuring the total

light flux in an interference pattern as a function of the path difference in the two arms of an interferometer. Such an interferometer was constructed by Kelsall (1959), the design being shown in Figure (8). Montgomery (1961) simplified this design and also employed a polarisation technique -Cerenkul (1964) used a shearing interfermoeter of this type to measure transfer functions in the presence of primary coma. He was able to obtain good agreement with the theoretical values of both modulus and phase of the transfer functions.

(5) Conclusion:

The two most successful methods to date appear to be the interfermoetric method, and the type of method as used by Born, Firth and Pringle, and Birch. It is a modified version of the latter method that is in fact used for the present work, and results suggest that this method is the simplest and most satisfying one.



S

CC1, CC2 – Corner Cubes.

BS – Beam Splitter.

P – Parallel Plates.

W – Small Angle Prism

P – produce relative lateral shear of the two wavefronts.

W – moved so that path difference follows saw tooth law.

CC – moved to get initially zero path difference.

Figure 8 Principle of the Transfer Function Measuring Interferometer.

References

Naish, J.M. and Jones, P.G. 1954, Nature, 173, 1241

Hopkins, R.E. 1951, N.B.S. Circular 526, 231.

Hopkins, R.E. and Carpenter, V. 1956, J.O.S.A., 46, 764.

Herriot, W. 1947, J.O.S.A. 37, 472.

Inglestam, E and Lindberg, P.J. 1951, N.B.S. Circular 526 171.

Sproson, W.N. 1953, B.B.C. Quarterly, 8, 55.

Schade, O. 1951, N.B.S. Circular 526, 183.

Born,M., Firth,R., and Pringle, R.W. 1946, Phil.Mag., 31, 1.

Birch, K.G. 1961 Proc. Phys. Soc., 77, 901.

Birch, K.G. 1962, Private Communication.

Baker, L.R. 1955, Proc.Phys.Soc.B., 68, 871.

Baker, L.R. 1964, Private Communication.

Kelsall, D. 1958, Proc.Phys.Soc. 73, 465.

Kelsall, D. 1959, Thesis, University of London.

Montgomery, A. 1961, Thesis, University of London.

Cœnkul, P. 1965 Proc. Phys. Soc., 86, 213.

CHAPTER IV

A General Description of the Optical Transfer Function Test Bench.

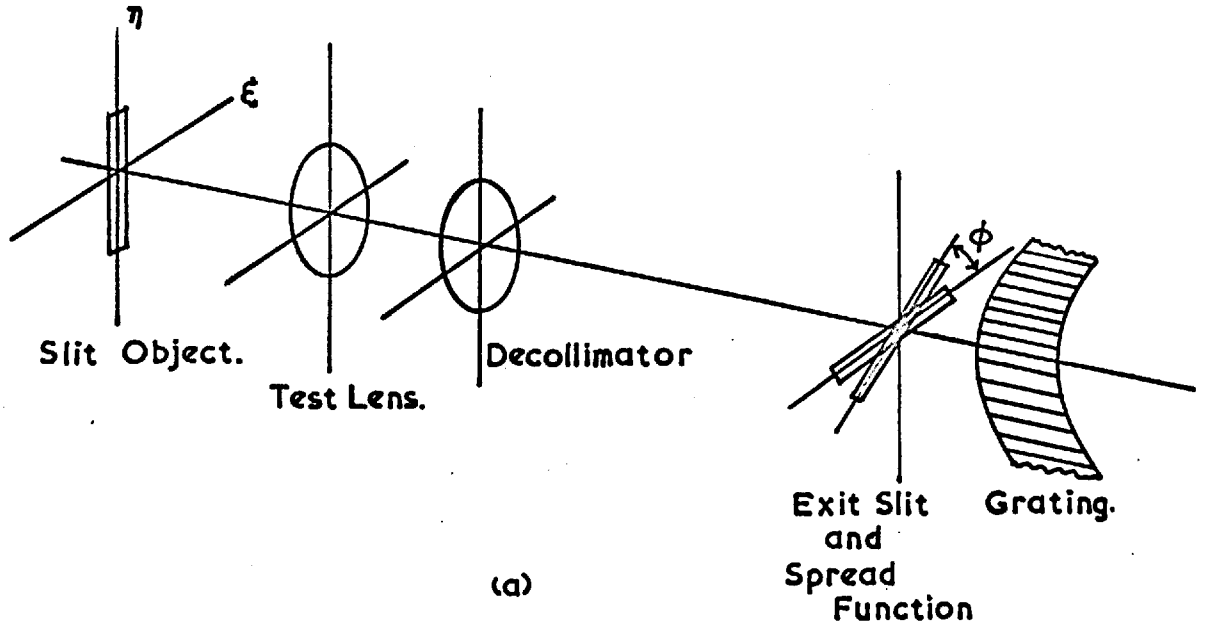
(1) Introduction:-

In this chapter a qualitative description of the methods involved, and the construction of the apparatus will be given. It is desirable that the general layout of the apparatus be known, in order that the theory, to be described in detail in the next chaper, may be followed. In chapter VI a piece-wise detailed description of the components will be given.

(2) A Method for Determining Optical Transfer Functions.

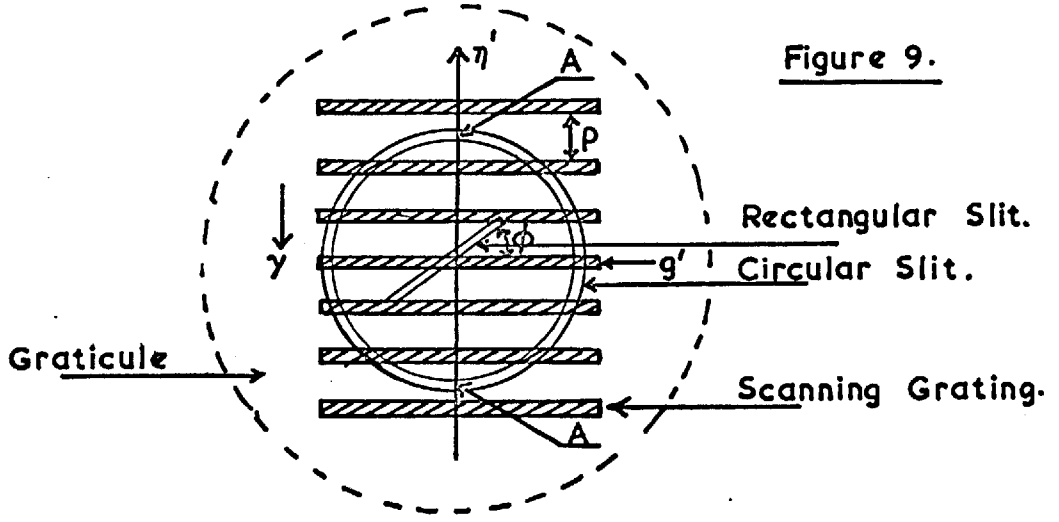
In order to determine the transfer function of an optical system, it is necessary to obtain the inverse Fourier transform of the point spread function or the line spread function. If the line spread function is considered, one convenient way of Fourier analysing it is as shown in Figure (9a), where the test lens is shown working with one infinite conjugate.

The distribution of intensity along the length of the exit slit when parallel to the ξ'-axis is in fact the line spread function. If the exit slit is now rotated through an angle φ, the distribution of intensity along its length is modified by a term dependent on φ. If the exit slit is also scanned by a moving grating (of fixed frequency or period),

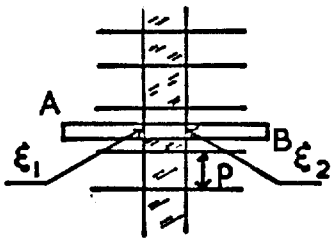


(a)

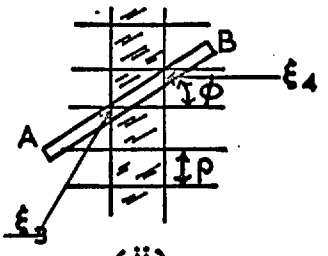
Figure 9.



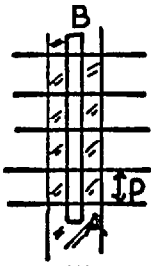
(b)



(i)



(ii)



(iii)

it may be shown (see following chapter) that the output light flux is, apart from numerical factors, the value of the inverse Fourier transform of the spread function for the spatial frequency $s_o \tan \varphi$, where s_o is the spatial frequency of the grating, and ϕ is the angle between the length of the slit and the lines on the grating. When φ is zero, that is parallel to the grating lines, the corresponding spatial frequency is also zero. Thus, by rotating the exit slit relative to the grating lines, a range of spatial frequencies varying upwards from zero to infinity may be obtained. In practice, one is interested only in spatial frequencies varying between zero and the value corresponding to the resolution limit, that is

$$0 \leqslant s \leqslant 2$$

where s is the reduced spatial frequency.

As mentioned above, the light output from the slit-grating combination contains the inverse Fourier transform of the line spread function, namely g(s). It would also be advantageous to obtain simultaneously the value g(0) because the ultimate aim is to determine D(s) where

$$D(s) = \frac{g(s)}{g(0)} = T(s) \exp \{i\, \theta(s)\}$$

A convenient way of doing this is illustrated in Figure (9b). This shows a graticule containing a straight slit and a circular slit, behind which is the scanning grating. The

shaded area indicates the intensity distribution in the line spread function. Suppose that the graticule is mounted accurately in a bearing. As the bearing rotates through an angle φ, the straight slit (or rectangular slit) effectively scans the spread function at spatial frequency s, where

$$s = \frac{1}{p} \tan \varphi$$

Also, the sections of the circular slit scan the spread function at spatial frequency

$$s = \frac{1}{p} \tan 0 = 0$$

Hence, it is possible in this way to obtain simultaneously the inverse Fourier transform of the line spread function at spatial frequencies $(\frac{1}{p} \tan \varphi)$ and zero. If then the corresponding light fluxes are compared, one may obtain the ratio $g(s)/g(o)$.

A qualitative way of seeing how s is dependent on $\tan \varphi$ is illustrated in Figure (9c), where the shaded area indicates the spread function distribution. In case (i), the scanning slit is parallel to the grating lines, and the scale of the spread function along the slit is $\xi_1 \xi_2$. In case (ii) the scale of the spread function is $\xi_3 \xi_4$ where

$$\xi_3 \xi_4 = \frac{\xi_1 \xi_2}{\cos \varphi}$$

Also, the separation of the lines of the scanning grating, as seen along the slit, is increased by the factor $\frac{1}{\sin \varphi}$, that is

$$p \rightarrow p/\sin \varphi$$

Hence the effective spation frequency at which the spread function is given by

$$\text{Spatial Frequency} = \frac{\sin \varphi}{p} \cdot \frac{1}{\cos \varphi} = \frac{1}{p} \tan \varphi = s$$

In case (iii) the scale of the spread function is infinite, while the line spacing of the grating along the slit is p. Hence the spatial frequency is infinite, which agrees with the value

$$s = \left(\frac{1}{p} \tan \varphi\right)_{\varphi=\pi_2} = \infty.$$

The light flux from the rectangular slit - referred to hereafter as the scanning slit - may be written in the form

$$F_\varphi = A(s) \cos \{\omega t + \theta(s)\}$$

where $A(s)$, $\theta(s)$ are functions of the orientation φ, and thus of spatial frequency s, $A(s)$ being an amplitude term and $\theta(s)$ a phase term. $\omega(=2\pi\nu)$ is the angular frequency of the signal, which depends on the grating frequency and its speed, and t is time. The light flux from the sections A of the circular slit - hereafter referred to as the reference slits - may be similarly written in the form

$$F_o = B(0) \cos (\omega t)$$

(The phase $\theta(s)$ is chosen to be zero at zero spatial frequency.)

If now these two light fluxes F_φ and F_0 are fed into one photomultiplier, the electrical signal output will take the form

$$F = F_\varphi + F_0 = A(s)\cos\{\omega t + \theta(s)\} + B(0)\cos(\omega t)$$

If the value of $\theta(s)$ is changed to a new value of $\pm\pi$ by shifting the spread function laterally (refer to chapter II), the resulting signal is

$$F = \{B(0) - A(s)\}\cos(\omega t)$$

If now the intensity $B(0)$ is attenuated until it is equal to $A(s)$, the resultant signal is zero in value.

This combination of rectangular and circular slits is, then, the basis of a null-setting method for determining the optical transfer function $D(s)$. The modulus $T(s)$ is determined as a function of the attenuation of the reference signal required, and the phase $\theta(s)$ is a function of the lateral shift of the spread function. The attenuation is produced by means of density wedges, and the lateral shift is produced by a parallel plate micrometer placed just in front of the scanning and reference slits.

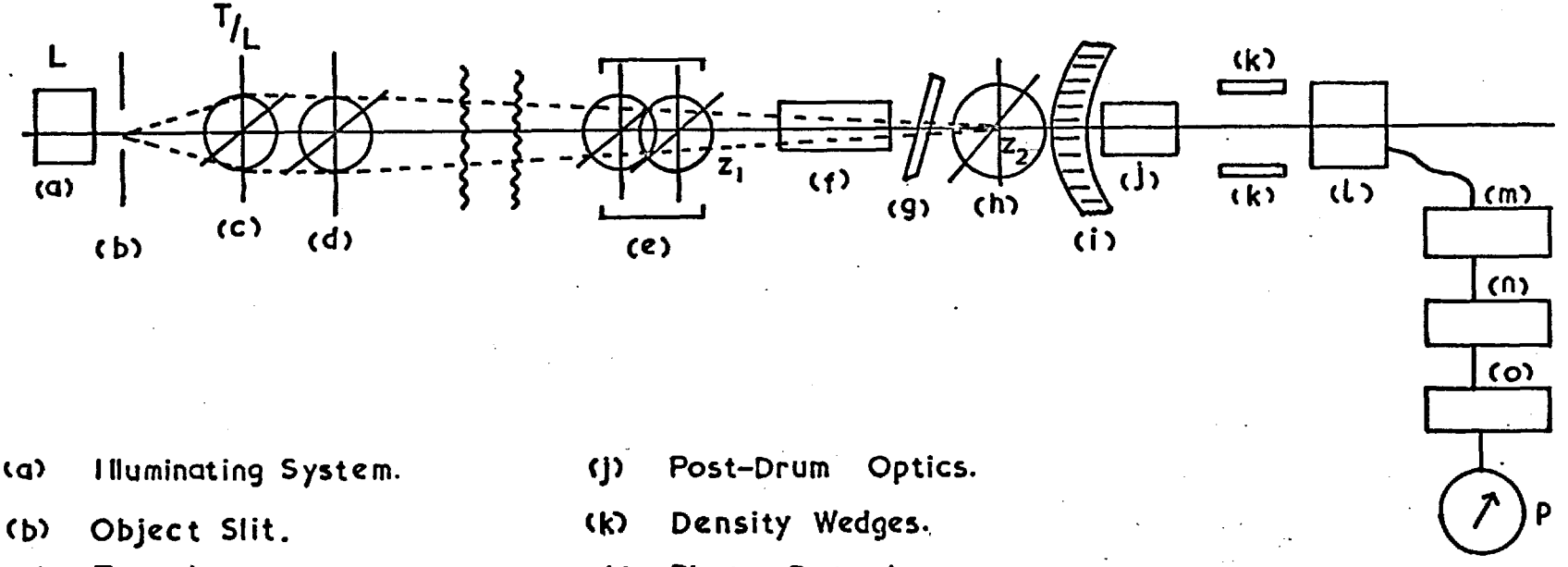
It is important to note that only one photodetector is used in this method, thus eliminating any errors due to fluctuations in photolultiplier sensitivity. Also, since a null-test is employed, amplifier linearity is not important.

Thirdly, any fluctuations of light intensity in the source introduce no errors, as both the scanning and reference signals are affected in a similar way. The accuracy of the null setting is thus determined solely by the signal to noise ratio, and the resulting measurements then rely only on the calibrations of the parallel plate micrometer and the density wedges used for attenuation.

(3) A General Description of the Apparatus:-

Figure (10) shows a block representation of the apparatus used. The light source L illuminates incoherently the object slit which is arranged to be in the back focal plane of the lens to be tested (T/L). The light emerging from the test-lens is thus collimated. This arrangement is desirable for testing systems working with one infinite conjugate. For systems working with finite conjugates, this arrangement would require a slight alteration. This is also true for telescopic systems.

Following the test-lens is a decollimator C which produces an image of the object slit at Z_1. Near to Z_1, however, is placed a magnifying system to enlarge this image to a suitable size. The magnification is chosen so that a useful range of spatial frequencies may be covered when the scanning slit is rotated through a maximum angle φ of 45°. The image of the object slit then appears at Z_2.



(a) Illuminating System.
(b) Object Slit.
(c) Test Lens.
(d) Decollimator.
(e) Magnifying System.
(f) Image Rotating Prism.
(g) Parallel Plate Micrometer.
(h) Scanning & Reference Slits.
(i) Scanning Grating.
(j) Post-Drum Optics.
(k) Density Wedges.
(l) Photo Detector.
(m) Frequency Selective Amplifier.
(n) Power Amplifier.
(o) Detector.
(p) Output Meter.
—— Optical Axis.
- - - - Ray Paths.

Figure 10

In the beam converging to Z_2 are placed a parallel plate micrometer and an image rotating prism. The former provides the means for obtaining phase measurements, as mentioned above, while the latter is used to return the image of the object slit to a direction perpendicular to the scanning grating lines when the object slit is in different azimuths. The image rotating prism must precede the parallel plate micrometer, as lateral shifts of the spread function are required in order to determine the phase of the transfer function.

In the plane through Z_2 and perpendicular to the optical axis, a graticule is placed containing the rectangular and circular slits. This graticule is mounted in a precision bearing which may be rotated through any angle φ. In close proximity to the graticule is the scanning grating containing lines of a fixed separation. It is in fact a square wave grating mounted around the periphery of a glass cylinder.

Following the scanning grating is an optical system which feeds the light from the scanning slit directly into a photomultiplier tube. The light from the reference slits is fed to the same photomultiplier tube after first passing through density wedges. The layout of these components is shown in Figure (11). The output from the photomultiplier is fed through a frequency-selective amplification system,

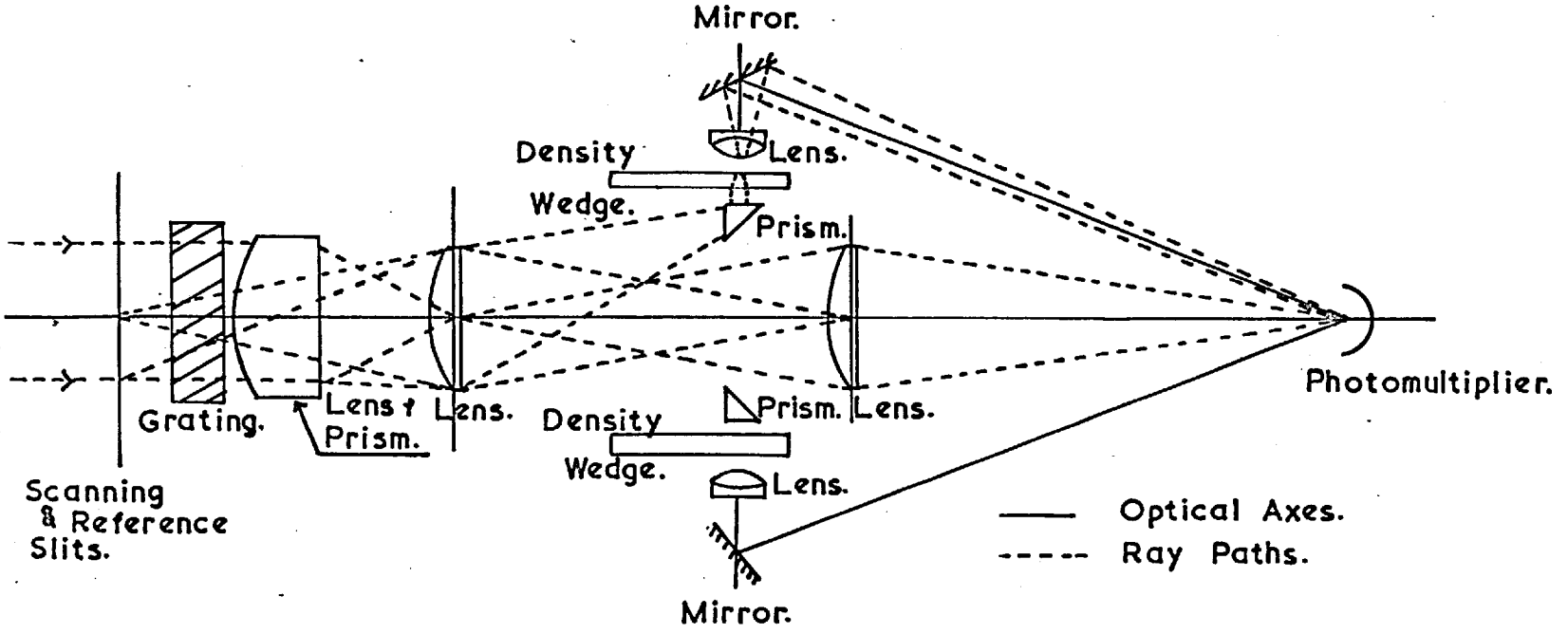


Figure II (not to scale)

and then to a final detecting circuit which enables the null-reading to be observed.

From this brief description of the apparatus, it is possible to visualise the apparatus as consisting essentially of two "black boxes" - one containing the illuminating system and object slit; the other containing the scanning system and detector. This concept is illustrated in Figure (12). Any optical system may then be placed between the two boxes and its transfer function determined. In addition, if the spread function is required to be scanned directly, a beam splitter may be inserted in the light path as shown in Figure (12).

The concept of two "black boxes" is very realistic, and thus makes the instrument an extremely versatile unit.

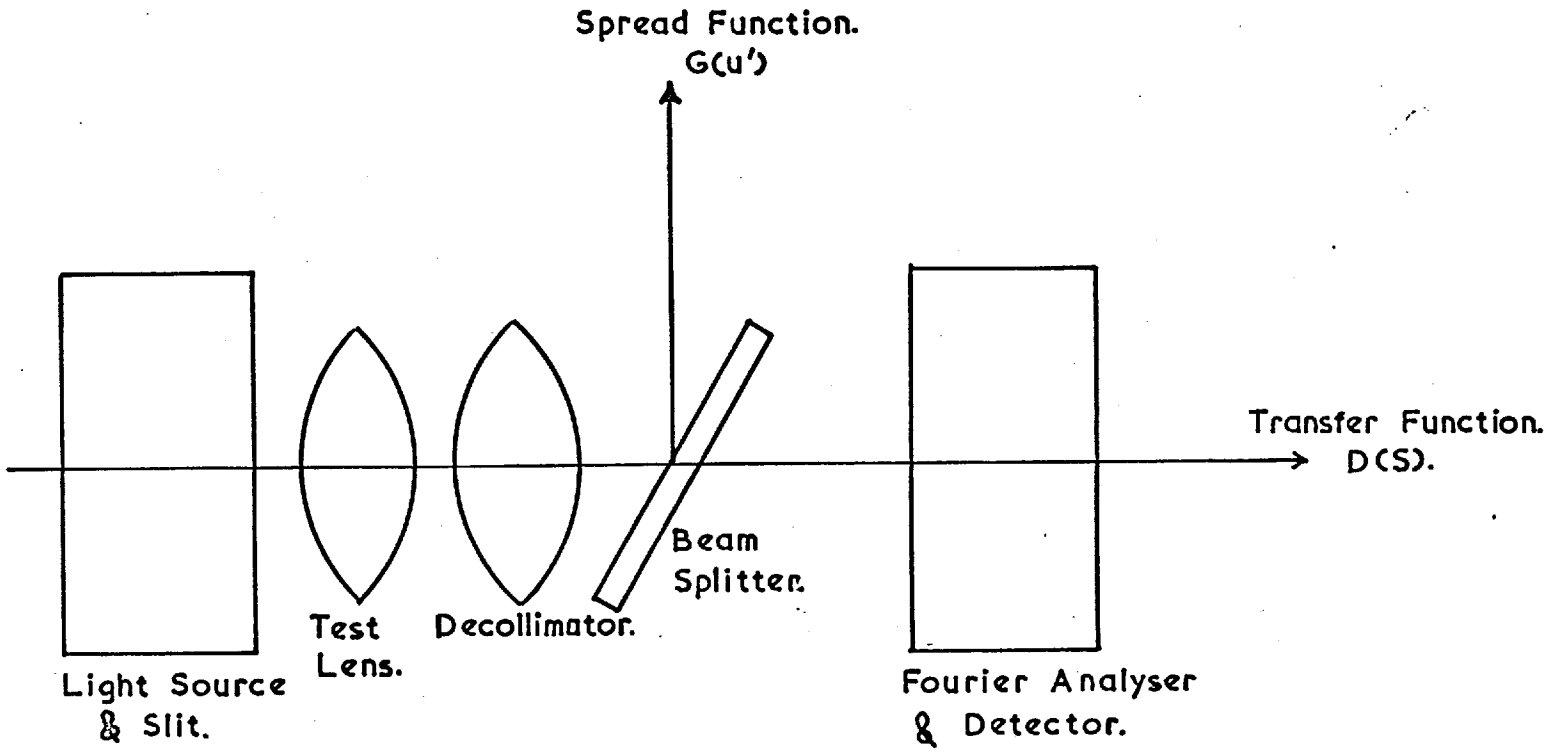

Spread Function.
G(u')
Transfer Function.
D(S).
Beam
Splitter.
Test
Lens.
Decollimator.
Light Source
& Slit.
Fourier Analyser
& Detector.

Figure 12

CHAPTER V

Theory of the Method of Instrument Operation.

(1) Introduction

In this chapter a detailed analysis of the methods of operation of the instrument will be given. Expressions for the light flux leaving the scanning grating will first be derived. Then it will be shown how the parameters in these expressions may be chosen in order that the signal to noise ratio may be optimised. Next, tolerances on, for example, the shape of the object slit, and other parameters will be derived. Finally, expressions for the actual signals fed to the photomultiplier will be obtained.

(2) Theoretical Analysis of Scanning Technique.

The notation to be used here is identical with that used in Chapter II.

Let B(u) be the distribution of intensity in the object plane of an optical system - in this case B(u) refers to the intensity distribution across the object slit. Also, let B'(u') be the intensity distribution in the image plane. Then one may write

$$B'(u') = \int_{-\infty}^{\infty} B(u)G(u'-u)\,du \qquad (1)$$

where G(u') is the line spread function in the image plane of the system. Taking inverse Fourier transforms, one obtains

$$b'(s) = b(s)\,g(s) \qquad (2)$$

where g(s) is the inverse Fourier transform of G(u') and b(s), b'(s) are the inverse Fourier transforms of B(u) and B'(u') respectively. s is the spatial frequency. Equations (1) and (2) express the fact that the convolution of functions in the space domain goes over to the product of functions in the frequency domain.

Referring now to Figure 13(a) where the relevant coordinates are shown, let ABCD be a rectangular slit, of length a and width b, placed in the image plane at an angle ϕ to the u'-axis. The image of the object slit, which is set to be in coincidence with the v'-axis, falls on the former slit, and it is necessary to find the distribution of intensity as seen through this "scanning" slit. The transparency of the slit may be represented by

$$T(u',v') = U(u').V(v')$$

where $U(u')=1, \quad |u'| \leqslant \frac{1}{2}a\cos\phi$

$V(v')=1, \quad u'\tan\phi - \frac{1}{2}b\sec\phi \leqslant v' \leqslant u'\tan\phi + \frac{1}{2}b\sec\phi$

Then, the distribution of intensity, as seen through the slit, is

$$B'(u').U(u').V(v') \qquad (3)$$

Suppose now a moving grating is placed behind the scanning slit as shown in Figure 13(b). Let this grating have a transparency varying with position, which at time t=o may be represented by the Fourier series

$$J'(v') = \sum_{n=-\infty}^{\infty} j_n \exp\{-i \frac{2\pi n}{p} v'\} \quad n= 0,1,2,... \qquad (4)$$

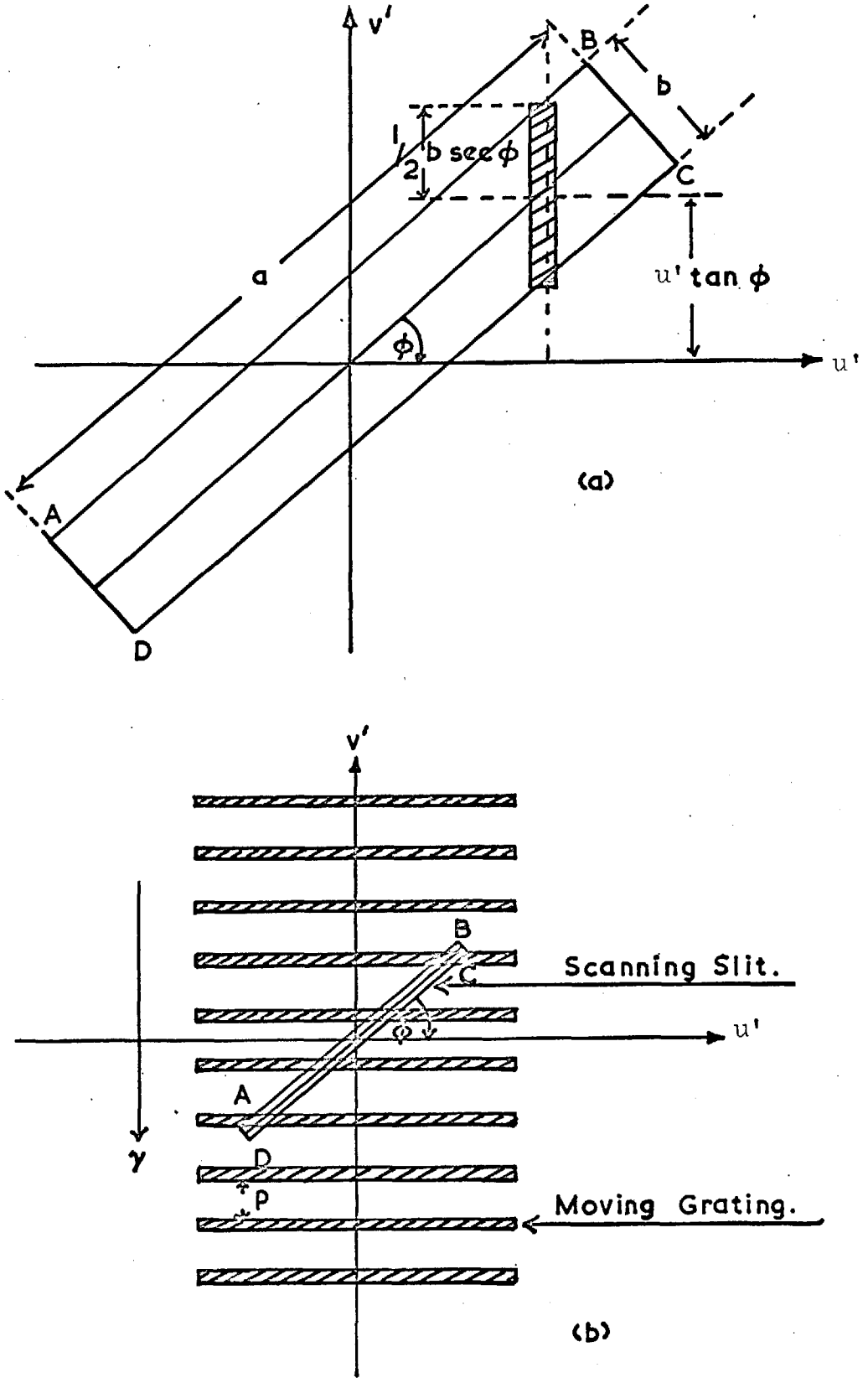

v'
B
b
1/2 b sec φ
C
a
u' tan φ
φ
u'
A
D
(a)
v'
B
Scanning Slit.
C
φ
u'
A
γ
D
P
Moving Grating.
(b)

Figure 13.

where p is the grating period (in reduced coordinates). At a later time t after the initial instant t=o, the transparency at the point v' will be

$$J'(v'-\gamma t) = \sum_{-\infty}^{\infty} j_n \exp\{-i \frac{2\pi n}{p}(v'-\gamma t)\}$$

or
$$J'(v'-\gamma t) = \sum_{-\infty}^{\infty} j_n \exp\{-i \frac{2\pi n}{p} v'\}.\exp\{i \frac{2\pi n}{p} \gamma t\} \quad (5)$$

where γ is the tangential speed of the grating.

Now the total light flux, as seen looking through the grating, is

$$F(\phi,t) = \iint_{u'v'} B'(u').U(u').V(v').J'(v'-\gamma t)du'dv' \quad (6)$$

We may allow the limits of integration for u' to extend to $\pm\infty$ if the length a of the scanning slit is such that

$$B'(u') = o \quad \text{for} \quad |u'| \geqslant \tfrac{1}{2}a\cos\phi$$

That is to say, the limits of integration may extend to $\pm\infty$ provided the image intensity distribution does not have a lateral dimension exceeding $a\cos\phi$ in value.

The limits of integration for v' are determined by the range of v' values for which the scanning slit is transparent, namely

$$u'\tan\phi - \tfrac{1}{2}b\sec\phi \leqslant v' \leqslant u'\tan\phi + \tfrac{1}{2}b\sec\phi$$

Thus

$$F(\phi,t) = -\int_{-\infty}^{\infty} \int_{u'\tan\phi-\frac{1}{2}b\sec\phi}^{u'\tan\phi+\frac{1}{2}b\sec\phi} B'(u') \sum_{-\infty}^{\infty} j_n \exp\{-i\,\frac{2\pi n}{p} v'\}\exp\{i\,\frac{2\pi n}{p}\gamma t\}du'dv'$$

or

$$F(\phi,t) = -\int_{-\infty}^{\infty} B'(u') \left\{ \int_{u'\tan\phi-\frac{1}{2}b\sec\phi}^{u'\tan\phi+\frac{1}{2}b\sec\phi} \sum_{-\infty}^{\infty} j_n \exp\{-i\,\frac{2\pi n}{p} v'\}dv' \right\} \exp\{i\frac{2\pi n}{p}\gamma t\}du' \qquad (7)$$

Now $$\int_{u'\tan\phi-\frac{1}{2}b\sec\phi}^{u'\tan\phi+\frac{1}{2}b\sec\phi} \sum_{-\infty}^{\infty} j_n \exp\{-i\,\frac{2\pi n}{p}v'\}dv' = \sum_{-\infty}^{\infty} j_n \exp\{-i\,\frac{2\pi n}{p}u'\tan\phi\} \cdot \frac{\sin\left(\frac{\pi nb}{p\cos\phi}\right)}{\left(\frac{\pi n}{p}\right)}$$

which substituted into (7) gives

$$F(\phi,t) = -\int_{-\infty}^{\infty} B'(u') \cdot \sum_{-\infty}^{\infty} j_n \cdot \exp\{-i\,\frac{2\pi n}{p}u'\tan\phi\} \cdot \frac{\sin\left(\frac{\pi nb}{p\cos\phi}\right)}{\left(\frac{\pi n}{p}\right)} \cdot \exp\{i\frac{2\pi n}{p}\gamma t\}\,du'$$

Collecting under the integral sign the terms in u', this last expression may be written

$$F(\phi,t) = \sum_{-\infty}^{\infty} j_n \cdot \frac{\sin\left(\frac{\pi nb}{p\cos\phi}\right)}{\left(\frac{\pi n}{p}\right)} \cdot b'\left(\frac{n}{p}\tan\phi\right) \cdot \exp\{i\,\frac{2\pi n}{p}\gamma t\} \qquad (8)$$

where $b'\left(\frac{n}{p}\tan\phi\right) = \int_{-\infty}^{\infty} B'(u')\exp\{-i2\pi(\frac{n}{p}\tan\phi)u'\}\,du'$ is, by definition, the inverse Fourier transform of $B'(u')$. Introducing now the notation

$$s_o = \frac{1}{p}\,, \quad s = s_o\tan\phi = \frac{1}{p}\tan\phi,$$

where s_o is the fundamental frequency of the grating, one obtains

$$F(\phi,t) = \sum_{-\infty}^{\infty} j_n \frac{\sin\left(\frac{\pi n s_o b}{\cos\phi}\right)}{\left(\pi n s_o\right)} .b'(ns).\exp\{i2\pi n s_o \gamma t\} \qquad (9)$$

From the relation (2), $b'(ns) = b(ns).g(ns)$ so that

$$F(\phi,t) = \sum_{-\infty}^{\infty} j_n \cdot \frac{\sin\left(\frac{\pi n s_o b}{\cos\phi}\right)}{(\pi n s_o)} .b(ns).g(ns).\exp\{i2\pi n s_o \gamma t\} \qquad (10)$$

Now the geometrical image of a rectangular slit is itself a rectangular slit. If it is assumed that the object slit is uniformly illuminated, then one may write

$$B(u) = K \quad , \quad |u| \leqslant \frac{d}{2}$$

$$= 0 \quad , \quad |u| > \frac{d}{2}$$

where d is the slit width in reduced coordinates.

Thus

$$b(ns) = \int_{-d/2}^{d/2} K.\exp\{-i2\pi ns.u\}\,du = K.\frac{\sin(\pi nsd)}{(\pi ns)}$$

Hence

$$F(\phi,t) = \sum_{-\infty}^{\infty} j_n \cdot \frac{\sin\left(\frac{\pi n s_o b}{\cos\phi}\right)}{(\pi n s_o)} \cdot K \cdot \frac{\sin(\pi n s d)}{(\pi n s)} \cdot g(ns) \cdot \exp\{i 2\pi n s_o \gamma t\} \qquad (11)$$

(11) shows that the light flux $F(\phi,t)$ leaving the grating varies periodically with time. $F(\phi,t)$ is real, and the right hand side of (11) is the complex Fourier series representing it. Now for a real function $F(t)$ of period T, the complex Fourier series has the form

$$F(t) = \sum_{-\infty}^{\infty} j_n \exp\{i \frac{2\pi n}{T} t\}$$

and writing

$$j_n = \tfrac{1}{2} \alpha_n \exp\{i \Phi_n\}, \quad j_{-n} = \tfrac{1}{2} \alpha_n \exp\{-i\Phi_n\}$$

this takes the form

$$F(t) = \sum_{o}^{\infty} \alpha_n \cos\{\frac{2\pi n t}{T} + \Phi_n\}$$

Thus, only the zero and positive values of n are selected, and then, in the complex series,

j_o = amplitude of the D.C. level

$2j_n$ = complex amplitude of the A.C. term of frequency (n/T).

Hence in (11), if only the D.C. term (n=o) and the fundamental frequency term (n=1) are selected, the light flux, as seen through the grating, may be written

$$F_{o,1}(\phi,t) = j_o.\left(\frac{b}{\cos\phi}\right).K.d.g(o) + 2|j_1|.\sin\frac{\left(\frac{\pi s_o b}{\cos\phi}\right)}{(\pi s_o)}.K.\sin\frac{(\pi sd)}{(\pi s)}|g(s)|.\cos\{2\pi\gamma s_o t + \arg(j_1)+\arg(g(s))\} \quad (12)$$

If the D.C. component is also removed, then

$$F_1(\phi,t) = 2|j_1|.\left(\frac{b}{\cos\phi}\right).\frac{\sin\left(\frac{\pi s_o b}{\cos\phi}\right)}{\left(\frac{\pi s_o b}{\cos\phi}\right)}.K.d.\frac{\sin(\pi sd)}{(\pi sd)}.|g(s)| .\cos\{2\pi\gamma s_o t+\arg(j_1)+\arg(g(s))\} \quad (13)$$

(13) gives the light flux $F_1(\phi,t)$ in terms of the different parameters of the system, and the modulus and phase of g(s), the inverse Fourier transform of the line spread function of the system under test.

If the value $\phi=0$ is chosen - that is, the scanning slit is arranged to be parallel to the u'-axis - the expression for the $A_2C_{\frac{1}{2}}$ component of the light flux, (13),

reduces to

$$F_1(0,t) = 2|j_1|b.\frac{\sin(\pi s_o b)}{(\pi s_o b)}.k.d.|g(0)|.\cos\{2\pi\gamma s_o t + \arg(j_1) + \arg(g(0))\} \quad (14)$$

Also, the ratio of the amplitudes of the fundamental frequency for $\varphi = \varphi$ and $\varphi = 0$ is given by

$$\frac{F_1(\varphi)}{F_1(0)} = \frac{\sin(\pi s_o b\cos\varphi)}{\sin(\pi s_o b)} \cdot \frac{\sin(\pi sd)}{(\pi sd)} \cdot T(s) \quad (15)$$

where $T(s) = \left|\frac{g(s)}{g(0)}\right|$ is the modulus of the optical transfer function of the system for the apatial frequency $s = s_o \tan\varphi$, where $s_o(=\frac{1}{p})$ is the spatial frequency of the fundamental of the grating.

The phase of the fundamental term (13) is

$$\arg(j_1) + \arg(g(s))$$

in which $\arg(j_1)$ is constant and

$$\arg(g(s)) = \theta(s)$$

is the phase of the optical transfer function. If the phase zero is chosen such that $\theta(0) = 0$, the transfer function may be written in the form

$$D(s) = \frac{g(s)}{g(0)} = T(s)\exp\{i\,\theta(s)\} \quad (16)$$

From (15) it may be seen that, apart from two correction factors, the optical transfer function at spatial frequency s is given by the ratio of two light

fluxes seen through the grating when the scanning slit is at angles of φ and zero relative to the grating lines. The two correction factors are due to the finite widths of

(a) the scanning slit - $\dfrac{\sin\left(\frac{\pi s_o b}{\cos\varphi}\right)}{\sin(\pi s_o b)}$

(b) the geometrical image of the object slit - $\sin\dfrac{(\pi sd)}{(\pi sd)}$

As will be seen in a later section, these factors are not negligible, and if omitted from (15) would lead to significant errors in the values of D(s).

In practice, the light from the scanning slit, together with the light from the two reference slits (formed by selecting the parts of the circular slit at which $\varphi = 0$) is fed into one photomultiplier. The output signal from the photomultiplier is thus proportional to the sum of the light fluxes from both the scanning slit and the two reference slits. The light from the scanning slit is phase shifted to give a minimum output signal, and the light from the reference slits is then attenuated until zero output signal is obtained.

(3) Optimisation of Parameters for Signal to Noise Ratio:-

The expression (12) gives the total light flux $F_{o,1}(\varphi,t)$ seen looking through the grating, namely

$$F_{o,1}(\varphi,t) = j_o\left(\frac{b}{\cos\varphi}\right).K.d.g(0) + 2|j_1|.\sin\frac{\left(\frac{\pi s_o b}{\cos\varphi}\right)}{\pi s_o}$$

$$.K.\frac{\sin(\pi sd)}{(\pi sd)}.d.|g(s)|.\cos\{2\pi\gamma s_o t + \arg(j_1) + \arg(g(s))\}$$

This light flux contains a D.C. term (first term), and an A.C. term (second term) of frequency $\gamma s_o (=\gamma/p)$. Rewriting the above in terms of the modulus T(s) and phase $\theta(s)$ of the optical transfer function, and taking

$$j_1 = |j_1|\exp\{i\beta_1\} \quad , \quad \theta(0) = 0 \quad ,$$

one obtains

$$F_{o,1}(\varphi,t) = j_o\left(\frac{b}{\cos\varphi}\right).K.d.g(0) + 2|j_1|.\frac{\sin\left(\frac{\pi s_o b}{\cos\varphi}\right)}{(\pi s_o)}.K.\frac{\sin(\pi ds)}{(\pi d)}.g(0).T(s).\cos\{2\pi\gamma s_o + \beta_1 + \theta(s)\} \quad (17)$$

and for $\varphi = 0$

$$F_{o,1}(0,t) = j_o.b.K.d.g(0) + 2|j_1|.b.K.d.g(0).\frac{\sin(\pi s_o b)}{(\pi s_o b)}.t(0)\cos\{2\pi\gamma s_o t + \beta_1\} \quad (18)$$

If one assumes uniform illumination of the object slit, and consequently uniform intensity along the length of its

image, the total light flux entering the photomultiplier will be

$$F = F_{o,1}(\varphi,t) + 2\,F_{o,1}(0,t)$$

where $F_{o,1}(\varphi,t)$ and $F_{o,1}(0,t)$ are given by (17) and (18) respectively. The flux $F_{o,1}(\varphi,t)$ is phase shifted to produce a minimum output signal, and then the flux $2\,F_{o,1}(0,t)$ is attenuated to produce zero output signal.

If $\{A(s)\}_{Bal.}$ is the attenuation required to produce zero A.C. output signal when φ has the value corresponding to the spatial frequency $s = s_o \tan\varphi$, then the total A.C. light flux equated to zero gives

$$F_1 = 2|j_1|.b.k.d.g(0)\left\{\frac{\sin\left(\frac{\pi s_o b}{\cos\varphi}\right)}{(\pi s_o b)} \cdot \frac{\sin(\pi sd)}{(\pi sd)} \cdot T(s) - 2\left\{A(s)\right\}_{Bal.} \cdot \frac{\sin(\pi s_o b)}{(\pi s_o b)}\right\} = 0 \qquad (19)$$

F_1 is the difference of the amplitudes of the A.C. components of (17 and (18), where, from definition $T(0) = 1$.

This relation gives

$$2\left\{A(s)\right\}_{Bal.} = \frac{\sin(\pi sd)}{(\pi sd)} \cdot \frac{\sin\left(\frac{\pi s_o b}{\cos\varphi}\right)}{\sin(\pi s_o b)} \cdot T(s) .$$

When near balance, an attenuation setting

$$A(s) = \{A(s)\}_{Bal.} + \delta A(s)$$

will correspond to an error $\delta T(s)$ in $T(s)$ given by

$$2\delta A(s) = \frac{\sin(\pi sd)}{(\pi sd)} \cdot \frac{\sin\left(\frac{\pi s_o b}{\cos\varphi}\right)}{\sin(\pi s_o b)} \cdot \delta T(s)$$

Thus, from (19), the A.C. component of flux when out of balance by an amount $\delta A(s)$ is given numerically by

$\delta F_1 = 2|j_1|.b.k.d.g(0).2\delta A(s).\frac{\sin(\pi s_o b)}{(\pi s_o b)}$ or, expressing $\delta A(s)$ in terms of $\delta T(s)$, and including a factor S which represents the signal sensitivity of the detector

$$\delta 0_1 = 2|j_1|.S.b.k.d.g(0).\frac{\sin(\pi sd)}{(\pi sd)}.\frac{\sin\left(\frac{\pi s_o b}{\cos\varphi}\right)}{(\pi s_o b)}.\delta T(s) \qquad (20)$$

In addition to the A.C. signal given by (20), there will be a noise signal generated. The noise is predominantly due to photon fluctuations in the light beam; this effect is taken to be much more significant than effects due to Johnson noise etc. In the classical approximation, that is for a large number of photons present, the root mean square fluctuation in photon flux density is given by

$$\sqrt{\delta\bar{n}^2} = \bar{n}$$

where $\bar{n}$ is the mean photon density. Thus the noise signal is given by

$$F_N = (\text{Total light flux})^{\frac{1}{2}}$$

Now the total D.C. light flux from both the scanning slit and the two reference slits, when the system is near balance is given, from (17) and (18) by

$$F_o = j_o \left(\frac{b}{\cos\phi}\right).K.d.g(o)+2A(s).j_o.b.K.d.g(o)$$

where $A(s)$ is the attenuation of the flux from the two reference slits. That is

$$F_o = j_o.b.d.K.g(o)\left\{\frac{1}{\cos\phi} + 2A(s)\right\} \qquad (21)$$

The bracketed term in (21) is insensitive to small variations in the values of s, b, and d, and varies in the range of approximately 1.3 ± 0.1 for values of ϕ $0 \leqslant \phi \leqslant \frac{\pi}{4}$. The remaining factors of (21) have the greatest effect on the D.C. flux. The noise signal due to photon fluctuations is therefore, to a good approximation,

$$O_N = S_N \left\{ \frac{j_o.b.K.d.g(o)}{1.3} \right\}^{\frac{1}{2}}$$

where S_N is the noise sensitivity of the detector. For an out of balance signal corresponding to an error $\delta T(s)$, the signal to noise ratio is given by

$$|\text{Signal/Noise}| = \frac{\delta O_1}{O_N} = \frac{1}{\sqrt{1.3}}\left(\frac{S}{S_N}\right)\left(\frac{2|j_1}{j_o^{\frac{1}{2}}}\right)\left(\frac{\sin(\pi sd)}{\pi sd^{\frac{1}{2}}}\right)$$

$$\cdot\left(\frac{\sin\left(\frac{\pi s_o b}{\cos\phi}\right)}{\pi s_o b^{\frac{1}{2}}}\right).\sqrt{g(o)}.\delta T(s) \qquad (22)$$

The factors in (22) have the following significance :-

(a) $\left(\frac{S}{S_N}\right) = \left(\frac{\text{Signal sensitivity of Photo-detector}}{\text{Noise sensitivity of Photo-detector}}\right)$

(b) $\left(\frac{|j_1|}{j_o^{\frac{1}{2}}}\right) = \left(\frac{\text{Amplitude of grating fundamental}}{(\text{Mean transmission of grating})^{\frac{1}{2}}}\right)$

(c) $\left(\frac{\sin(\pi sd)}{\pi sd^{\frac{1}{2}}}\right)$ = Effect due to finite height of object slit.

(d) $\frac{\sin\left(\frac{s_o b}{\cos\phi}\right)}{\pi s_o b^{\frac{1}{2}}}$ = Effect due to finite height of scanning slit.

(e) $\sqrt{g(o)}$ is a photometric term.

It should be noted that the noise signal O_N will be modified to some extent by the bandwidth $\Delta\nu$ of the detecting apparatus. However, this is a separate effect, and will not be considered at this juncture.

It is clear from (22) that the signal to noise ratio should be made as large as possible in order that the sensitivity or accuracy of the instrument be maximised. The larger the signal to noise ratio, the smaller is the value of $\delta T(s)$ that can be sensibly detected. Alternatively, for a

small error $\delta T(s)$ in $T(s)$ to be detected, the factors in (22) must be maximised.

Considering first the factor (c) in (22), for this to be a maximum

$$\frac{\partial[(c)]}{\partial d} = 0$$

This is so when

$$\tan(\pi sd) = 2(\pi sd)$$

Similarly for the factor (d) in (22), one obtains as a condition for maximum value

$$\tan\left(\frac{\pi s_o b}{\cos\phi}\right) = 2\left(\frac{\pi s_o b}{\cos\phi}\right)$$

Solving these equations graphically gives

$$\left.\begin{aligned} \pi sd &= \pi\left(\frac{d}{p}\right) \quad \tan\phi = 1.167 \\ \frac{\pi s_o b}{\cos\phi} &= \pi\left(\frac{b}{p}\right)\frac{1}{\cos\phi} = 1.167 \end{aligned}\right\} \qquad (23)$$

As may be seen, a particular angle ϕ must be chosen at which to maximise the signal to noise ratio. Now the signal strength will, in general, decrease with increasing spatial frequency, so that it would appear advantageous to have a maximum signal to noise ratio at a high spatial frequency. From practical considerations it appears useful to choose $\phi = \frac{\pi}{4}$. Then one obtains from (23)

$$\frac{d}{p} = 0.372 \quad ; \quad \frac{b}{p} = 0.262 \ .$$

If a different value of ϕ is chosen for optimisation, different values of $(\frac{d}{p})$ and $(\frac{b}{p})$ will be obtained. Figure 14(a) shows the variation of $(\frac{d}{p})$ with ϕ to give maximum signal to noise ratio. The relation between $(\frac{b}{p})$ and ϕ gives a similar curve.

Figure 14(b) shows the variation of signal to noise ratio with $(\frac{d}{p})$ for a fixed value of $\phi(=\frac{\pi}{4})$. The value 100 has been chosen arbitarily as the maximum value. As may be seen, the curve is slowly varying, so that the value of $(\frac{d}{p})$ is not particularly critical. The same holds for $(\frac{b}{p})$.

Turning now to the factor (b), the value of $\frac{2|j_1|}{\sqrt{j_o}}$ is determined by the mark: space ratio of the scanning grating. The grating may be considered to have a transparency $J(v')$ where

$$J(v') = 0 \quad , \quad -p/2 < v' < \tau$$

$$= 1 \quad , \quad -\tau < v' < \tau \qquad \text{see Figure (15)}$$

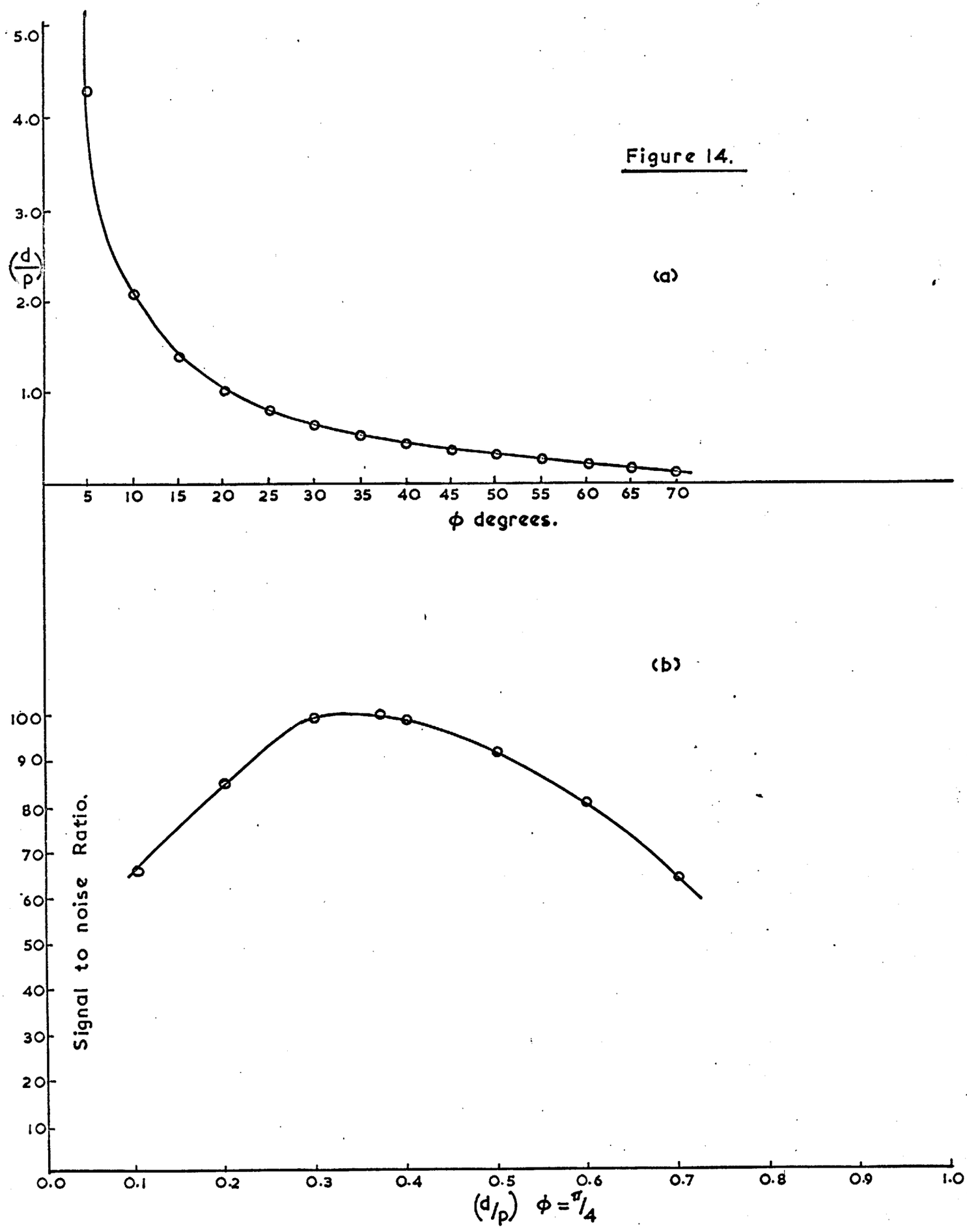
$$= 0 \quad , \quad \tau < v' < p/2$$

This transparency is represented by the Fourier series

$$J(v') = \sum_{-\infty}^{\infty} j_n \exp\{-i \frac{2\pi n}{p} v'\}$$

where

$$j_n = \frac{1}{p} \int_{-p/2}^{p/2} J(v') \exp(i 2\pi \frac{n}{p} v') \, dv'$$


Figure 14.
(a)
5.0
4.0
3.0
(d/p)
2.0
1.0
5
10
15
20
25
30
35
40
45
50
55
60
65
70
φ degrees.
(b)
100
90
80
70
60
50
40
30
20
10
Signal to noise Ratio.
0.0
0.1
0.2
0.3
0.4
0.5
0.6
0.7
0.8
0.9
1.0
(d/p) φ = π/4

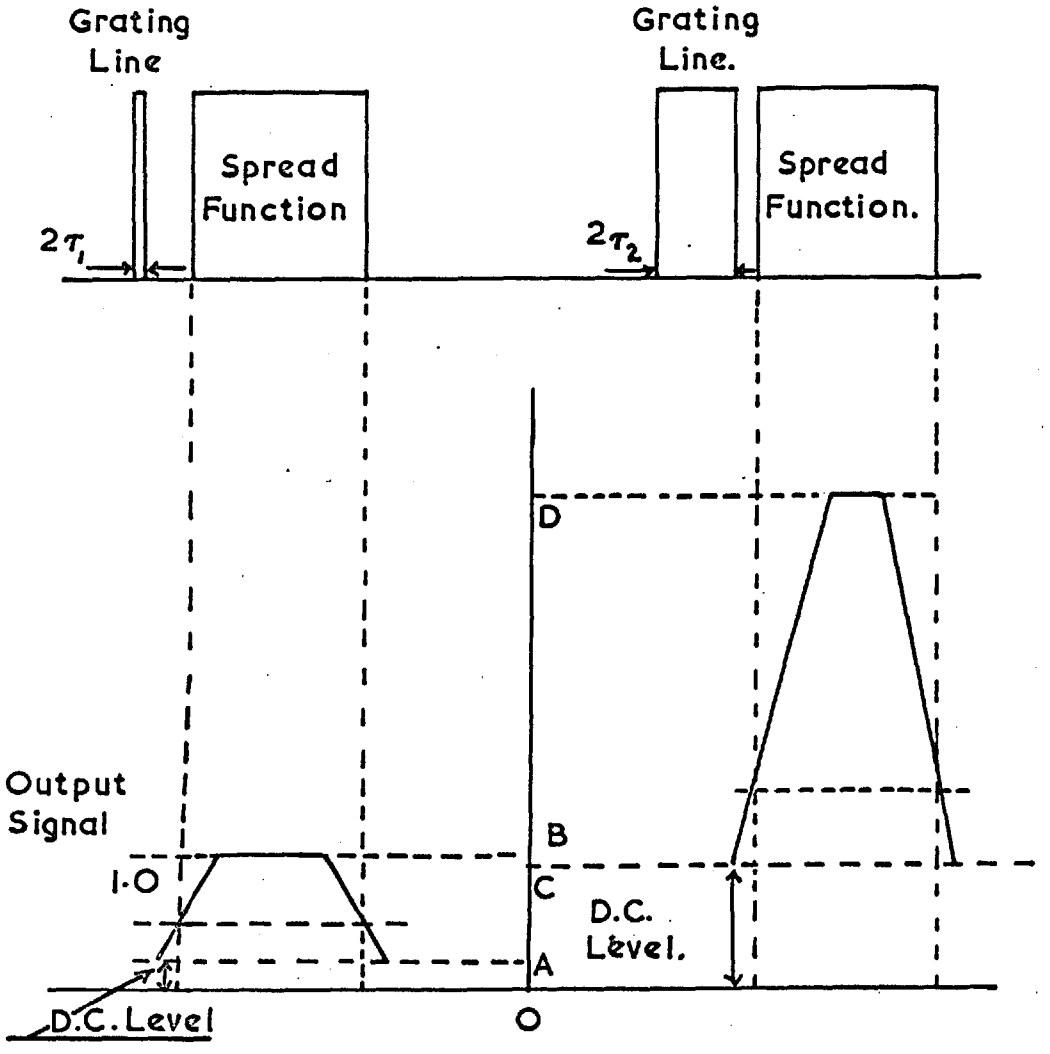

Grating Line
Spread Function
$2\tau_1$
Grating Line.
Spread Function.
$2\tau_2$
D
B
C
A
O
D.C. Level.
Output Signal
I·O
D.C. Level
$\frac{\text{Signal}}{\text{Noise.}} \propto \frac{\text{O.B.}}{\text{O.A.}^{\frac{1}{2}}}$
$\frac{\text{Signal}}{\text{Noise}} \propto \frac{\text{O.D.}}{\text{O.C.}^{\frac{1}{2}}}$

Figure 15.

If the terms of order n=0 (D.C) and n=1 (fundamental) are chosen, then

$$j_o = \frac{1}{p}\int_{-\tau}^{\tau} d\tau = \frac{\tau}{p}$$

$$j_1 = \frac{1}{p}\int_{-\tau}^{\tau} \exp\left(i\,\frac{2\pi}{p}v'\right) dv' = \frac{\sin\left(\frac{2\pi\tau}{p}\right)}{\pi}$$

Thus $$\frac{2|j_1|}{\sqrt{j_o}} = \frac{2}{\pi} \cdot \frac{\sin\left(\frac{2\pi\tau}{p}\right)}{\left(\frac{\tau}{p}\right)^{\frac{1}{2}}}$$

This has a maximum value when

$$\frac{2\pi\tau}{p} = 1.167 \quad \text{or} \quad \frac{2\tau}{p} = 0.372.$$

Hence the mark to space ratio required to maximise $\frac{2|j_1|}{\sqrt{j_o}}$ is

$$M:S = 0.372 : 0.628 \approx 4:9$$

The physical significance of this result may be seen in Figure 15. For a fine line scanning the spread function, there will be a small D.C. level and a small A.C. level. As the line width increases, so does the D.C. level and also the A.C. level, the ratio of these levels being given by $\frac{2|j_1|}{\sqrt{j_o}}$. As the line width increases still further, the D.C. level rises until it eventually swamps any A.C. present.

The factor (a) in (2) is a function of the sensitivity of the photodetector, and thus represents a constant in the signal to noise ratio expression $(\delta 0_1 / 0_N)$

(4) Influence of Variation in Intensity in Spread Function

In all the foregoing discussion it has been assumed that the intensity distribution in the spread function is the required distribution. This in turn requires uniform illumination of the object slit, which itself must be truly rectangular in form. In addition, the transmission through the optical system has been assumed uniform. If any of these assumptions are not correct, the measured spread function will not usually be the true function required for analysis

Let $G(u')$ be the true spread function, and let $G(u',v')$ be the measured spread function. It is now assumed that the relation between $G(u')$ and $G(u',v')$ is of the form

$$G(u',v') = G(u').L(u').M(v')$$

where $L(u') = (1 + \alpha_1 u' + \alpha_2 u'^2 + \ldots)$, $M(v') = (1 + \beta_1 v' + \beta_2 v'^2 + \ldots)$

Then, if only terms of the zero and first order in u' and v' are considered

$$G(u',v') = G(u')\{1 + \alpha_1 u'\}\{1 + \beta_1 v'\}$$

Now the variation of intensity along the v'-direction will result only in different attenuations being required for the

two reference signals - this difference, if present, may be determined experimentally, and so may be neglected here. Thus the relation between the measured and true spread functions may be written

$$G(u',v') \rightarrow \tilde{G}(u') = G(u')\{1 + \alpha_1 u'\}$$

Taking inverse Fourier transforms, and noting that

$$g(s) = \int_{-\infty}^{\infty} G(u') \exp\{-i\, 2\pi\, u's\}\, du'$$

one obtains

$$\tilde{g}(s) = \int_{\infty}^{\infty} g(s-s')T^{-1}\{1 + \alpha_1 u'\}_{s=s'} ds'$$

where T^{-1} denotes an inverse transform.

Using the relations

$$\delta(s) = \int_{-\infty}^{\infty} \exp\,[-i2\pi u's\}du' \;,\; \delta'(s) = \int_{-\infty}^{\infty} (-i2\pi u')\exp\{-i2\pi u's\}$$

where $\delta(s)$, $\delta'(s)$ are the delta function and its derivative respectively, one obtains

$$\tilde{g}(s) = \int_{\infty}^{\infty} g(s)\; \{\delta(s) + \frac{i\alpha_1}{2\pi}\, \delta'(s)\}\, ds'$$

or

$$\tilde{g}(s) = g(s) + \frac{i\alpha_1}{2\pi}\; g'(s)$$

Hence the required spread function is given by

$$g(s) = \tilde{g}(s) - \frac{i\alpha_1}{2\pi} g'(s) \qquad (24)$$

To obtain quantitative values of this effect, a simple example is chosen.

Choose $G(u') = 1 \qquad |u'| \leqslant d/_2$

$$= 0 \qquad |u'| > d/_2$$

Then $g(s) = \frac{\sin(\pi ds)}{\pi s}$, $g'(s) = \frac{\pi ds.\cos(\pi ds) - \sin(\pi ds)}{\pi s^2}$

Figure 16 shows the function g(s) plotted against s, and also the variation of g'(s) with s.

From (24) we have

$$|g(s) - \tilde{g}(s)| = \frac{\alpha_1}{2\pi} g'(s)$$

If the optical transfer function is to be measured with an accuracy of $1^{o}/o$, then

$$|g(s) - \tilde{g}(s)| = 0.01 = \frac{\alpha_1}{2\pi} g'(s)$$

or

$$\alpha_1 \approx \frac{0.06}{g'(s)} \qquad (25)$$

The expression (25) gives the permissible value of α_1 consistent with a $1\ ^{o}/_{o}$ accuracy in g(s), for any value of s. For example, take s = 1/d. Then

$$g'(s) = -d^2 \quad , \quad \alpha_1 = \frac{-0.06}{d^2}$$

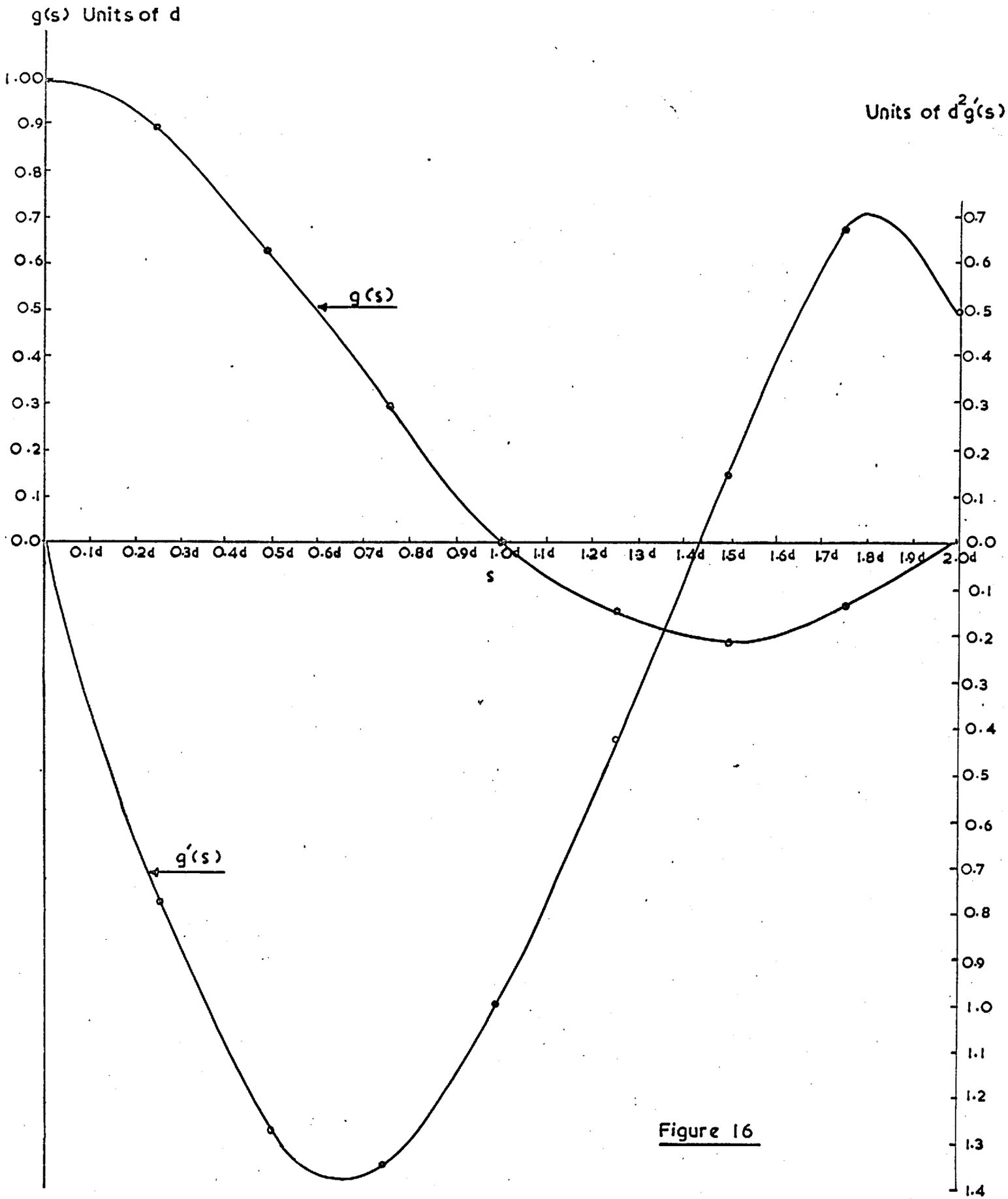

g(s) Units of d
Units of d²g'(s)
1.00
0.9
0.8
0.7
0.6
0.5
0.4
0.3
0.2
0.1
0.0
0.7
0.6
0.5
0.4
0.3
0.2
0.1
0.0
0.1d 0.2d 0.3d 0.4d 0.5d 0.6d 0.7d 0.8d 0.9d 1.0d 1.1d 1.2d 1.3d 1.4d 1.5d 1.6d 1.7d 1.8d 1.9d 2.0d
s
g(s)
g'(s)
0.1
0.2
0.3
0.4
0.5
0.6
0.7
0.8
0.9
1.0
1.1
1.2
1.3
1.4

Figure 16

Remembering that d is the reduced height of the object slit, and taking

$$D = 4\times10^{-3}\text{inches, where } d = \frac{n\sin\alpha}{\lambda} D ,$$

one obtains, for a $1^{o}/o$ accuracy in g(s)

$$(F/No.)_{\text{Image Space}} \approx 55$$

That is, for a given value of D and λ, the F/No. in the image space must not be less than about 55. This condition is satisfied in practice.

(5) Influence of Decollimator and Magnifying System Aberrations on the Spread Function.

Let $W(s,y)_T$, $W(x,y)_C$, $W(x,y)_M$ be the aberrations of the test lens, decollimator, and magnifying system respectively. The total aberration is then

$$W = W(x,y)_T + W(x,y)_C + W(x,y)_M$$

or

$$W = W(x,y)_T \left\{ 1 + \frac{W(x,y)_R}{W(x,y)_T} \right\}. \qquad (26)$$

where $W(x,y)_R = W(x,y)_C + W(x,y)_M$.

From (26) it may be seen that the better the correction state of the test-lens, the greater the effect have the residual aberrations. Thus it is important that both the decollimator and the magnifying system are well corrected. The conditions under which the decollimator and magnifying system work are

advantageous in this respect since they are working at a much lower F/No. than is the test lens.

One method of estimating this effect is to consider a perfect lens defocussed by, say, $\lambda/4$. At each spatial frequency, the quantity

$$\delta T(s) = T(s)_o - T(s)_{\lambda/4}$$

may be determined. The maximum value of $\delta T(s)$ for this case is approximately

$$\delta T(s) = \delta T(0.8) \approx 0.20$$

This implies that if the decollimator and magnifying system contribute only $\lambda/4$ to the total aberration of the complete system, then the error in T(s) may be as high as 0.20 at this particular spatial frequency. For the error $\delta T(s)$ to be reduced to about 0.01, the aberration introduced by the decollimator and magnifying system would need to be approximately $\lambda/50$. It is to be stressed that these values apply only in the case of a perfect test-lens. For a normal test-lens, the tolerance on the aberrations of the decollimator and magnifying system would not be as severe.

In practice, the decollimator and magnifying system are working on axis at very low apertures, so that the abberations introduced are negligibly small. This statement is verified by the fact that good agreement is obtained between theory and experiment when the test-lens is stopped

down to F/40 - it is then working as a perfect lens.

(6) Aberrations Introduced by Image Rotating Prisms.

The image rotating prisms in this instrument take the form shown in Figure 17. The primary spherical aberration introduced by such a prism is

$$|W_{40}| = \frac{1}{8}|S_I| = \frac{1}{8}\,\frac{(\mu^2 - 1)}{\mu^3}\,u^4 d$$

where μ = refractive index
d = thickness
u = ray angle

} Here the prism is considered equivalent to a plane parallel plate.

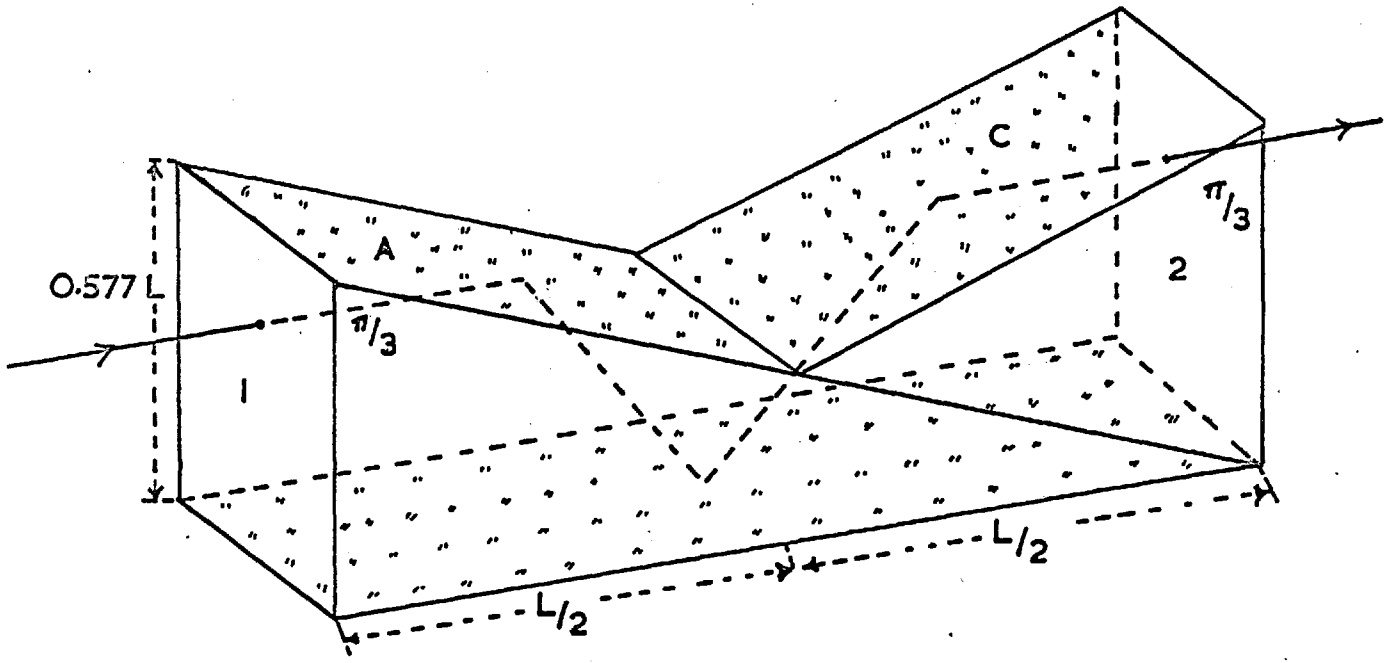
For $\mu = 1.5$ and $d = 7.5$ cm.

$$W_{40} \approx 0.3u^4$$

If the prism is working in parallel light

$$u = o \quad \text{and} \quad W_{40} = 0$$

If $u \neq o$, $W_{40} \neq o$, and a value of u may be found such that W_{40} is less than some specified value. For W_{40} to be less than $\lambda/50$, u must be less than 0.04. That is, the aperture ratio must be less than F/12. This tolerance is met in practice, since the prism in the object space works in parallel light, and the prism in the image space works at apertures less than F/50. For this reason, other types of aberration introduced by the prisms will be negligibly small.



Surfaces A, B, C, reflecting.
Surfaces 1, 2, transmiting.

Figure 17.

Of far greater importance, therefore, is the optical accuracy of the reflecting surfaces of the image rotating prisms. Over the aperture of these surfaces used, the flatness is better than $\lambda/20$.

The theory of operation of an image rotating prism is given in Appendix I.

(7) Aberrations Introduced by Parallel Plate Micrometer

As is shown in Appendix II, the expression for the lateral shift produced by a parallel plate micrometer is

$$\delta y = BC = t \sin I \left(1 - \frac{N \cos I}{N' \cos I'}\right)$$

and for small I, I'

$$\delta y = BC = t \sin I \left(1 - \frac{N}{N'}\right)$$

Now the aberrations (first order) introduced by a parallel plate are given by

$$S_I = -\left(\frac{\mu^2 - 1}{\mu^3}\right) t u_1^4$$

$$S_{II} = \left(\frac{\mu^2 - 1}{\mu^3}\right) t\theta u_1^3$$

$$S_{III} = -\left(\frac{\mu^2 - 1}{\mu^3}\right) t\theta^2 u_1^2$$

$$S_{IV} = 0$$

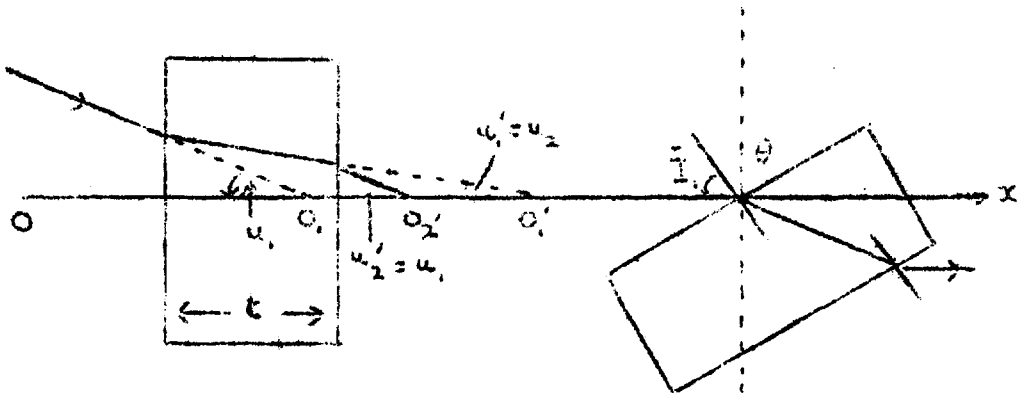
$$S_V = \left(\frac{\mu^2 - 1}{\mu^3}\right) t\theta^2 u_1$$

where μ = refractive index of plate

t = thickness of plate

u = angle between incident ray and axis ox

θ = angle of tilt of plate



The above formulae are obtained by substituting

$$u_{pr} = \theta$$

in the standard formulae for the aberrations of a parallel plate (see Wave Theory of Aberrations p.141). In the present case

$$t = 0.25'' \ , \quad \mu = 1.5 \ , \quad u_1 \approx 0.01$$

Thus

$$S_I = 1.67 \times 10^{-9} \ , \quad S_{II} = 1.67 \times 10^{-7}.\theta$$

$$S_{III} = 1.67 \times 10^{-5}.\theta^2, \quad S_V = 1.67 \times 10^{-3}.\theta^3$$

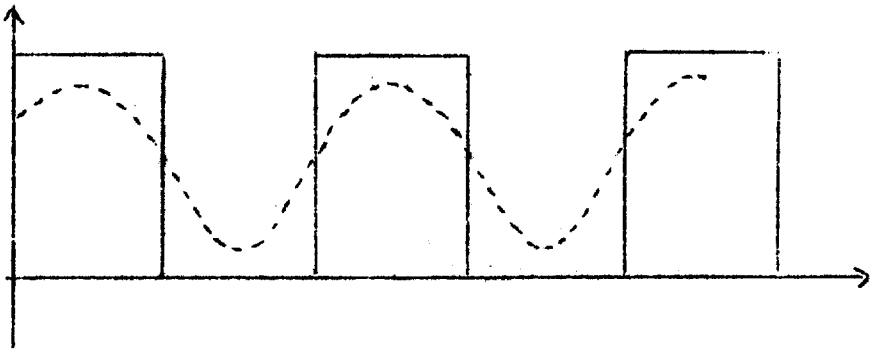
It may be seen that for any reasonable value of θ, the

aberrations introduced by the parallel plate are negligible.

(8) Effect of Position and Shape of Scanning Grating

In developing the above theory, it has been assumed that the spread function, scanning slits, and scanning grating all lie in the one plane. In practice this is not so, it being impossible to make the scanning slits and grating exactly coplanar.

If all three were exactly coplanar, the scanning grating would behave as a true rectangular grating as shown below (heavy line)



Due to defocussing effects however, the grating will behave as shown by the dotted line. There will, in general, be a reduction in contrast together with a small change in the D.C. level. The frequency content in the light output from such a defocussed grating will be the same, but will appear with reduced amplitude .

Using a cylindrical drum involves a further photometric factor due to the circular slit being further from the grating than the scanning slit. This is one reason why it is desirable to use two reference slits - the A.C. signal from the reference slits will then always be greater than that from the scanning slit.

(9) Influence of Circular Slit on Reference Signal:

Ideally, the reference slits should be parallel to the grating lines. However, as will be demonstrated below, the effect due to these slits being circular is negligible.

In a diffraction limited system, the diameter of the first Airy ring is given by

$$d' = \frac{1.22\lambda}{n'\sin\alpha'} = 2.44\lambda\ (\text{F/no.})$$

The spread function, even in badly corrected systems, will not in general exceed ten times this diameter, that is

$$(d')_{S/F} \leqslant 25\lambda\ (\text{F/no.})$$

Taking $\lambda = 5.5 \times 10^{-4}$ mm. and $(\text{F/no.})_{max.} = 200$,

$$\{(d')_{S/F}\}_{max.} \leqslant 2.5 \text{ mm.}$$

If the diameter of the circular slit is taken to be 12.7 mm., then the sagitta for an aperture of 2.5 mm. is approximately 0.05 mm. If the scanning grating has 4 lines

per millimetre on it, this sagitta is 20% of the grating period. Hence the reference light flux from one slit will contain frequency dependent terms in addition to the zero frequency term. That is

$$(\text{Flux})_{\text{Ref.1}} = \frac{B}{2} \cos \omega t + B_1 \cos(\omega t + \theta_1) + B_2 \cos(\omega t + \theta_2) + \ldots$$

If now the diameter of the circular slit is arranged to be an integral number of grating periods, the light flux from the other reference slit will be

$$(\text{Flux})_{\text{Ref.2}} = \frac{B}{2} \cos \omega t + B_1 \cos(\omega t + \theta_1 + \pi) + B_2 \cos(\omega t + \theta_2 + \pi) + \ldots$$

The total A.C. light flux from the two reference slits is, then,

$$(\text{Flux})_{\text{Ref.1,2}} = \frac{B}{2} \cos \omega t + B_1 \cos(\omega t + \theta_1) + B_2 \cos(\omega t + \theta_2) + \ldots + \frac{B}{2} \cos \omega t - B_1 \cos(\omega t + \theta_1) - B_2 \cos(\omega t + \theta_2) + \ldots$$

or $(\text{Flux})_{\text{Ref.1,2}} = B \cos \omega t.$

Hence, any effects due to the reference slits being circular and not rectangular are cancelled out. This is the second, and most important, reason for employing two reference slits.

(10) Tolerance on Calibration of Density Wedges:

The density wedges are employed to attenuate the reference signals until the A.C. component of their sum is equal to that of the scanning signal. If A(s) is the attentuation coefficient of the wedges, then effectively

$$A(s) = k\left\{\frac{T(s')}{T(0)}\right\} = k\left\{\text{Contrast Transfer Function}\right\}$$

where $k \simeq 1$

Hence $$\delta A \simeq \delta\left\{\frac{T(s)}{T(0)}\right\}$$

For a 2% accuracy in $\frac{T(s)}{T(0)}$, we must have the value of A accurate to 2%.

Now the density D of the wedges is given by

$$D = -\log_{10} A$$

or

$$A = 10^{-D}$$

Differentiation of this relation gives

$$\delta A = -2.302485A\ \delta D$$

For $\delta A = 0.02$, $A = 1$, $|\delta D| = 0.008$

That is, for a 2% accuracy in the contrast transfer function, the density of the wedges must be known with an accuracy of 0.008 units.

If circular wedges are used, with a linear density range 0→2.0, then

$$D = 0.00575\psi$$

where ψ degrees is the angle through which the wedges are totated. Thus the above tolerance may be achieved if the angle ψ can be set to within one degree.

(11) The A.C. Components of the Signals Fed to the Photomultiplier:

Referring to expression (17), the A.C. signal fed to the photomultiplier from the scanning slit is

$$2|j_1|.K.\frac{\sin\left(\frac{\pi s_o b}{\cos\varphi}\right)}{(\pi s_o)}.\frac{\sin(\pi sd)}{(\pi s)}.g(0).T(s)$$

$$.\cos\{2\pi\gamma s_o t + \beta_1 + \theta(s)\}$$

while the A.C. signal from the reference slits is

$$4|j_1|.K.d.\frac{\sin(\pi s_o b)}{(\pi s_o)}.g(0).T(0).\cos\{2\pi\gamma s_o t + \beta_1\}$$

The signal from the scanning slit is first phase shifted using the parallel plate micrometer until its phase relative to that of the reference signal is equal to π. The shift of the parallel plate micrometer required for this is given by

$$\pi - \theta(s) = -2\pi R \tan\varphi\ \delta\xi'$$

where R tan φ is the number of lines per inch in the image plane, and $\delta\xi'$ inches is the lateral shift of the image produced by the micrometer.

The two reference signals are then each attenuated by an amount A(s) to prduce zero A.C. output. For exactly zero output, the value of A(s) is

$$2A(s)_{Bal.} = \frac{\sin(\pi sd)}{(\pi sd)} \cdot \frac{\sin\left(\frac{\pi s_o b}{\cos\varphi}\right)}{\sin\left(\pi s_o b\right)} \cdot \frac{T(s)}{T(o)}$$

But, A(s) is a function of the density of the attenuating wedges; that is

$$A(s) = 10^{-D} = 10^{-0.00575\,\psi}$$

where $D = 0.00575\,\psi$ is the relation between density D and angle of rotation ψ of the wedges.

Thus

$$\frac{T(s)}{T(0)} = 2\left\{10^{-0.00575\,\psi}\right\} \cdot \frac{\sin(\pi s_o b)}{\sin\left(\frac{\pi s_o b}{\cos\varphi}\right)} \cdot \frac{(\pi sd)}{\sin(\pi sd)} \qquad (27)$$

(27) then gives the value of $\frac{T(s)}{T(0)}$ as a function of spatial frequency s, and the angle of rotation ψ of the density wedges.

References.

Hopkins, H.H. - Proc. Phys. Soc. 1962, Vol.79. P.889.

Birch, K.G. - Proc. Phys. Soc. 1961, Vol.77. P.901.

Mandl, L. - Progress in Optics, Vol.II. P.183.

Hopkins, H.H. - The Wave Theory of Aberrations (Clarendon 1950).

CHAPTER VI.

A Detailed Description of The Apparatus Construction.

(1) Introduction:

This chapter describes in detail the apparatus used for the measurement of optical transfer functions. Referring to Figure 10, each component will be discussed separately, working from left to right.

(2) General Remarks:

In designing the apparatus, five main points were taken into account. These were

(a) Availability of a 115" focal length decollimator and a 20" test lens initially.

(b) Availability of a scanning drum of frequency 100 lines per inch.

(c) Magnification through the complete system must be such that (i) a reasonable range of spatial frequencies in the object space may be obtained; (ii) the slit sizes are near those required to optimise the signal to noise ratio.

(d) Mechanical tolerances required on various components are not too severe.

(e) Minimum amount of optics so as to eliminate possible errors in the obtained measurements.

With these points in mind, an initial layout was obtained as shown in Figure 18(a).

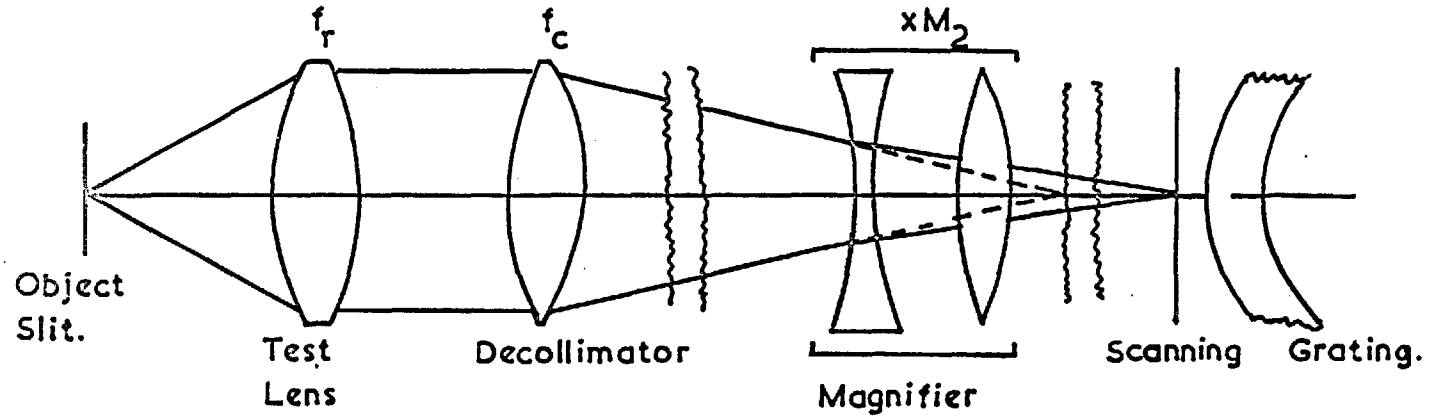
To be able to use the test lens at near its resolution limit, it is desirable that the object slit has a width less than this limit. Figure 18(b) shows the resolution limits at various apertures, and it may be seen that very narrow slits are required. (Ideally, the slits should have a width of about one quarter the resolution limit.) To eliminate the need for a reducing system here, it was decided to use an available slit width and adjust the aperture of the test lens accordingly. Should the lens be tested at higher apertures, the corresponding range of spatial frequencies would be reduced.

Another factor involved is that it was considered advisable to check the operation of the apparatus initially with the test lens working paraxially. Under these conditions the lens could be considered as diffraction limited. Taking these thoughts into consideration, it was decided to test the lens initially at F/40 using a 7.5 micron object slit, and to design the apparatus to suit these figures.

It has been shown that, for maximum signal to noise ratio, the width of the image of the object slit should be 0.372 that of the scanning grating period. Thus for a grating period of 0.01", the width of the imaging slit should be

$$D = 0.00372"$$

(a)



Total Magnification. $= M_2 \left(f_c / f_r\right)$

(b)

$\lambda = 5461\ \mathring{A}$.

Aperture. $F/_{No.}$	40	20	10	5	2·5	1·25
Resolution Limit (μ)	21·8	10·9	5·45	2·72	1·36	0·68.

Figure 18.

Also, using the same criterion, the width of the scanning slit should be

$$B = 0.00262".$$

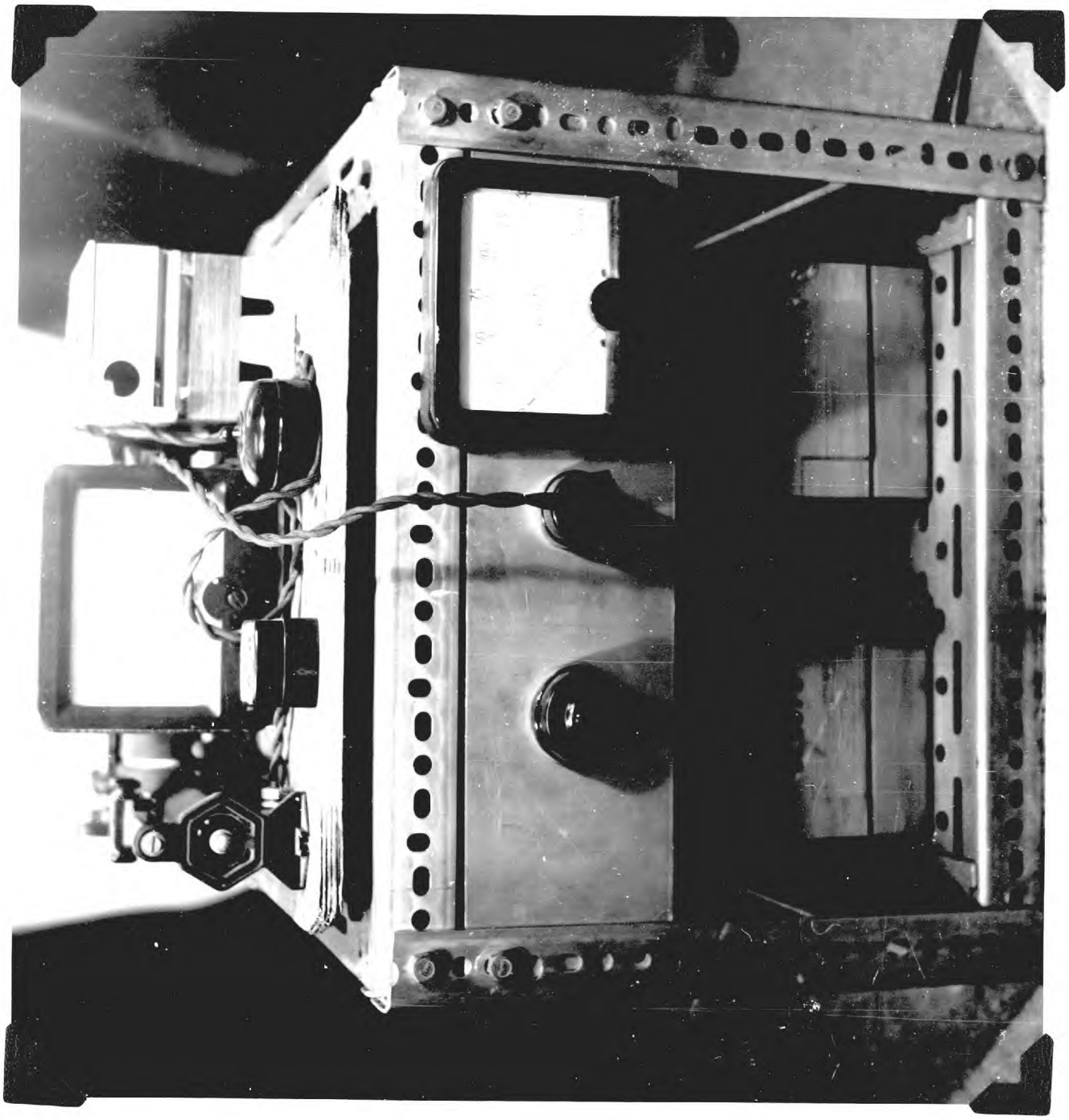
The value D = 0.00372" means that the total magnification required in the optical train is × 12. The magnification produced by the test lens and decollimator combination is approximately × 6, so that an auxiliary system having a magnification of × 2 is required.

With these general remarks, we may proceed to describe each component in detail.

(3) Illuminating System:

It is essential that the object slit be illuminated incoherently. This requires the aperture of the condensing system to exceed that of the test lens, and that the light be provided by a thermal source. Also, the object slit must be able to rotate so that measurements for different azimuths may be made.

The layout of components in the illuminating system is shown in Figure 19. The light source is a standard Philips medium pressure merucry arc source rated at 125 watts with the pearl glass envelope removed. The source supply is obtained from a Westat constant D.C. output unit. The current drawn by the source is regulated by means of series resistances, and is maintained at about 0.7 amps. The output voltage from the supply is 180 volts. The



POWER SUPPLY FOR LIGHT SOURCE

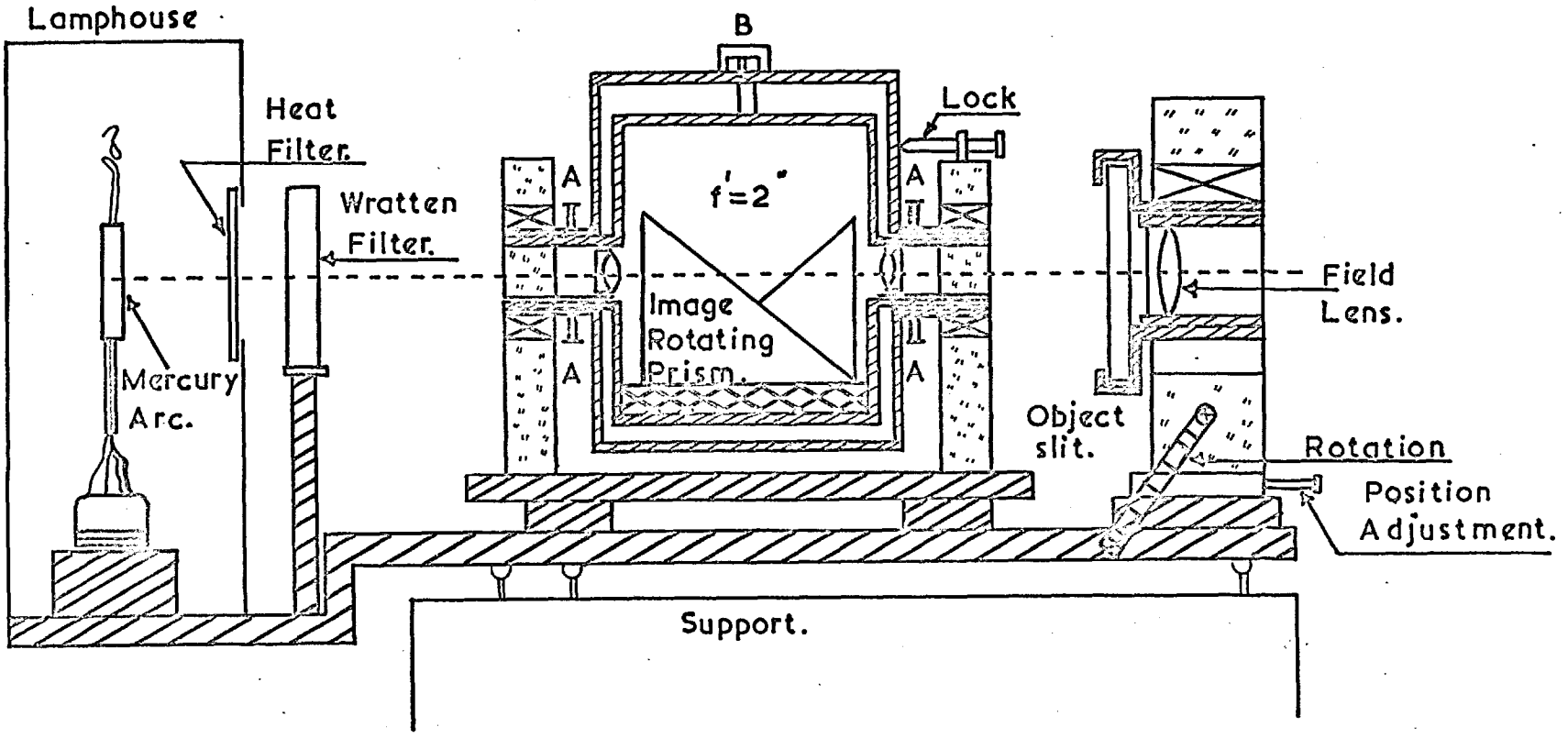
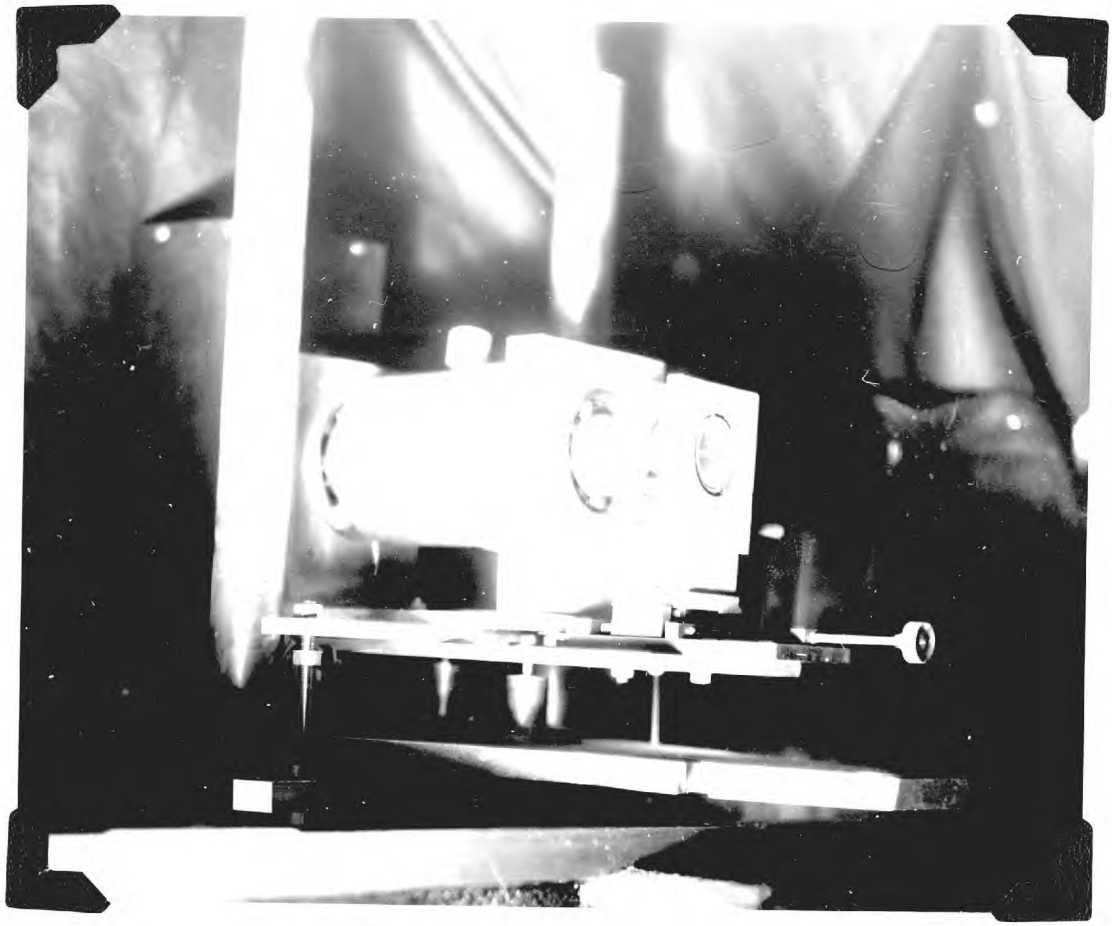

Lamphouse
Heat
Filter.
Wratten
Filter.
Mercury
Arc.
B
Lock
A
A
f'=2"
Image
Rotating
Prism.
A
A
Field
Lens.
Object
slit.
Rotation
Position
Adjustment.
Support.

Figure 19.



ILLUMINATING SYSTEM

mercury arc is enclosed in a lamp house to eliminate stray light. A heat filter is included to minimise the risk of damage to the Wratten filter, which is next to the lamp house. The Wratten filter is a gelatin type 77, which isolates the 5461A$^{\circ}$ line of the mercury spectrum. The characteristics of this filter are shown in Figure 20.

Following the lamp house and filter assembly is the condensing system. This consists essentially of two doublet lenses, each of focal length 2". The first doublet collimates the mercury arc source, and the second acts as a decollimator, the arc being brought to a focus in the plane of the object slit. Between the two doublets is placed an image rotating prism, thus enabling the image of the arc source to be made to coincide with the object slit. This makes possible uniform illumination of the object slit for any azimuthal setting.

The image rotating prism is mounted inside a duralium cylinder, whose position relative to an outer cylinder (also duralium) is controlled by the four adjusting screws A and the spring loaded plunger B. (see Figure 19). The outer cylinder is mounted in good quality ball bearings. With this arrangement it is possible to adjust the image rotating prism so that when the outer cylinder is rotated, the motion of the arc image is purely rotational, with no lateral shift from the optical axis. (See Appendix I for the operation of the image rotating prism.)

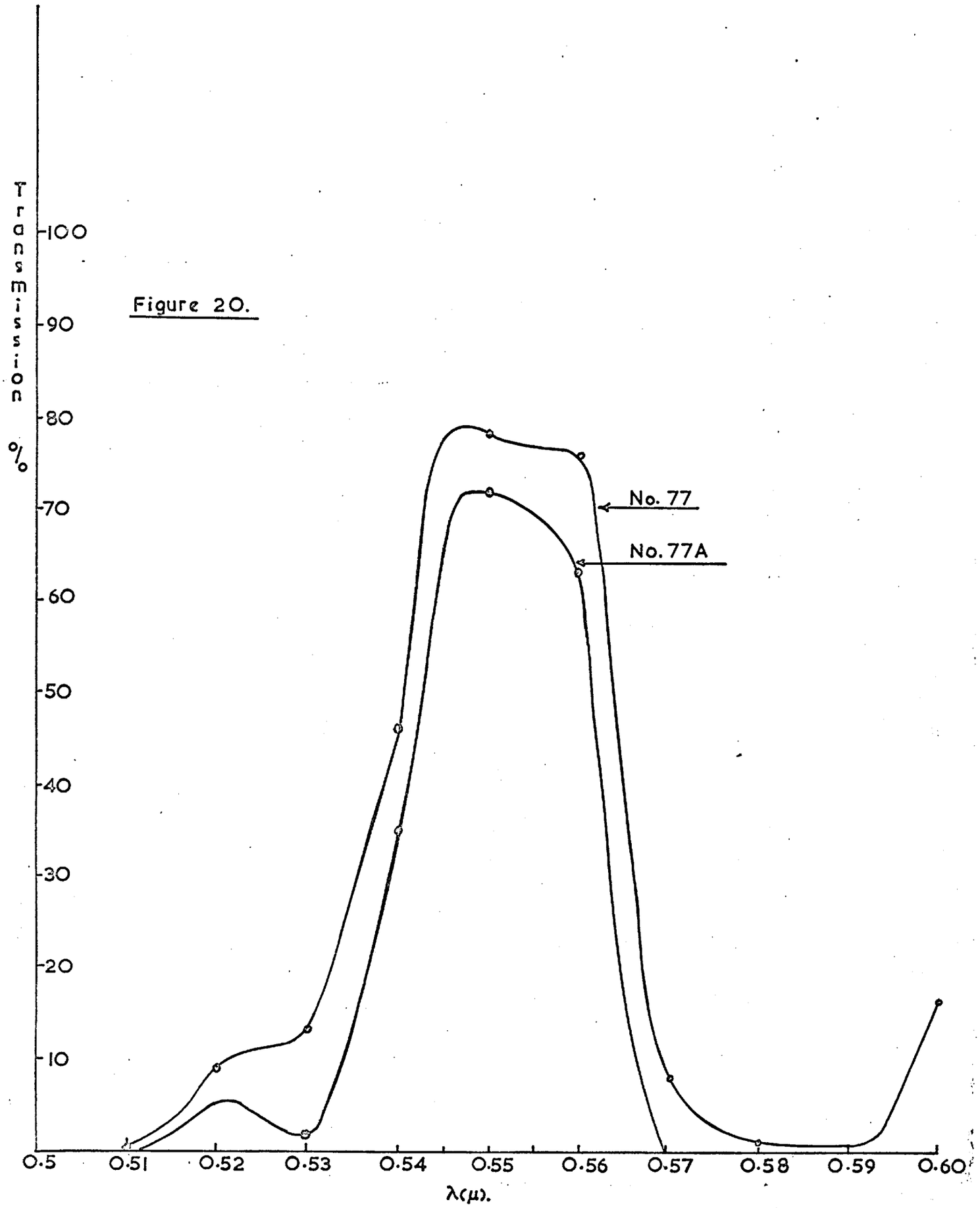

Transmission %
100
90
80
70
60
50
40
30
20
10
No. 77
No. 77A
0·5
0·51
0·52
0·53
0·54
0·55
0·56
0·57
0·58
0·59
0·60
λ(μ).

Figure 20.

The aperture of the condensing system is chosen to be F/5 so that incoherent illumination is ensured. With 2" focal length lenses, this means the clear aperture of the image rotating prism and the lenses must be at least 0.4". This requirement determines the physical dimensions of the prism needed. The value obtained for the minimum prism length is 2.1". The actual prism used has a length of 2.55", and is made with glass of refractive index n_e = 1.51738.

The 2" focal length condensing lenses are fitted in mounts which slide along the inner cylinder. Their position is adjusted to leave a minimum air gap between them and the image rotating prism. As each doublet is separately corrected for working with one infinite conjugate, the resulting aberration function will contain only astigmatic terms, and at F/5 these are not serious. (Note the image rotating prism is working in parallel light so that no aberrations are introduced here).

The object slit is supported in a bearing which may be rotated by means of a worm-drive, thus allowing the slit to be set in various azimuths. The slit itself is ruled on a chrome plated class disc about $\frac{1}{8}$" thick. A second disc of glass is cemented to the first to protect the slit. The length of the slit is 1 cm.

Some difficulty was experienced in determining the width of the object slit, due to the thickness ($\frac{1}{8}$") of the glass discs. No direct measurement, using a high power microscope, was possible as the working distance of such an instrument is less than $\frac{1}{8}$". Two other methods were employed, namely a projection method and a measurement of the diffraction pattern produced by the slit.

In the first method, an image of the slit produced by a lower power microscope was projected onto a screen. The size of the image projected depends on the distance from the microscope eyepiece. Having selected a suitable distance, the slit being measured was replaced by a calibrated graticule and the image size again measured. The width of the slit is then given by

$$\text{Slit width} = (\text{Size of graticule spacings}) \Big/ \left(\frac{\text{Graticule Image Size}}{\text{Slit Image Size}}\right)$$

The second method involved measuring the Fraunhofer diffraction pattern produced by the slit. The slit was illuminated with collimated light (λ = 5461 A°) and the diffraction image formed using a corrected 2" focal length lens. The image was recorded photographically, and measured with a travelling microscope. To check the calibration of the system, the diffraction pattern of a slit of known width was also measured.

Both methods gave good agreement for the value of the slit width, the former 7.44 μ, and the latter 7.48 μ. This second measurement was considered to be more accurate than the other, as a larger number of readings was obtained. The size of the object slit was, then, taken to be

$$7.48\ \mu\ .$$

No non-uniformity of intensity in the diffraction lines was observed, so that the parallelism of the object slit is assumed to be within the toleranced value (see Chapter V Section (4)).

Mounted as close as possible to the object slit is a field lens of focal length of 2.25 inches. The function of this lens is to image the pupil of the condensing system into the entrance pupil of the lens under test. The field lens is also a corrected doublet.

The assembly containing the object slit and field lens has provisions for both lateral and longitudinal movements, thus permitting accurate alignment of the optical axis. The longitudinal movement may be set with an accuracy of bettern than 0.001". The image rotating prism assembly and the lamp house may be moved independently of the slit assembly, so that maximum illumination of the object slit may be obtained without altering the position of the object slit itself.

The entire illuminating system is supported on a table attached to the optical bench, and may be moved vertically relative to the bench. This enables correct height adjustments to be made.

(4) Test Lens and Nodal Slide:

As mentioned previously, the first test lens has a focal length of 20". This lens is a wartime aerial survey lens, and has the following design parameters:-

Surface	Curvature In^{-1}	Thickness In	N_e	$N_{e'}$
1	.196502	.6080	1.0	1.61509
2	.049652	.5140	1.61509	1.0
3	.126295	.1760	1.0	1.57217
4	.126295	.2055	1.57217	1.0
5	.00 (stop)	.2055	1.0	1.0
6	.115848	.1736	1.0	1.55414
7	.131130	.5680	1.55414	1.0
8	.054466	.4880	1.0	1.61509
9	.197941		1.61509	1.0

Equivalent Focal Length = 19.786"
Back Focal Length = 18.473"
} Maximum Aperture F/5.6

The lens is mounted on a nodal slide so that off axis measurements may be made. The nodal slide and accompanying oprical bench are supported on heavy steel girders, the girders themselves resting on a thick layer of foam rubber. In this way, any vibrations due to movements of the building are minimised, and no effects due to vibrations have been detected in practice. The total weight of the nodal slide test bench is estimated to be about one ton.

The test lens may be rotated in its mount on the nodal slide, and this facility is used to determine approximately the correct height of the optical axis. The exact position of the test lens is determined by a micrometer screw/dial gauge combination attached to the bench.

(5) Decollimator:

The decollimator lens has a focal length of 115 inches and a diameter of 8". It is a triplet type objective with small air spaces between components. Its state of correction was judged by examining qualitatively the interferogram produced by it in a common path interferometer. There appeared to be negligible spherical aberration and about $\frac{1}{10}$ wavelength of coma present at full aperture (F/14.5). As the decollimator is always used at much lower apertures, this amount of aberration is insignificant. (Should the aberration not be insignificant, this would appear as a discrepancy in the measured results. No such discrepancy has been observed.)



TEST-LENS MOUNT, NODAL SLIDE, & DECOLLIMATOR

The decollimator is mounted on a fixed support attached to the end of the nodal slide bench. Adjustments to position are achieved by means of three levelling screws 120 degrees apart.

(6) Magnifying System:

This is to be a x 2 system working at a maximum aperture of F/28. The requirements for this system are

(i) Aberrations introduced are negligible

(ii) Distance from final image plane sufficient to allow room for an image rotating prism and a parallel plate micrometer.

The detailed design of the system is given in Appendix III, but the final parameters are as below:-

Surface	1	2	3	4
Radius (In.)	11.8565	3.9515	−8.9977	−5.0489
Thickness (In.)	0.10	9.925	0.25	
N_e	1.0	1.5094	1.0	1.5152
N_e'	1.5094	1.0	1.5152	1.0

Object distance = 11"

Image Distance = 20"

The aberrations of the system may be written in the form

$$W(r,\varphi) = {}_0W_{40}r^4 + {}_1W_{31}\,\tau\, r^3\cos\varphi + {}_2W_{20}\,\tau^2r^2 + {}_2W_{22}\,\tau^2r^2\cos^2\varphi + {}_3W_{11}\,\tau^3 r\cos\varphi$$

where $_0W_{40} = \frac{1}{8} S_I$, $_1W_{31} = \frac{1}{2} S_{II}$, $_2W_{20} = \frac{1}{4}\{S_{III} + S_{IV}\}$,

$_2W_{22} = \frac{1}{2} S_{III}$, $_3W_{11} = \frac{1}{2} S_V$

and S_I, S_{II}, S_{III}, S_{IV}, S_V are the Seidel aberration coefficients.

The resultant aberrations of the magnifying system are

$$S_I = 0.000210, \quad S_{II} = 0.086551, \quad S_{III} = 0.546811$$

$$S_{IV} = 0.290840 \qquad S_V = 5.493466$$

At F/28, the total aberration present is completely negligible.

The components of the magnifying system are mounted on a small auxiliary optical bench placed so that the back component is about 20" from the desired final image position. Provisions are made for adjusting precisely the position of these components.

(7) Image Rotating Prism: This is of the same form as in the illuminating system, but of slightly smaller dimensions, the base length being 1.852". The prism is mounted in a similar way to the one in the illuminating system, but here more precision is desirable. When aligned to the optical axis by means of the adjusting screws, on rotating the prism the axis does not shift more than 10^{-4} inches from its mean position. This figure is determined by passing near-collimated light rhough the prism and observing the movement of a pair of

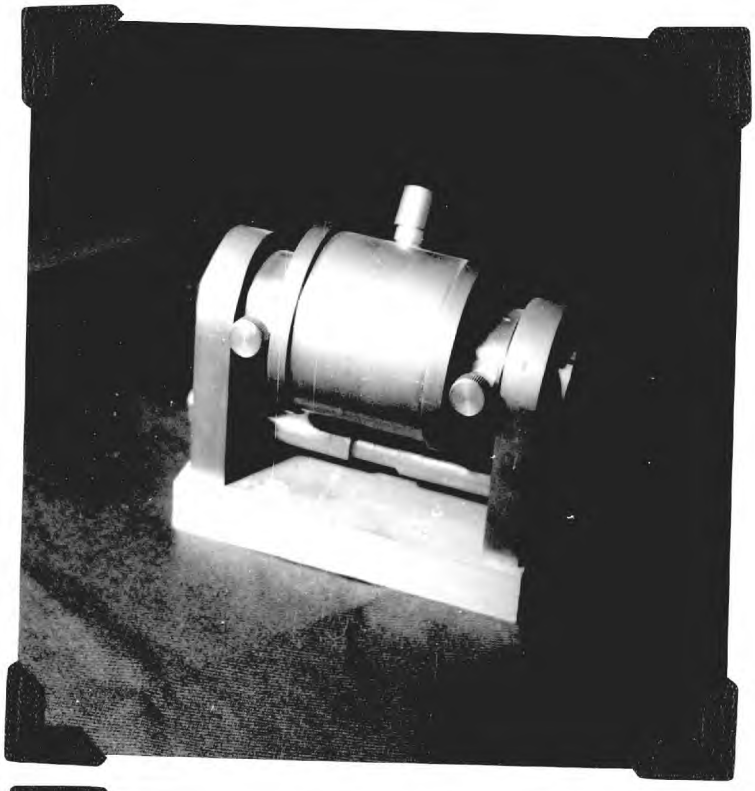
cross-wires as the prism is rotated.

The tolerance of 10^{-4} inches on the shift of the optical axis was originally determined by the fact that phase measurements were required to an accuracy of $\pm 1\%$. This was assuming that the spread function was to be rotated for each spatial frequency. However, as the spread function is fixed in orientation relative to the scanning drum for each azimuthal setting of the object slit, this tolerance may be relaxed somewhat. All that is required is that the image rotating prism rotates the spread function to be normal to the lines of the scanning drum in such a way that the illumination remains constant across the diameter of the circular slit. As the physical length of the spread function exceeds 5 cm., this is no problem. Any lateral shift of the spread function due to rotation of the prism may be corrected by initially readjusting the zero phase setting. The accompanying photograph shows the mounting of the image rotating prism.

(8) Parallel Plate Micrometer:

The accuracy required for phase measurements is $\pm 1\%$. For a grating period of 0.01", this means that the lateral shift of the spread function must be known to 10^{-4} inches. Hence a parallel plate micrometer calibrated to this accuracy must be obtained.

A modified version of the Hilger and Watts standard 1" parallel plate micrometer was obtained. The modifications



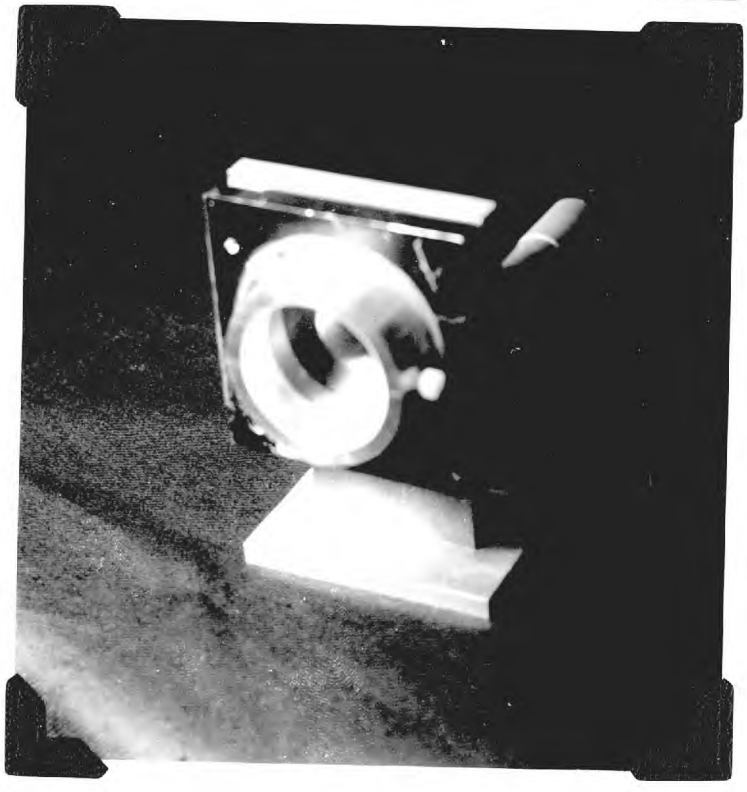


IMAGE ROTATING PRISM MOUNT & PARALLEL PLATE MICROMETER

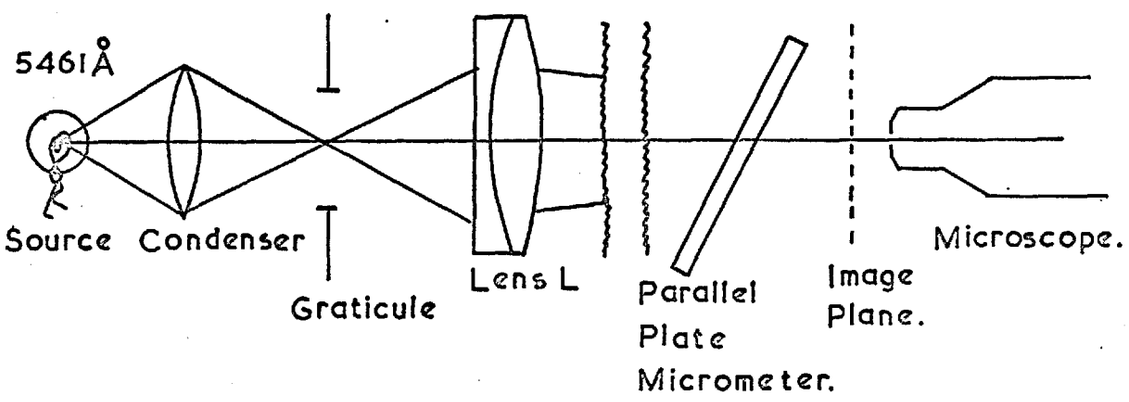
consisted of altering the parallel plate to be 0.25" thich and correspondingly altering the calibration. This is specified in terms of the lateral shift of the image, and is recorded on a micrometer screw head which actuates the parallel plate. The range of shift possible with this parallel plate is 0-0.020 inches the graduation on the scale being in steps of 10^{-4} inches.

For small values of φ, the angle through which the scanning slit is rotated, the effective period of the scanning grating exceeds 0.020". For example, if φ is $(\pi/18)$, the effective grating period is increased by cosec $(\pi/18)$, so that for a grating of 100 lines per inch, the effective period becomes 0.0575". If there is no phase term present in the transfer function, then the lateral shift required to obtain a minimum signal is 0.0288". This is beyond the range of the parallel plate micrometer, and therefore erroneous values will be obtained for the modulus of the transfer function.

To overcome this difficulty, a second parallel plate micrometer was made with a plate about 1" thick. This is shown in the accompanying photograph. The setting is again achieved by using a micrometer screw.

To calibrate the parallel plate micrometers, an arrangement as shown in Figure 21(a) is used. A graticule containing a pair of cross-wires is illuminated by light of wavelength 5461 A°. The image of this graticule produced

(a)



(b)

"Mic. Setting."	"Image Shift."
0.0	0.0
0.0005	0.0005
0.0010	0.0010
0.0015	0.0015
0.0020	0.0021
0.0030	0.0030
0.0040	0.0039
0.0050	0.0049
0.0060	0.0060
0.0070	0.0070
0.0080	0.0081
0.0090	0.0091
0.0100	0.0102
0.0110	0.0111
0.0120	0.0123
0.0130	0.0132
0.0140	0.0141
0.0150	0.0152
0.0160	0.0164
0.0180	0.0183
0.0200	0.0204

(c)

"Mic Setting mm"	"Image Shift."
0.0	0.0
0.25	0.0079
0.50	0.0162
0.75	0.0236
1.0	0.0312
1.25	0.0395
1.50	0.0477
1.75	0.0554
2.00	0.0632
2.25	0.0711
2.50	0.0789
2.75	0.0872
3.00	0.0952

Figure 21

by lens L is observed with a microscope and micrometer eyepiece, the light first passing through the parallel plate micrometers. The aperture of the converging beam is arranged to be near that used in practice. The microscope itself was calibrated using a graticule with known line spacings on it.

Figures 21(b) and (c) show tables giving the mean image shift produced by each parallel plate micrometer as a function of the movement of the micrometer screws. Figure 22 shows graphically these calibrations. In both cases the curves are very nearly straight lines. For curve (b) the maximum error involved in assuming the curve to be a straight line of slope 1.1 is 1% except for the encircled region where the error is 3%. For curve (c) the slope is taken to be 0.0313 in./mm., and the maximum error is less than 1%. Hence, for all practical purposes we take

(b) (Image shift)" = 1.1 (Scale reading)"

(c) (Image Shift)" = 0.0313 (Scale reading)mm.

noting tha (b) does not hold for scale readings between 0.0045" and 0.0055". (In practice, this range is used infrequently.)

(9) Scanning and Reference Slits:

As mentioned previously, these are respectively a rectangular slit and a circular slit. They are ruled in a chrome film on a glass disc $\frac{1}{8}$" thick, and have the following

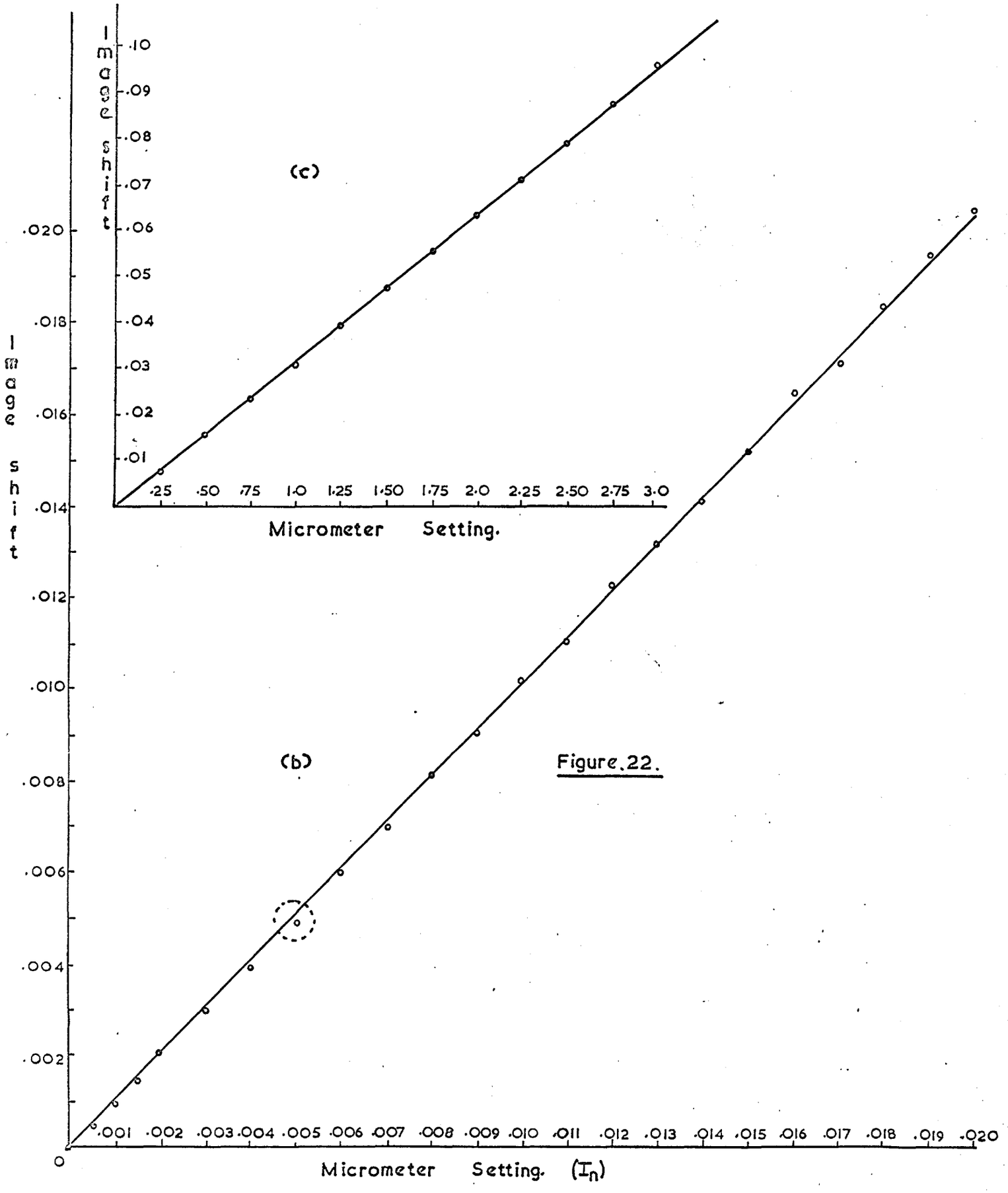

Image shift
.10
.09
.08
.07
.06
.05
.04
.03
.02
.01
(c)
.25 .50 .75 1.0 1.25 1.50 1.75 2.0 2.25 2.50 2.75 3.0
Micrometer Setting.
Image shift
.020
.018
.016
.014
.012
.010
.008
.006
.004
.002
0
(b)
.001 .002 .003 .004 .005 .006 .007 .008 .009 .010 .011 .012 .013 .014 .015 .016 .017 .018 .019 .020
Micrometer Setting. (In)

Figure.22.

specifications:-

Width of Rectangular Slit = 0.003"

Width of Circular Slit = 0.003"

Length of Rectangular Slit = 0.330"

Mean Diameter of Circular Slit = 0.500"

These dimensions were determined using a high power (× 80) microscope. They satisfy the following requirements:

(a) Slit widths correct for optimum signal to noise ratio (Theory predicts optimum width of 0.0026").

(b) Length of scanning slit greatly exceeds the lateral dimension of the spread function. At F/400, the maximum width of the spread function does not exceed 0.20", even in the presence of very large aberrations.

(c) Diameter of the circular slit is such that uniform illumination of the spread function is ensured across this diameter. With a diameter of 0.5" and a total magnification of about 12 through the system, only 0.04" of the object slit is being used.

The mounting of the graticule containing the slits has the tightest tolerance of any component in the whole instrument. In order to maintain a 1% accuracy in phase, the graticule must be able to rotate about its centre with an accuracy of 1% of the grating period, that is to within 10^{-4} inches. To this end a special bearing was constructed and this is illustrated in Figure 23. The bearing is of the

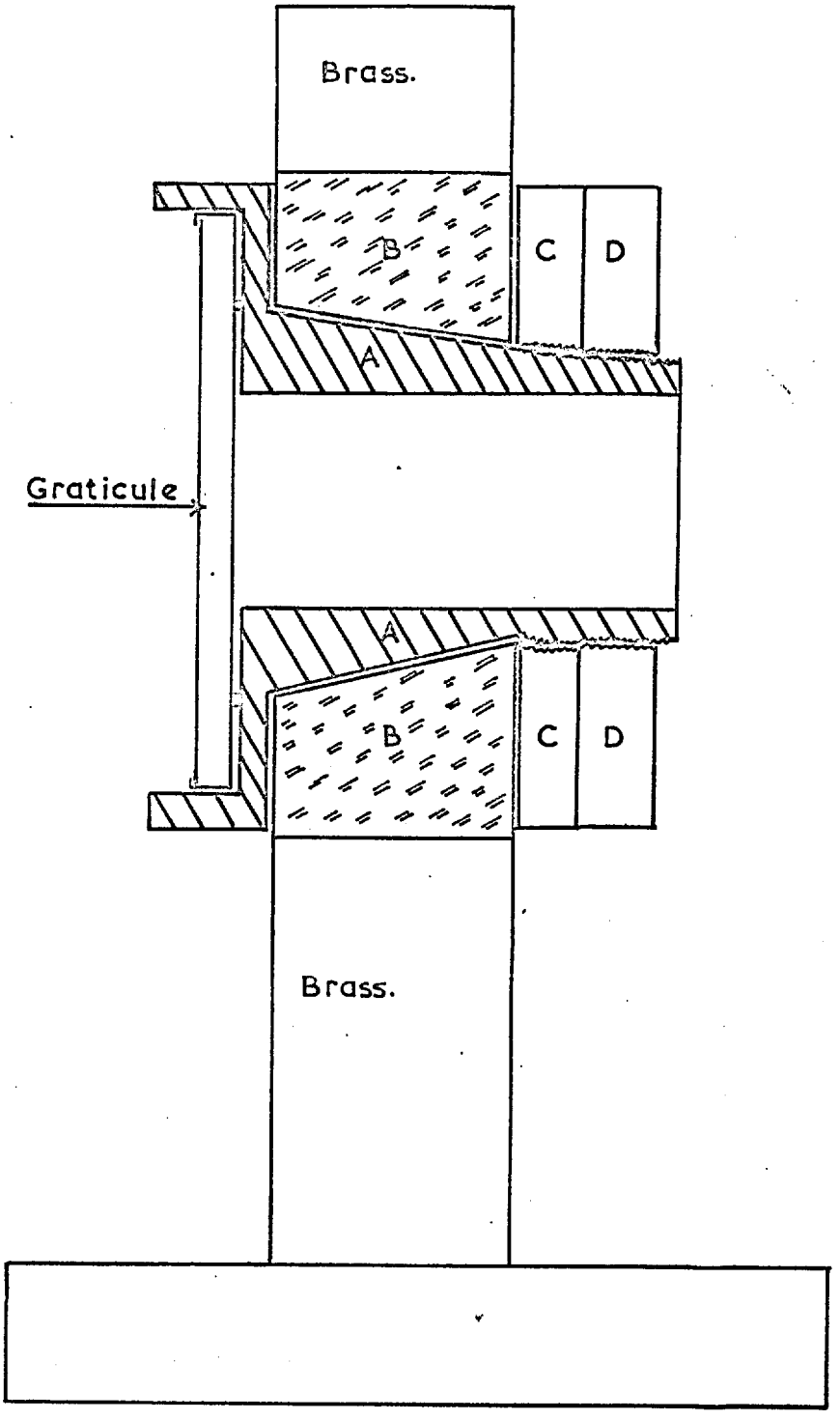


Figure 23

taper type, with a taper angle of about three degrees. The shaft A is made of hardened steel, and the seating B is a softer lead-like material. The rear end of the steel shaft has a 20 threads per inch screw cut on it, and is held firmly in the seating by means of a brass locking nut C. A second nut D is included to prevent C from loosening. As the soft seating B wears, nuts C and D may be tightened to remove any slackness which may develop.

Space is provided in the steel shaft for inserting the graticule containing the slits. This space has a diameter slightly larger than the diameter of the graticule to allow for any errors in centring the slits on the graticule. Using a high power (× 80) microscope, the movement of the slits on rotating the bearing shaft could be noted. The position of the graticule was adjusted until the shift of the edges of the circular slit was less than 10^{-4} inches. The movement of the rectangular slit was then checked and found to be central. The final decentring error of the slits was better than 6×10^{-5} inches over a complete revolution of the graticule. The graticule was then firmly fixed in place with a mixture of beeswax and resin, and checked for any accidental movement.

(10) Scanning Drum and Grating:

The scanning drum is a glass cylinder of diameter 3.55" and width 1.125". The wall thickness is approximately

0.25", and the glass is of good optical quality, so that transmission through it may be considered uniform over the entire circumference.

The grating is a square wave grating and takes the form of a photographic film wrapped around the inside circumference of the drum. The film has lines printed on it with a frequency of 100 lines per inch, and a mark to space ratio of 1:1. (This is contrary to the theoretical value of 4:9 predicted for maximum signal to noise ratio, but due to availability, a grating with a mark to space ratio of 1:1 was used.) The film was produced by contact printing a master grating.

With a grating frequency of 100 lines per inch, the number of periods around the circumference of the drum exceeds 1,200. Hence, the effect of mis-match at the join in the film is negligible, since the width of the join is of the order of one period. Any non-negligible effect could, however, be filtered out in the electronic circuitry later.

The scanning drum is driven at constant speed by a synchronous motor coupled to the drum through a 1:6 reduction gear box. The motor is connected to the gear box by means of a rubber shaft which helps to minimise any vibrations present. For a motor speed of 1500 r.p.m., the rate of rotation of the scanning drum is 250 r.p.m. The A.C. carrier frequency generated is given by

$\nu = (\gamma/p)$ c/s where γ is speed (ins.sec^{-1})

p is grating period (in)

or

$\nu = 2\pi\sigma\, r/60p$ where σ is the number of r.p.m.

r is the drum radius

For σ = 250 r.p.m., 2r = 3.55", p = 0.01" ,

ν = 4,648 c/s.

This, then, is the frequency at which signals will be detected, and standard audio amplifier and detector circuits may be used with no difficulty. It is important to note that this frequency is no multiple of the mains 50 c/s. frequency, so that mains interference is automatically eliminated. The frequency is also sufficiently high to avoid excessive bulkiness of the electronic components required for frequency selective devices.

(11) Post Drum Optics: The layout of components following the scanning drum is illustrated in Figure 24, where a plan view is shown.

Immediately following the drum is a 45° prism which deviates the light beams by 90° in order to make them accessible. The prism has a base length of 0.8" so that the equivalent air path through the prism is 0.533" (refractive index 1.5). The prism is mounted on an adjustable support so that the deviated optical axis may be

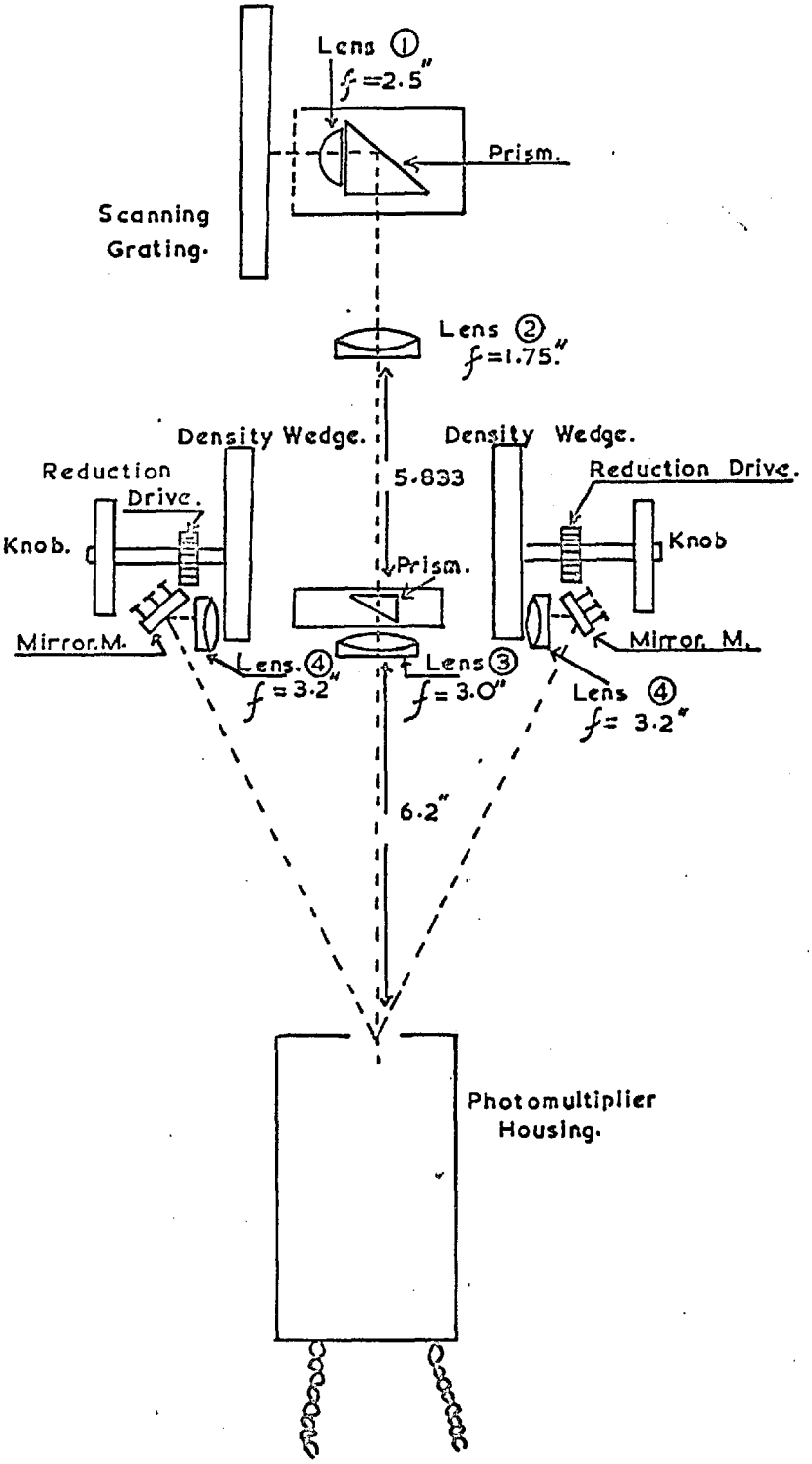

Lens ①
f=2.5"
Prism.
Scanning
Grating.
Lens ②
f=1.75"
Density Wedge.
Density Wedge.
Reduction
Drive.
5.833
Reduction Drive.
Knob.
Prism.
Knob
Mirror M.
Lens ④
f=3.2"
Lens ③
f=3.0"
Mirror M.
Lens ④
f=3.2"
6.2"
Photomultiplier
Housing.

Figure. 24.

made truly horizontal.

Cemented to the front face of the prism is a plano-convex lens (1) of focal length 2.5". The purpose of this lens is to image the decollimator pupil into the pupil of lens (2). As the decollimator pupil may be considered to be at infinity, the pupil image will be formed approximately 2" behind the rear face of the prism.

Lens (2) is used to form an image of the circular and rectangular slits. The size of this image must be such that the light from the parts of the circular slit acting as reference slits may be tapped off without interfering with the light from the scanning slit. Also, mechanical problems must be taken into account here. Referring to the dimensions of the rectangular and circular slits, it seemed desirable to have a magnification of about × 2.5. The length of the rectangular slit would then be 0.825, and the diameter of the circular slit would be 1.25". For an object distance of 2.5", this means that lens (2) must have a focal length of 1.79", and that the image distance is 6.25". In practice, a lens of focal length 1.75" is used, giving an image distance of 5.833" and a magnification of × 2.33. With these final parameters, the diameter in the image of the circular slit is 1.165", and the length of the image of the rectangular slit is 0.777".

Lens (2) is a corrected doublet and is held in a mount which fits in a threaded support, thus producing a focussing control.

In front of lens (3) two small prisms of $\frac{1}{4}$" face are placed to deflect the light from the reference slits onto the density wedges. The prisms are fixed, on one edge to a plane parallel glass plate which acts as a support, one prism fixed to the top, and one to the bottom. The outer edges of the prisms are fixed to small metal rods which are attached to a mounting framework. The width of the parallel plate is 0.9". In this way the light from the scanning slit passes through the parallel plate to form an image in the pupil of lens (3), while the light from the two reference slits is deflected by the prisms, and comes to a focus in the planes of the density wedges.

The mounting of the circular density wedges is shown in the accompanying photograph. The wedges are mounted on shafts which rotate in good quality bearings. The shafts are connected through a 1:5 reduction gear to a control knob and calibrated scale. The scale is a circular metal disc with radial lines at intervals of 15° ruled on it. The order of accuracy of setting the pointer attached to the knob is better than 5°, so that the density wedges may be set to an accuracy exceeding 1°.

The range of density chosen for the wedges is 0-2.0. This coverage theoretically enables measurements of moduli of transfer functions in the range $1 \geqslant T(s) \geqslant 0.01$ to be made. It is desirable that the density range vary linearly with the angle of rotation of the wedges, and that the relation between density and the angle of rotation be the same for both wedges. A pair of matched wedges was obtained from a commercial source, and their calibration checked using a Hilger and Watts recording photometer. The resulting calibration curves are shown in Figure 25 where density is plotted against the angle of rotation ψ. It may be seen from the curves that the two wedges are well matched, and that the relation between density D and angle of rotation ψ is linear. (Note that for practical purposes a linear relation between ψ and the transmission A would be preferable, but it is not possible to obtain such density wedges). The mean slope of the lines is found to be 0.00575 density units per degree of rotation, and the error in assuming

$$D = 0.00575\ \psi$$

over the whole range amounts to less than 1%.

Now, the image of the scanning slit is formed in the pupil of lens (3). This lens has a focal length of 3.0" so that the pupil of lens (2), containing light from the scanning slit, is imaged 6.2" behind it onto P.

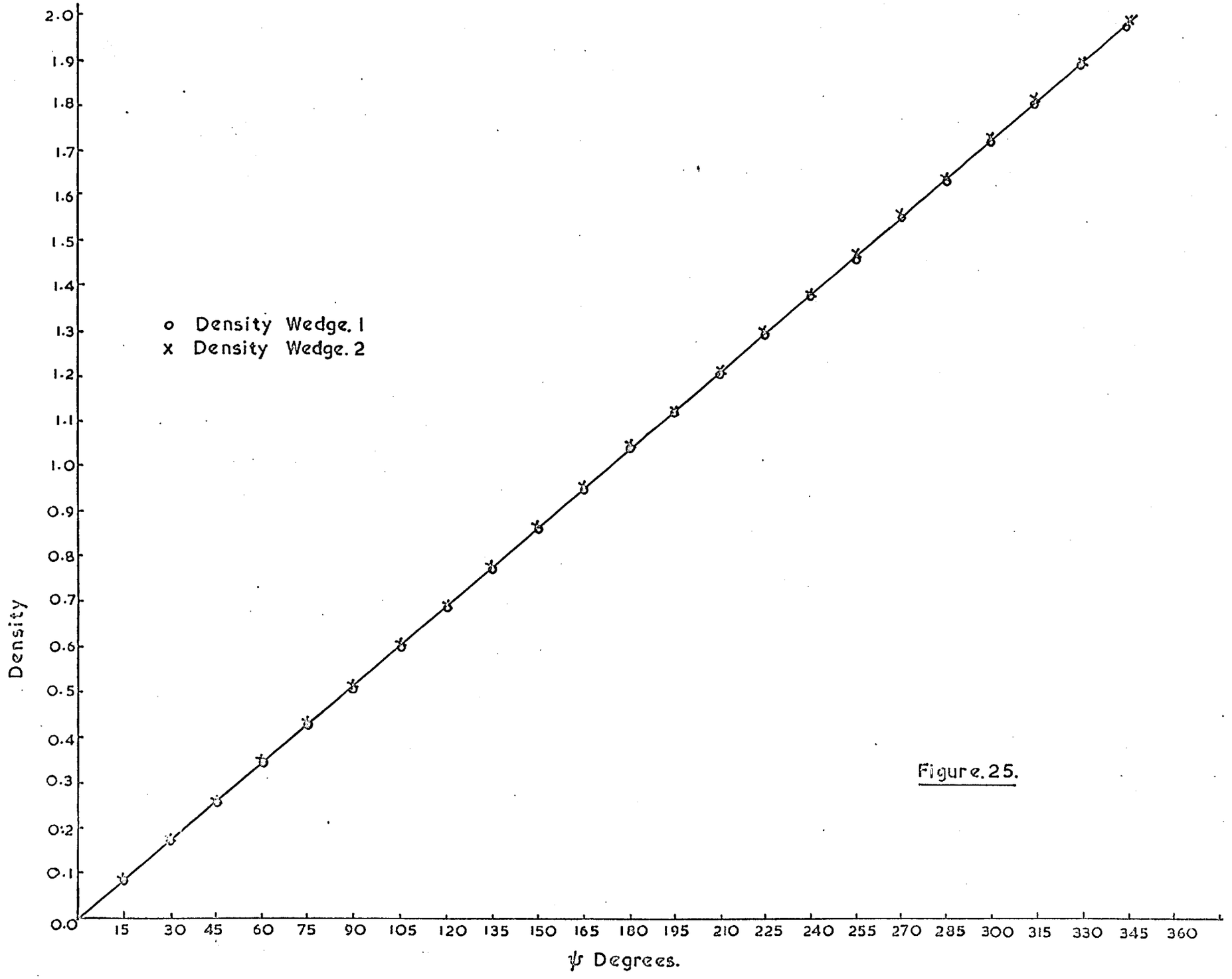

o Density Wedge. 1
x Density Wedge. 2
Density
2.0
1.9
1.8
1.7
1.6
1.5
1.4
1.3
1.2
1.1
1.0
0.9
0.8
0.7
0.6
0.5
0.4
0.3
0.2
0.1
0.0
15 30 45 60 75 90 105 120 135 150 165 180 195 210 225 240 255 270 285 300 315 330 345 360
ψ Degrees.

Figure. 25.

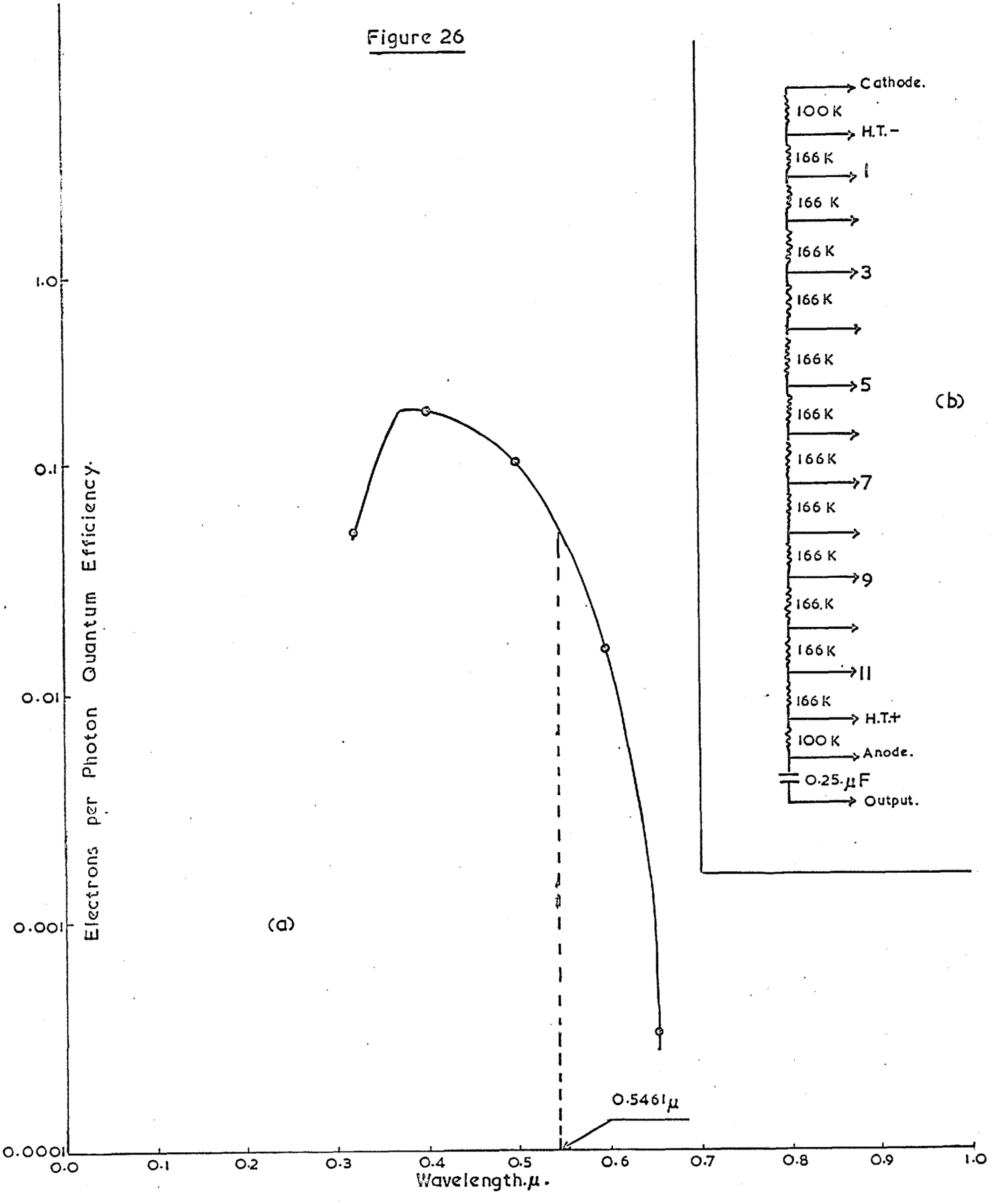
Immediately behind the density wedges are placed lenses (4) of focal length 3.2", which, together with the mirrors M, image the pupil of lens (2), containing light from the reference slits, onto the same plane through P. The lenses (4) are attached to the mounts of the density wedges, while the mirrors M are supported on adjustable mounts close to the lenses (4). Focal lengths and path lengths have been adusted so that all three images are in focus, and coincide at P. Lens (3) is supported in a mount similar to that for lens (2), thus providing a method of achieving focal coincidence.

(12) Photomultiplier Detector:

A photomultiplier is employed to convert the sinusoidally varying light fluxes into sinusoidally varying electrical signals. The photomultiplier, mounted in a blackened brass tube, is arranged so that the centre of the photocathode coincides with the point P. Provisions are made for the position of the photomultiplier to be adjustable in three dimensions.

The photomultiplier used is an E.M.I. type 6094 B, Having a spectral response as shown in Figure 26(a). The 6094 B is an eleven dynode, venetian blind type tube, with a 1 cm. diameter photocathode. Just in front of the photocathode a lenticular screen is placed to diffuse the incident light. Thus effects due to variations in

Figure 26


Electrons per Photon Quantum Efficiency.
1.0
0.1
0.01
0.001
0.0001
0.0
0.1
0.2
0.3
0.4
0.5
0.6
0.7
0.8
0.9
1.0
Wavelength. μ.
0.5461 μ
(a)
(b)
Cathode.
100 K
H.T.-
166 K
1
166 K
166 K
3
166 K
166 K
5
166 K
166 K
7
166 K
166 K
9
166.K
166 K
11
166 K
H.T.+
100 K
Anode.
0.25. μF
Output.

sensitivity across the photocathode are eliminated.

The high tension for the tube is obtained from a stabilised 2000 volt D.C. supply coupled with a potentiometer unit. Figure 26(b) shows the resistor chain used to supply equal potential differences between each pair of dynodes. Typical operating characteristics for the 6094 B are as follows

E.H.T. = 1400 v

Voltage between dynodes = 117 v

Current Drain = 0.705 mA

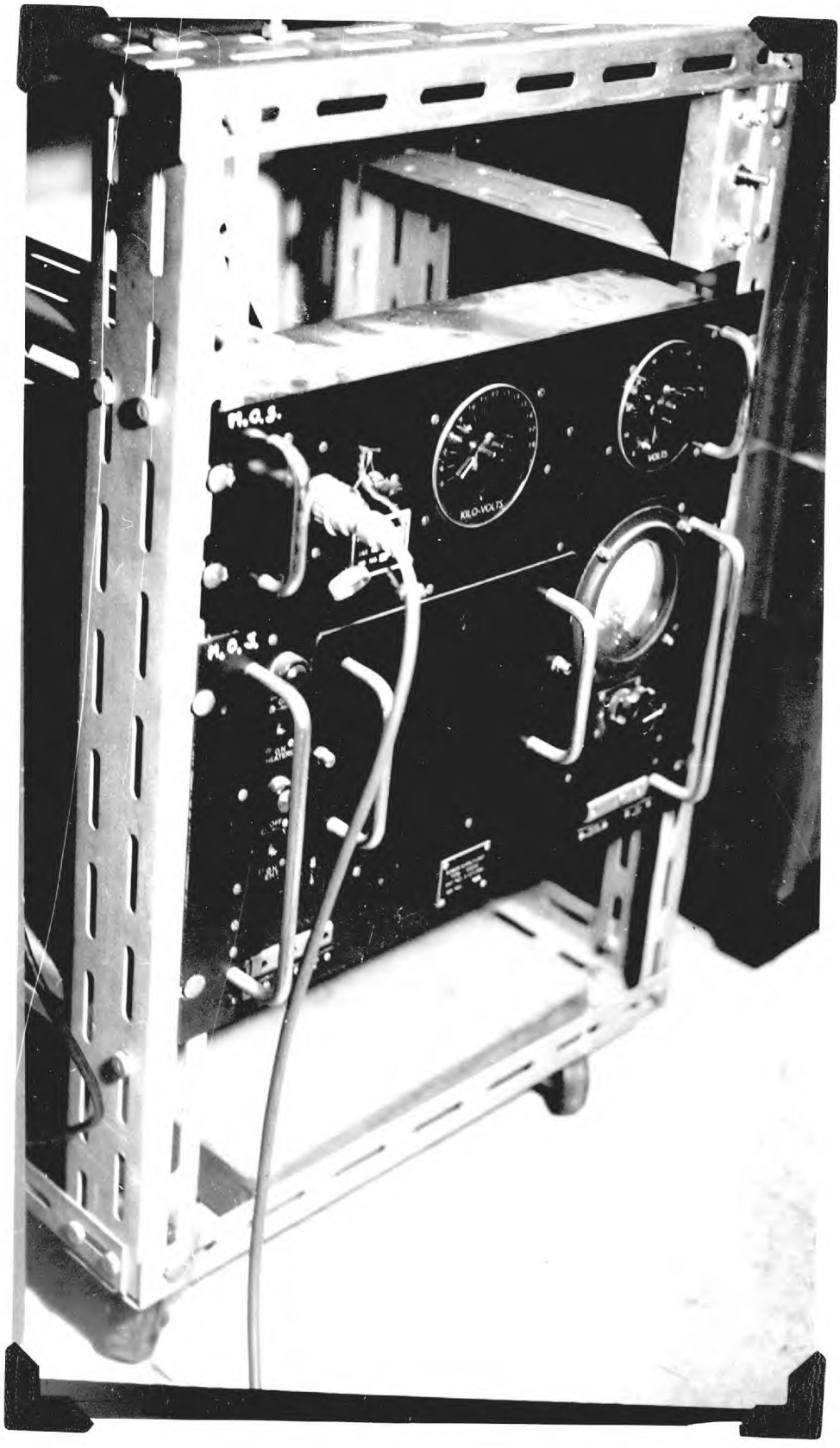
Dark Current = 3×10^{-10} A

Sensitivity = 200 A/Lumen.

The 100 KΩ resistor at the cathode end of the resistor chain is a safety precaution . The choice of 166 KΩ resistors in the chain were chosen to permit the safe use of 2000v across the tube. In practice this is found unnecessary. A load resistor of 100 KΩ was chosen to match the impedance of the following electronics.

(13) Frequency Selective Amplifier:

The output from the photomultiplier is fed into a frequency selective amplifier which filters out all but the fundamental frequency produced by the moving grating. This frequency is 4,648 c/s. The circuit of the amplifier is shown in Figure 27. Frequency selection is achieved by employing tuned circuits in feedback loops, as shown in the



E.H.T. SUPPLY FOR PHOTOMULTIPLIER

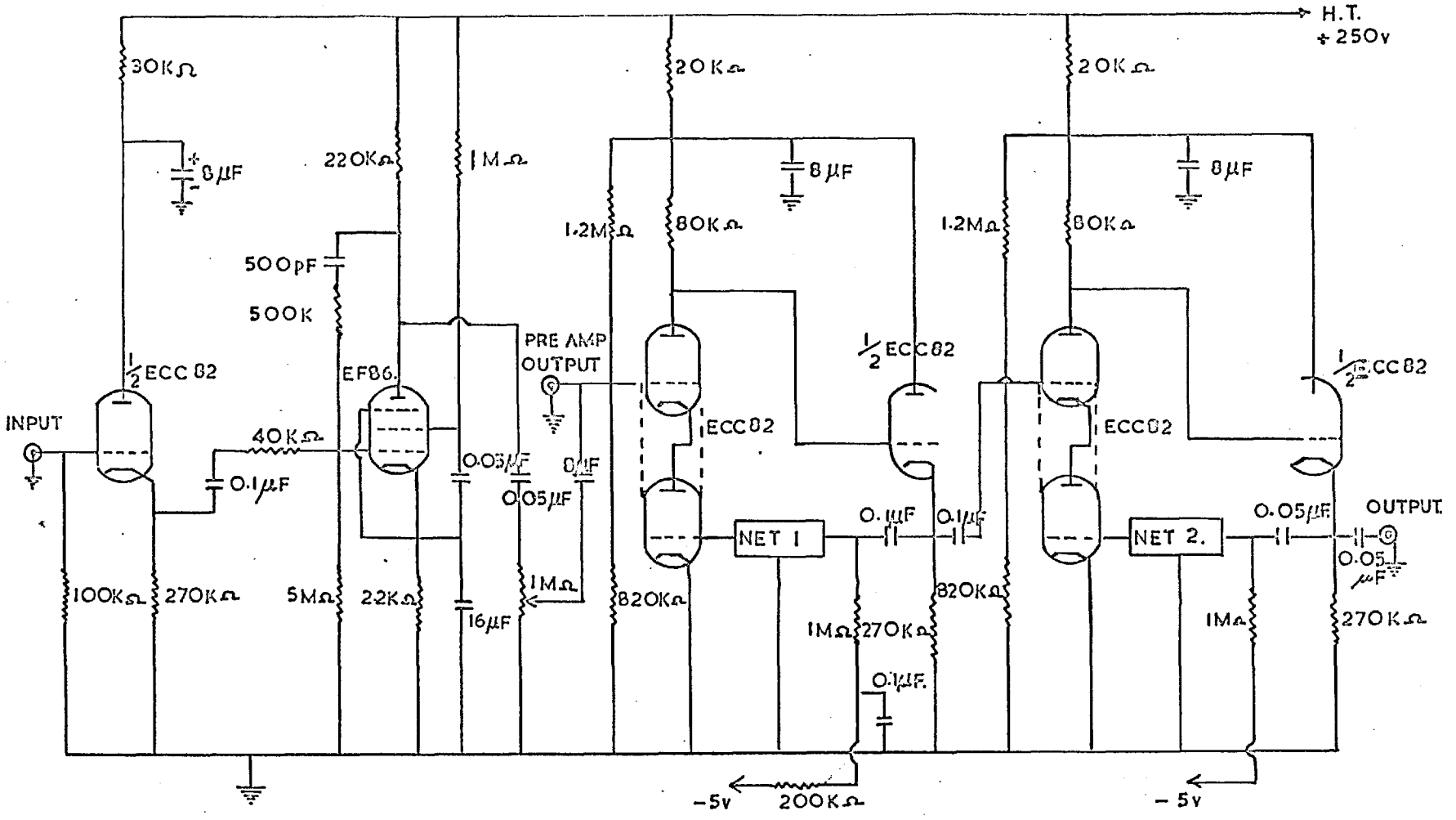

H.T.
+250v
30KΩ
8μF
220KΩ
1MΩ
500pF
500K
½ ECC 82
EF86
INPUT
40KΩ
0.1μF
100KΩ
270KΩ
5MΩ
22KΩ
0.05μF
16μF
PRE AMP
OUTPUT
0.05μF
1MΩ
20KΩ
8μF
1.2MΩ
80KΩ
ECC82
820KΩ
NET 1
0.1μF
0.1μF
1MΩ
270KΩ
0.1μF
-5v
200KΩ
½ ECC82
20KΩ
8μF
1.2MΩ
80KΩ
ECC82
NET 2.
1MΩ
½ ECC 82
0.05μF
OUTPUT
0.05μF
270KΩ
-5v

Figure 27.

figure. The tuned circuits are of the twin-T rejection type, the rejection frequency here being 4,648 c/s. Figure 28(a) shows the actual tuned circuits used. The resistances are made variable to allow the circuits to be "peaked". Two filter circuits are employed in the amplifier, and these are stagger tuned to allow for small variations in the speed of rotation of the scanning grating. The final selective characteristic of the amplifier is shown in Figure 28(b), and it may be seen that the second harmonic contributes less than 1% to the total output.

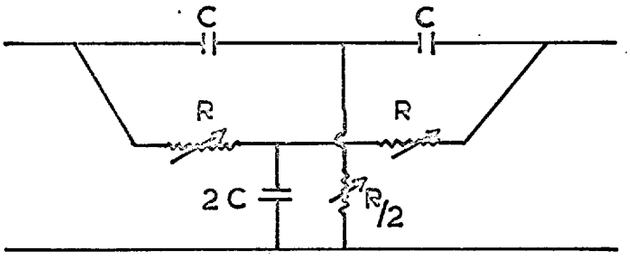
The input voltage from the photomultiplier is on the average, after attenuation, 0.005 volts, and the frequency selective amplifier works with a gain of about 300, giving an output of about 1.5 v.

(14) Main Power Amplifier:

The output from the frequency selective amplifier is fed into a Mullard 5-10 power amplifier, the circuit of which is shown in Figure 29. The signal output is taken from one anode of the push-pull output valves. Normally, the voltage gain is about 10, although this may be increased considerably is required. The output voltage then is about 15 volts, and the output impedance about 4,000 ohms.

(15) Detector and Output Control:

The output from the main amplifier is fed to a detector and measuring circuit which is shown in Figure 30.



(a)

$\nu = {}^{1}/_{2\pi}(RC)^{-1}$: $\nu = 4,648$ R = 50KΩ C = 680pF
(0 → 100KΩ)

(b)

Attenuation.

0
-2
-4
-6
-8
-10
-12
-14
-16
-18
-20
-22
-24
-26
-28
-30
-32
-34
-36

1450 2250 3050 3850 4650 5050 6250 7050 7850 8650

ν c/s.

Figure 28.

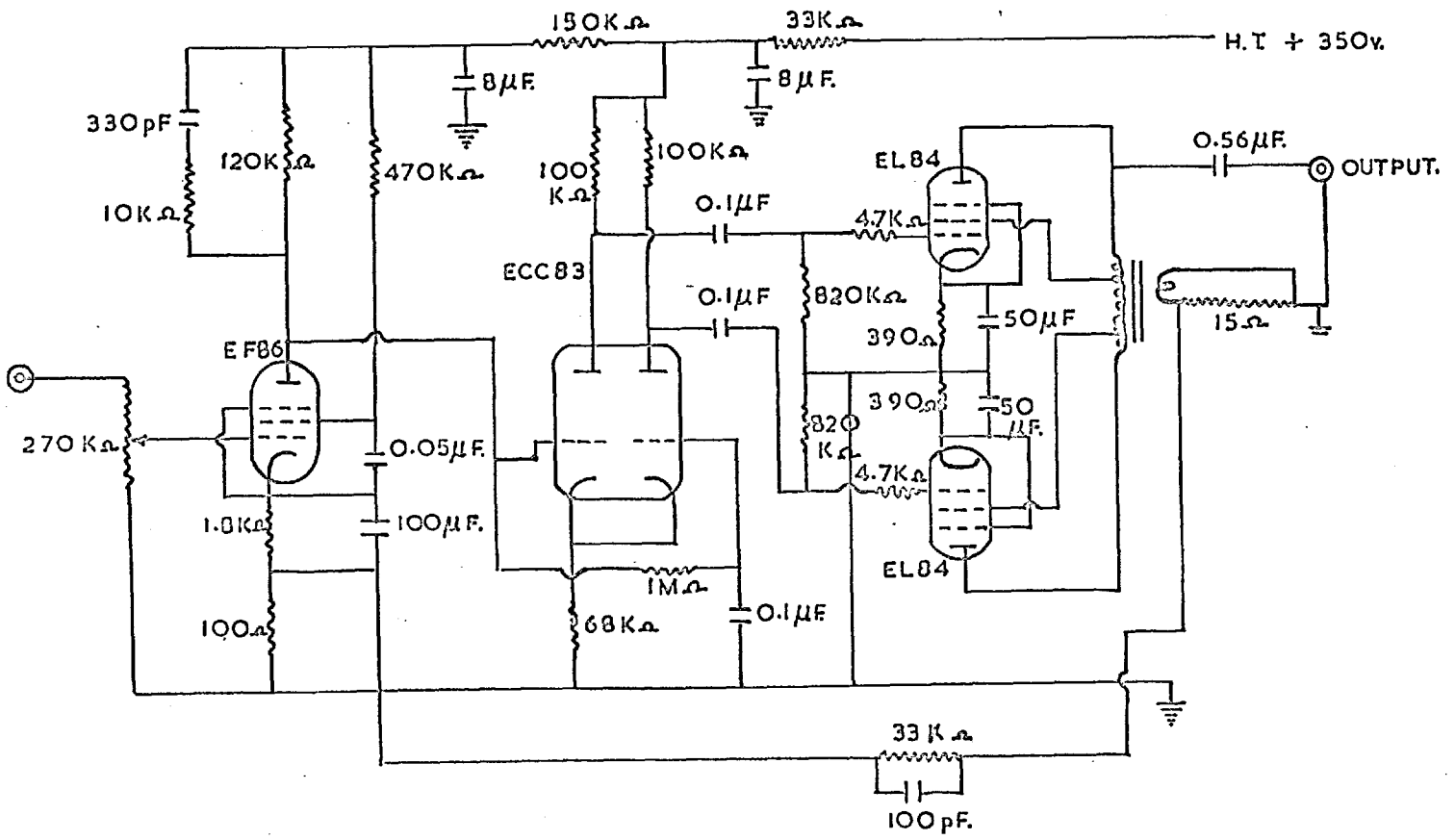

150K Ω
33K Ω
H.T + 350v.
8μF.
8μF.
330pF
120K Ω
10K Ω
470K Ω
100 K Ω
100K Ω
0.1μF
EL84
4.7K Ω
0.56μF.
OUTPUT.
ECC83
0.1μF
820K Ω
390Ω
50μF
15Ω
EF86
270 K Ω
0.05μF.
390Ω
50 μF.
820 K Ω
4.7K Ω
1.8K Ω
100μF.
EL84
1M Ω
68K Ω
0.1μF
100Ω
33 K Ω
100 pF.

Figure 29.

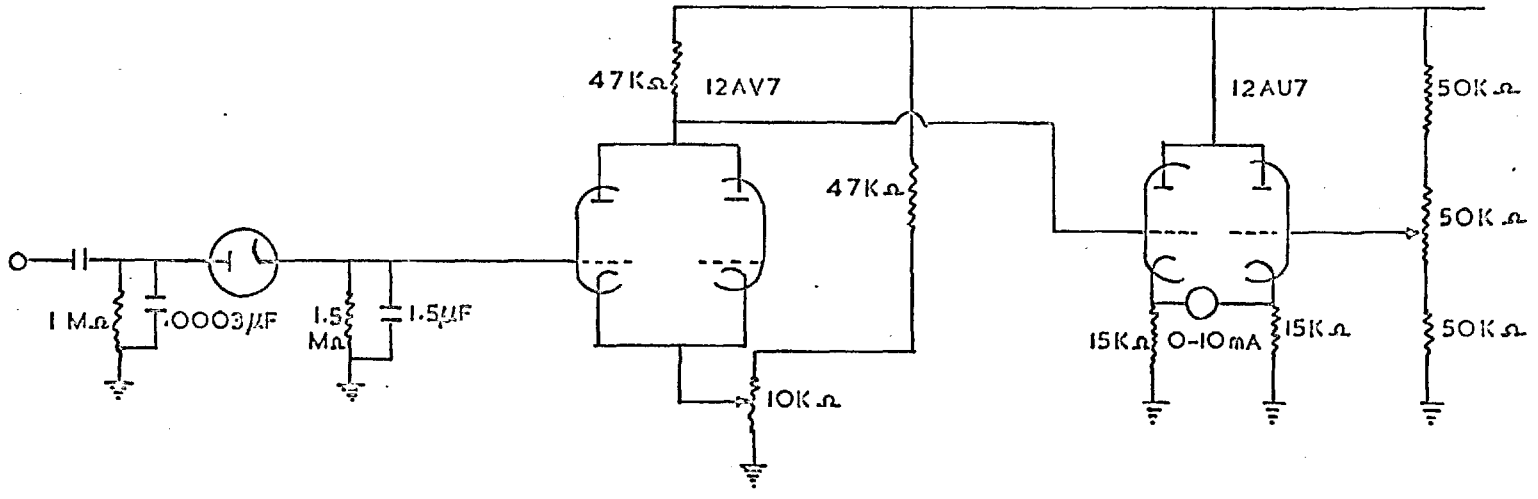

47KΩ
12AV7
47KΩ
12AU7
50KΩ
50KΩ
50KΩ
1 MΩ
.0003μF
1.5 MΩ
1.5μF
10KΩ
15KΩ
0-10mA
15KΩ

Figure 30.

Firstly the A.C. signal is rectified, using one half of a 6 AL5 valve. The rectified output then passes into a R-C integrating circuit which has a time constant exceeding 1 second. This removes any A.C. signals which may be superimposed on the D.C. signal. An important feature here is that a very large percentage of the voltage fluctuations due to photomultiplier noise, variations in scanning grating transmission, and valve noise are removed.

The signal then passes into a D.C. amplifier and bridge circuit. The output meter measures the "out of balance" of the bridge circuit. Adjustments are provided for ensuring the non-saturation of the D.C. amplifier valve, and for controlling the out of balance current in the bridge network. Linearity of the detector circuit may be obtained by suitably setting the adjustments. This is not necessary though, as a zero reading only is required.

The meter for measuring the out of balance current, and hence the output signal, is a standard 0-10mA. meter. A large capacitance may be connected across the meter to bypass any residual signal fluctuations.

(16) Method of Operation:

The gains of the amplifiers are first adjusted so that the initial incoming signal gives a suitable output on the meter. The parallel plate micrometer and the density wedges are then adjusted to give an approximately zero output.

The amplifier gains may then be increased and readjustments made to the micrometer and density wedges. This process is repeated until an accurate null is obtained. The only limitation on accuracy is how effectively noise fluctuations have been eliminated, and this in turn depends on the time constants in the detector.

CHAPTER VII

Setting Up and Alignment of the Apparatus.

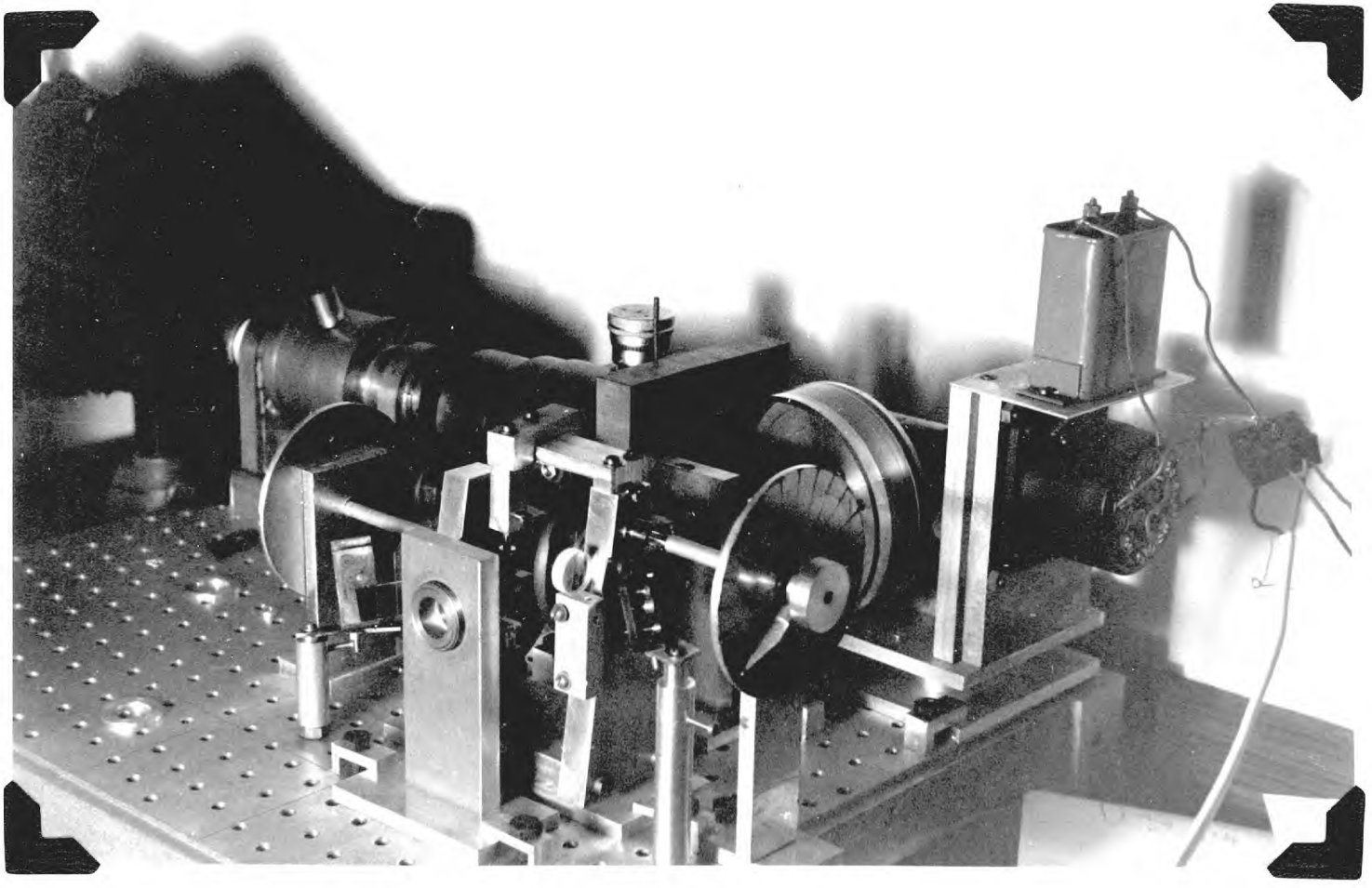
(1) Introduction:

This chapter describes the methods used to align all the components in the instrument. The alignment is achieved in eight stages, each of which will be described in detail. Once the alignment has been carried out, the instrument is ready for testing and the taking of measurements.

(2) Mounting of Components on a Base-Plate:

The base-plate is a machine finished die-cast duralium chassis measuring 18" × 15" × 2.5", The surface contains a large number of tapped holes, and each mounted component is held in place by right angle brackets screwed to the base-plate. Each component is supported in its mount at a standard height of three inches above the base-plate surface.

It is important that each component be mounted perpendicular to the optical axis, and to meet this requirement the following procedure was adopted. An autocollimator, with a setting accuracy of one second of arc, was set in a fixed position, and the base-plate adjusted until its surface was parallel to the autocollimator axis. This was done by autocollimating off a mirror attached to the side of the base-plate. Next, the bearing mount containing



the graticule was positioned, and autocollimation used to obtain both the correct orientation and normality of the graticule to the optical axis. The graticule remained normal to the axis when the bearing was rotated. (The major area of the graticule has a high reflectivity which provides an ideal surface for autocollimation.)

The parallel plate micrometers were then positioned and their angular settings adjusted until no shift of the optical axis was observed in the autocollimator pupil. The setting accuracy here is one second of arc, which corresponds to a shift of about 10^{-5} inches of the optical axis.

The image rotating prism was then placed on the base-plate, and its position adjusted using the above procedure. A check was made to ensure that the rotation axis of the prism coincided with the optical axis. (Refer to the previous chapter for details concerning the adjustement of the image rotating prism in its mount.)

Following this, the scanning drum and its associated drive mechanism were fixed to the base-plate, the drum being placed as close as possible to the graticule. Normality of the drum surface to the optical axis was obtained by sliding feeler gauges between the external surface of the drum and the rear of the graticule bearing.

The prism, with lens attached, for turning the optical axis through 90° was next placed as close as possible to the inner surface of the scanning drum. To ensure that the optical axis was turned through exactly 90°, the autocollimator was moved and autocollimation obtained off a small mirror attached to one side of the graticule bearing mount. The orientation of the prism was then adjusted so that its rear face was normal to the autocollimator axis.

The scanning graticule was next illuminated, through the image rotating prism and the parallel plate micrometers, by a collimated point source. A small pinhole in a mount at the standard height above the base-plate surface was used to locate the image of this point source produced by lens (1), attached to the prsim. Having located the image position, the pinhole was removed and replaced by the first imaging lens (lens (2)).

As lens (2) produces an image of the scanning and reference slits, the same procedure as above was adopted to locate the position of lens (3). However, an extended source was used here so that the reference slits were illuminated.

Having located the position of lens (3), the mount containing the glass plate with the small prisms attached to it was placed in such a way that the image of the

scanning slit did not alter its position, while the light forming images of the reference slits was turned through 90° by the small prisms. These image planes were determined, and the density wedges fixed in position

The image produced by lens (3), of the pupil of lens (2), was next located. Lenses (4) were then fixed to the density wedge mounts as described previously. Placing a large pinhole in the image plane of lens (3), and then blocking out the light from the scanning slit, the mirrors M were adjusted until maximum light from the reference slits passed through the pinhole.

(3) Determination of the Optical Axis:

The optical axis of the complete system was determined using a series of pinholes. Initially the decollimator and test-lens were removed from their mounts. Two small pinholes, one supported in the test-lens mount and the other in an auxiliary mount, were placed on the nodal slide at the same height above the T-bar. The auxiliary mount was placed on the object side of the test-lens mount. The two pinholes were illuminated by a point source whose position was adjusted to give maximum light transmission. The auxiliary mount was then moved to the other side of the test-lens mount, that is towards the decollimator position. A third pinhole was then placed in the approximate focal plane of the decollimator/ magnifying system, and its position adjusted to give maximum

light transmission.

Two more pinholes were placed in the lens mounts of the magnifying system. Their positions and heights were adjusted to give maximum light transmission. To ensure that the axis of the auxiliary optical bench, on which these mounts move, was parallel to the true optical axis, the mounts were moved some distance from their correct positions in both directions. Being supported on an adjustable table, adjustments could be made to the bench in order that maximum light was transmitted through the pinholes for any position of the lens mounts.

The light source was then placed behind the pinhole in the image plane of the decollimator/magnifying system. The object slit was replaced by a pinhole. and its position adjusted for maximum light transmission.

The optical axis between object and image planes was thus determined by six accurately aligned pinholes.

Following this, the lenses of the magnifying system were placed in their mounts. Next, the decollimator was placed on its support, and its position adjusted to again give maximum light transmission. Then the test-lens was placed in its mount. On rotating this lens in its mount it was found that the light intensity through the pinhole in the object-plane varied. The azimuth giving maximum light transmission was chosen. (It will be shown later that

this intensity variation is due to the decentring of one or more components in the test-lens. This gives rise to a discrepancy between predicted and measured values of the transfer function which arises from the presence of on-axis coma.)

Having determined the position of the object slit, the other components of the illuminating system were added, their position being adjusted in order that the pinhole in the object slit mount received maximum light from the source.

(4) Determination of Image Plane:

To determine the image plane precisely, a collimator was used to form an image at infinity of a pair of cross-wires. The collimator was placed along the optical axis between the test lens and the decollimator. The image of the cross-wires produced by the decollimator and magnifying system was located using a finely ground glass screen and a microscope. The position of this image was marked for future reference, as this is the position to be occupied by the scanning graticule.

(5) Positioning of the Base-Plate:

Once the final image plane was located, the base-plate was moved into position. The base-plate itself is supported on a table and framework attached to the steel girders which hold the nodal slide in place. This table is adjustable in three dimensions, and provisions are made for lateral movements of the base-plate relative to the table.

In order to determine the correct position of the scanning graticule, an image of it when illuminated was observed with an autocollimator placed along the optical axis in front of the decollimator. When the scanning graticule is in the correct position, the image of it, as seen in the autocollimator, should be sharp. Also, on rotating the graticule, the image of the rectangular slit should only rotate about the optical axis of the autocollimator. To obtain the sharpest focus, one of the lenses of the magnifying system was shifted a small distance. This was necessary as the decollimated beam passes through a finite thickness of glass before striking the scanning graticule.

The autocollimator was also used to check the normality of the scanning graticule to the optical axis, and coonsequently the coincidence of the optical axes of the base-plate components and the rest of the instrument. When these axes coincide, the reflected beam from the graticule is coincident with the incident beam. Also, the image of the rectangular scanning slit coincides exactly with the centre of the autocollimator pupil. This adjustement is achieved using the four screws which control the lateral movement of the base-plate mentioned earlier. A final coincidence setting is obtained by adjusting the parallel plate micrometer.

(6) Magnification of Object:

With the position of the components of the magnifying system adjusted in order that the final image plane coincided with the plane of the scanning graticule, the total magnification throug the system could be determined. To do this, the size of the image of a pinhole in the object slit mount was measured using a medium power microscope and a micrometer eyepiece. In order to make this image accessible a 45° prism was placed in the beam just ahead of the image rotating prism. A considerable number of measurements of the image size were made in order to eliminate errors. The pinhole object was then removed from its mount and measured using the same microscope and eyepiece. The total magnification of the system was found to be

$$M = 9.16(24)$$

so that D, the width of the geometrical image of the object slit is

$$D = 6.8(5) \times 10^{-3} \text{ cm.}$$

The magnification measurement is quite critical as D determines the magnitude of the correction factor

$$\frac{\sin(\pi sd)}{(\pi sd)} = \frac{\sin(\pi DR \tan \varphi)}{(\pi DR \tan \varphi)}$$

to be included when calculating the transfer function from

the measured quantities. For example, if

$$R = 4 \text{ lines/mm} , \quad \varphi = \pi/4 , \quad D = 0.0685 \text{ mm} ,$$

then

$$\frac{\sin (\pi DR \tan \varphi)}{(\pi DR \tan \varphi)} = 0.8812 .$$

If there is a 10% error in the value of D, the correction factor takes the value 0.8591, which would lead to a 3% error in the value of T(s). However, as the value of T(s) here would be small, the error is not so significant when considered as a percentage of T(0).

(7) Positioning of the Test-Lens:

As mentioned in previous chapters, the transfer function is to be determined initially with the test-lens working "paraxially". This requires that the object slit be in the back focal plane of the test-lens. Knowing the design parameters, this distance was calculated and measured, and found to be

$$f' = 18.473 \text{ inches}$$

A metal rod of this length, less the thickness of the object slit cover glass, was made and placed between the object slit and the test-lens. One end of the rod just touched the cover glass of the object slit. The test-lens was then moved back until it just touched the other end of the metal rod. The reading of the dial gauge attached to the lens

mount was noted, and the metal rod removed. (It was necessary to move the lens in order to remove the rod)

A second and more sensitive method of checking the focal setting will be given in the next chapter.

(8) Determination of the Nodal Point of the Test-Lens:

For measurements of the transfer function with the test-lens in an off-axis position, the test-lens must be rotated about an axis passing through its rear nodal point. When this occurs, the light emerging from the test lens follows the same path as when the lens is on axis, so that the final image is not shifted at all. To determine this pivot point, the final image was observed with a microscope, the test-lens being initially on-axis. The nodal slide was then moved and the test-lens shifted off-axis. Adjustements to the position of the pivot point were made until the final image shifted by less than 10^{-4} inches. A little refocussing of the test-lens was required for shifts off-axis of about fifteen degrees.

(9) Positioning of the Photomultiplier:

Illuminating the scanning graticule with an extended source, the position of the pupil images prodcued by lenses (3) and (4) was located. The photomultiplier was then placed so that the photocathode coincided with this image position. Provisions for adjustments in three dimensions were made, so that this positioning was not difficult.

CHAPTER VIII

THE MEASUREMENT OF OPTICAL TRANSFER FUNCTIONS

(1) Introduction:-

This chapter describes the measurements made and the results obtained with three separate lens systems. These systems were

(a) 20" focal length F/5.6 Anastigmat

(b) 19" focal length F/8 Plano-Convex Singlet

(c) 8" focal length F/2.9 Pentac.

Initially, measurements were made with the object slit in the meridional section. Later, results were obtained for other azimuthal settings of the object slit, both for on-axis and off-axis images.

To obtain theoretical values of the transfer function, a computer programme (written by J. Hindley) was employed. A critical examination of the relations between the theoretical and measured values has been made, and the conclusions to be drawn from this examination are given.

(2) Measurements on the 20" lens:-

As mentioned previously, the 20" Anastigmat lens is a wartime aereal survey lens, having the following constructional data

Surface	C in^{-1}	t'in.	No	No'
1	0.196502	0.6080	1.0	1.61509
2	0.049652	0.5140	1.61509	1.0
3	0.126295	0.1760	1.0	1.57217
4	0.126295	0.2055	1.57217	1.0
5	0.0 (stop)	0.2055	1.0	1.0
6	0.115848	0.1736	1.0	1.55414
7	0.131130	0.5680	1.55414	1.0
8	0.054466	0.4880	1.0	1.61509
9	0.197941		1.61509	1.0

For this system, calculation gives

Equivalent Focal Length = 19.786" Maximum Aperture = F/5.6

Back Focal Length = 18.473"

The wavefront aberration coefficients were calculated, using the first part of the Hindley programme, with the results listed below:

ON-AXIS (λ=5461A$^{\circ}$)

W_{20} = 0.0

W_{40} = 18.219

W_{60} = $\overline{12.647}$

12° OFF-AXIS

(W_{11} = 0.4462)

(W_{20} = $\overline{0.8544}$)

W_{22} = $\overline{6.3024}$

W_{31} = 4.9409

W_{33} = $\overline{2.5461}$

W_{40} = 28.325

$$W_{42} = 6.9990$$
$$W_{51} = \overline{4.1443}$$
$$W_{60} = \overline{19.525}$$

The coefficients $W_{p,q}$ have the following significance:-

W_{11} = Transverse focal shift

W_{20} = Longitudinal focal shift

W_{22} = Primary astigmatism

W_{31} = Primary coma

W_{51} = Secondary coma

W_{40} = Primary spherical aberration

W_{60} = Secondary spherical aberration

W_{33} = Higher order coma - type aberration

W_{42} = Higher order astigmatism - type aberration.

Initially, the lens was stopped down to F/40 by placing the appropriate size of aperture in it, in coincidence with the stop plane. To check that the object slit was exactly in the rear focal plane of the test lens, measurements at a fixed spatial frequency at various focal settings were made, following adjustment of the test-lens position to give a maximum output signal at zero spatial frequency. The reduced spatial frequency chosen was s = 0.138 corresponding approximately to 3 lines /mm. in the object plane. This

corresponds in turn to setting the scanning slit at an angle $\phi = 5^{\circ}$ from the zero spatial frequency position.

The coefficient specifying the defocussing introduced is given by

$$W_{20} = \frac{n\lambda}{\pi} = -\frac{1}{8} (F/no.)^{-2} \, dL$$

n having the values 0,1.2,...

where λ = wavelength

dL = Longitudinal shift of focus

W_{20} = Wavefront aberration.

The table below gives the values of dL and W_{20} for various values of n, when an aperture of F/40 is used.

($\lambda = 5461A^{\circ}$)

n	0	1	2	3
dL/mm.	0	$\overline{2.2256}$	$\overline{4.4512}$	$\overline{6.678}$
W_{20}	0	0.318λ	0.636λ	0.954λ

The lens could be positioned to an accuracy of ± 0.01 mm which in terms of W_{20} is less than $\pm 0.002\lambda$. This amount of defocussing would, of course, produce an undetectable effect on the transfer function.

Several sets of measurements were made on-axis, the lens being moved either side of the mechanically determined paraxial focus. The resulting values of the modulus and phase of the measured transfer function are shown in Figure 31.

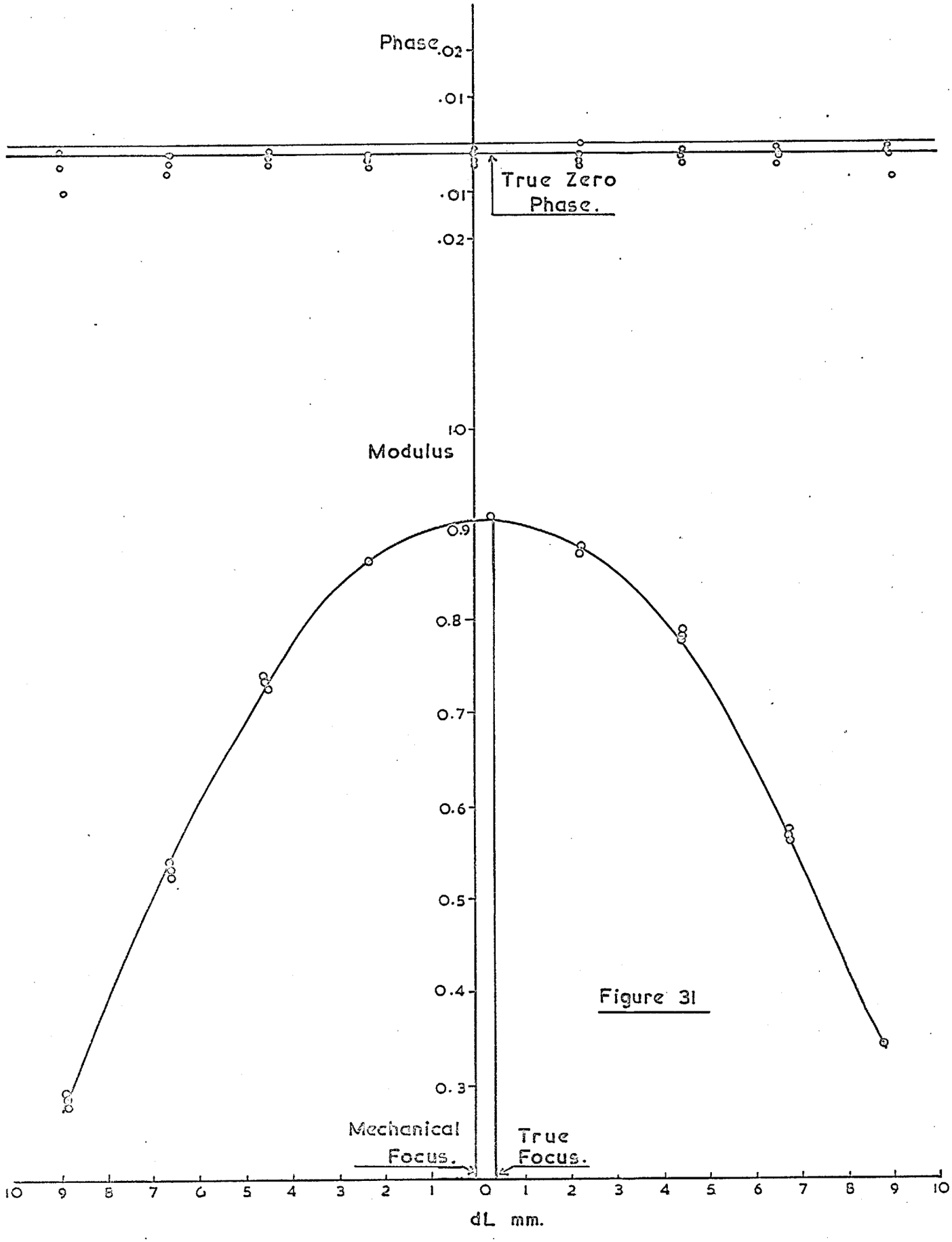
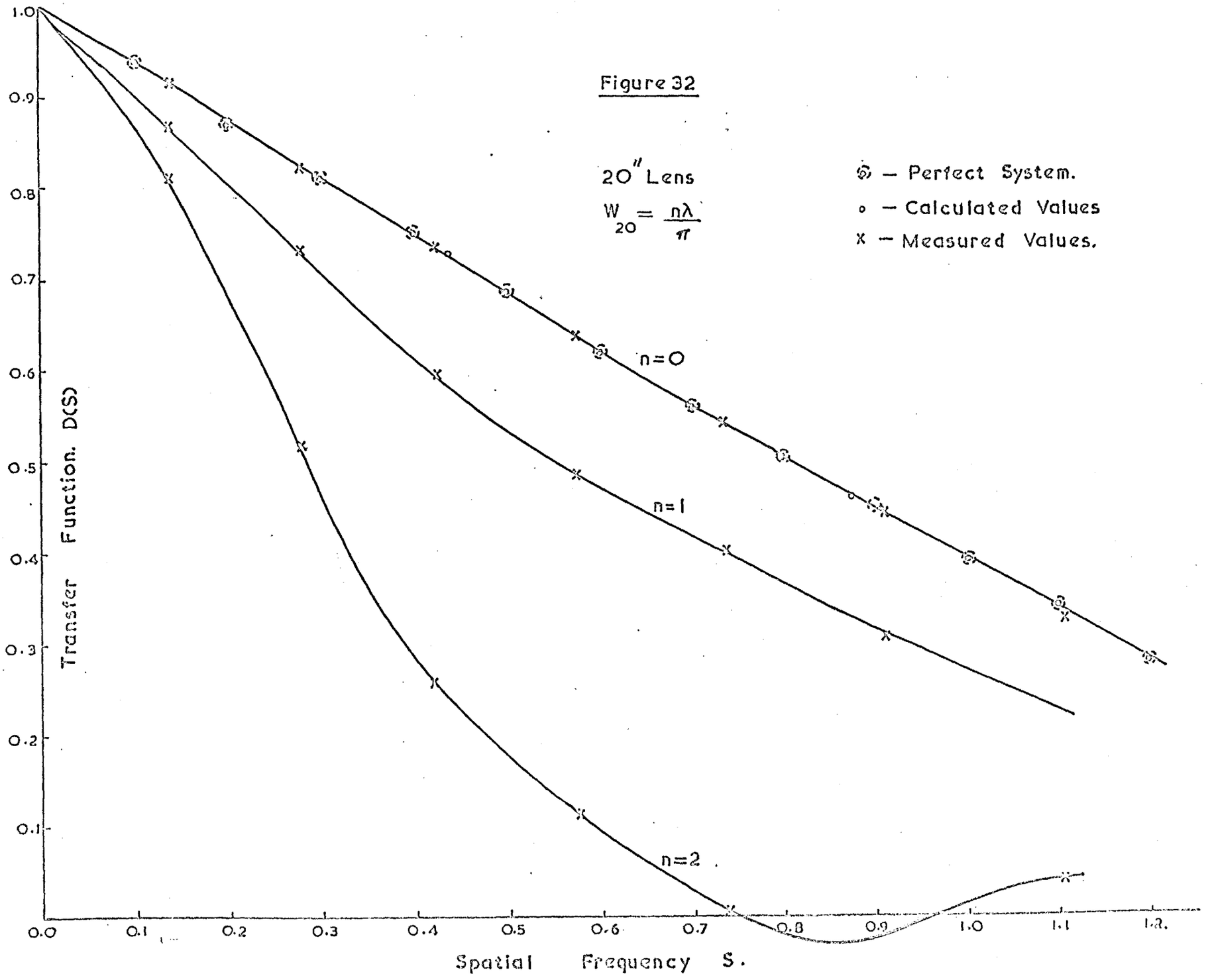

Phase
.02
.01
.01
.02
True Zero
Phase.
1.0
Modulus
0.9
0.8
0.7
0.6
0.5
0.4
0.3
Mechanical
Focus.
True
Focus.
10 9 8 7 6 5 4 3 2 1 0 1 2 3 4 5 6 7 8 9 10
dL mm.

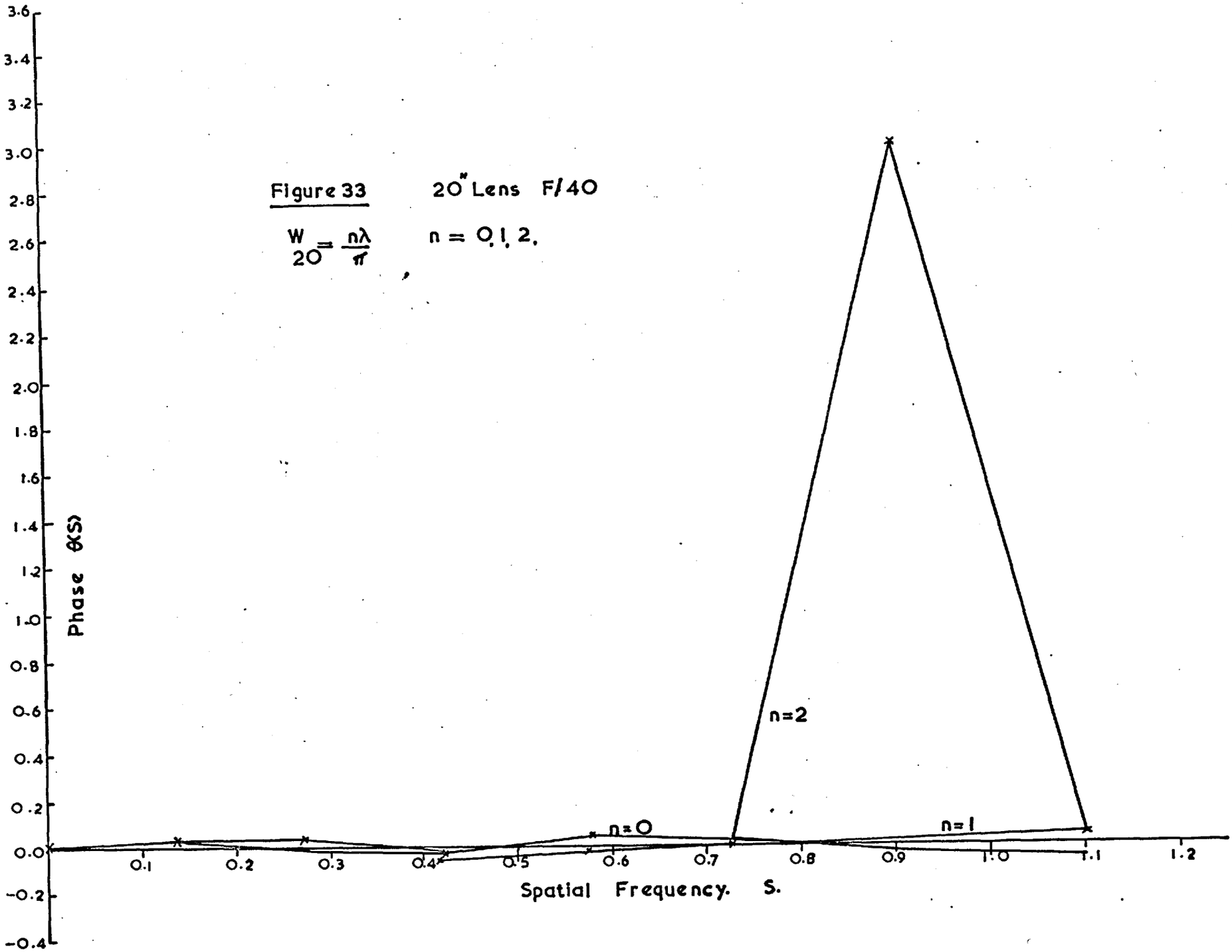
Figure 31

As may be seen there is a small discrepancy in the setting of both the paraxial focal position and the zero phase position. This is shown by an asymmetry in the modulus curve, and a lateral shift of the zero phase mean axis. The focal error is + 0.11 mm, and the phase error is 0.0014 radians, the latter corresponding to a lateral shift of the image of about 5×10^{-4} inches.

Having checked the focal setting in the above manner, measurements at F/40 were obtained. Defocussing by the amounts specified above were then introduced, and values of both modulus and phase determined for the range of spatial frequencies $0 \leqslant s \leqslant 1.104$. The results are shown graphically in Figures 32 and 33. For these measurements the object slit was in the vertical section. It may be seen from the upper curve in Figure 32 that the agreement between theoretical and measured values is very good. The maximum error in the modulus measurement is 0.02 (2%). From Figure 33 it may be seen that the maximum error in the measurement of phase is 0.015 radians (less than 1%). These results confirm that the instrument is working satisfactorily.

Referring again to the upper curve in Figure 32, the theoretical values of the modulus are those expected for a diffraction limited system. As the measured values agree precisely with the theoretical ones, it is clear that at F/40


Figure 32
20" Lens
$W_{20} = \frac{n\lambda}{\pi}$
⊛ — Perfect System.
∘ — Calculated Values
x — Measured Values.
n=0
n=1
n=2
Transfer Function. D(S)
Spatial Frequency S.
1.0
0.9
0.8
0.7
0.6
0.5
0.4
0.3
0.2
0.1
0.0
0.1
0.2
0.3
0.4
0.5
0.6
0.7
0.8
0.9
1.0
1.1
1.2.


Figure 33
20" Lens F/40
$\frac{W}{20} = \frac{n\lambda}{\pi}$ n = 0, 1, 2,
Phase θ(S)
Spatial Frequency. S.
n=0
n=1
n=2
3.6
3.4
3.2
3.0
2.8
2.6
2.4
2.2
2.0
1.8
1.6
1.4
1.2
1.0
0.8
0.6
0.4
0.2
0.0
-0.2
-0.4
0.1
0.2
0.3
0.4
0.5
0.6
0.7
0.8
0.9
1.0
1.1
1.2

the test lens is working as a diffraction limited system. This was not found to be so at higher apertures.

Unfortunately, there are no theoretical values of the transfer function for a perfect system defocussed by the above small amounts. Hence no comparison between theoretical and measured values was possible at this aperture (F/40). The remaining curves in Figures 32 and 33 show the measured values of modulus and phase obtained at F/40. For the case n = 1, the contrast for spatial frequencies above s = 0.3 is about 70% that for a perfect system. The amount of defocussing corresponds to a wavefront aberration of 0.32λ which is just outside the Rayleigh $\lambda/4$ tolerance value.

For the case n = 2, there is a rapid decrease in contrast above s = 0.2, falling to zero at s = 0.75. At higher spatial frequencies there is spurions resolution, accompanied by a reversal of contrast between s = 0.75 and s = 0.96. In this region, the transfer function is negative, there being present a phase change of π relative to the phase at zero spatial frequency. The phase change appears to be rather sudden, but it must be remembered that measurements are made with finite steps in the values of spatial frequency s. It will be demonstrated later, however, that this phase change is in fact quite abrupt.

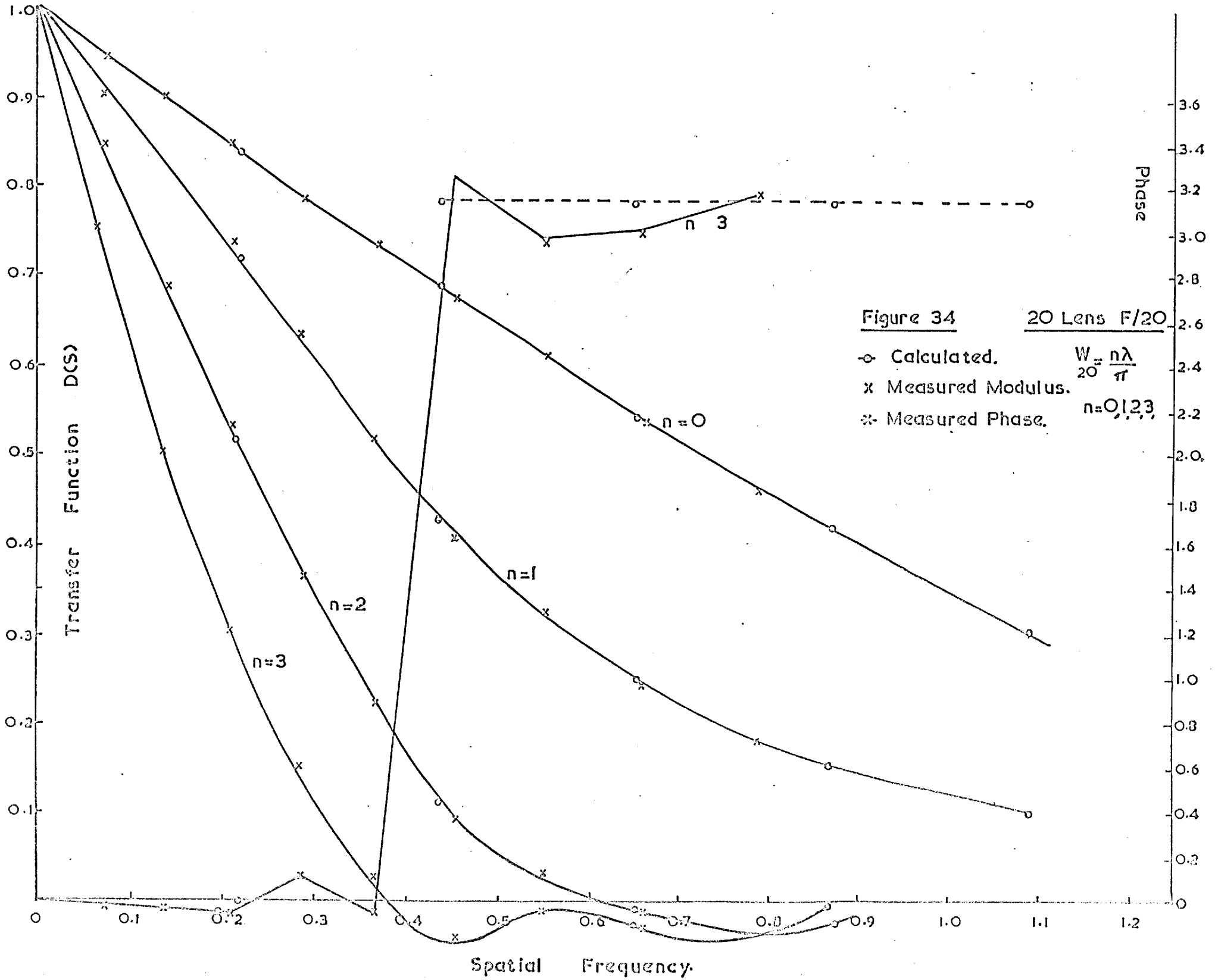
The lens was next tested on-axis at F/20 with the object slit again in the vertical position. Here the defocussing coefficient is given by the table following:

n	0	1	2	3
dL m.m.	0	0.5564	1.1128	1.6692
W_{20}	0	0.318λ	0.636λ	0.954λ

The results are again shown graphically in Figure 34, where only the phase measurements for the case n = 3 are plotted. Again there is good agreement between theory and measurement, the errors amounting to no greater than 2% for both modulus and phase. In terms of the angular measurement of phase, this error is about 7° or $\pi/26$. The phase error when the value of the phase term is near to π is mainly due to the fact that the parallel plate micrometer requires only a movement corresponding to an image shift of a few ten-thousandths of an inch in order to obtain a minimum output signal. An error of 10^{-4} inches in the lateral shift of the image will produce a 25% error in the phase term when its value is close to π.

It may also be seen that the phase change from zero to π is quite sudden, the change taking place between spatial frequencies 0.368 and 0.455. This corresponds to a reversal of contrast, the term exp i $\theta(s)$ in the expression

$$D(s) = T(s) \exp i\, \theta(s)$$


Transfer Function D(S)
Phase
Spatial Frequency.
n=0
n=1
n=2
n=3
n 3
Figure 34
20 Lens F/20
Calculated.
Measured Modulus.
Measured Phase.
$W_{20} = \frac{n\lambda}{\pi}$
n=0,1,2,3

taking the value -1. This is in conformity with there being no asymmetry in the line spread function, so that the aberrations present are proportional to even powers of the aperture. Since the rest lens is working on-axis, the aberration terms present are spherical aberration and defocussing, and these depend on even powers of the aperture.

Following the measurements at F/20, the lens was tested at F/10. Again the object slit was in the vertical position, and the defocussing introduced is given below

n	0	1	2
dL m.m.	0	$\overline{0.139}$	$\overline{0.278}$
W_{20}	0	0.318λ	0.636λ

The results, shown in Figure 35, show a slight disagreement with theoretical values, both in modulus and phase. The discrepancy in the modulus term increases with increasing spatial frequency, and the phase term increases approximately linearly as s increases. This suggests the presence of some asymmetric aberration on-axis, and is possibly coma introduced by the decentring or tilting of one or more components in the test lens. This question will be returned to shortly.

The lens was next tested at F/5.6 with the object slit in the same position as for F/10, and with no defocussing introduced. The resulting values of modulus and phase are shown in Figure 36. Again there is a marked

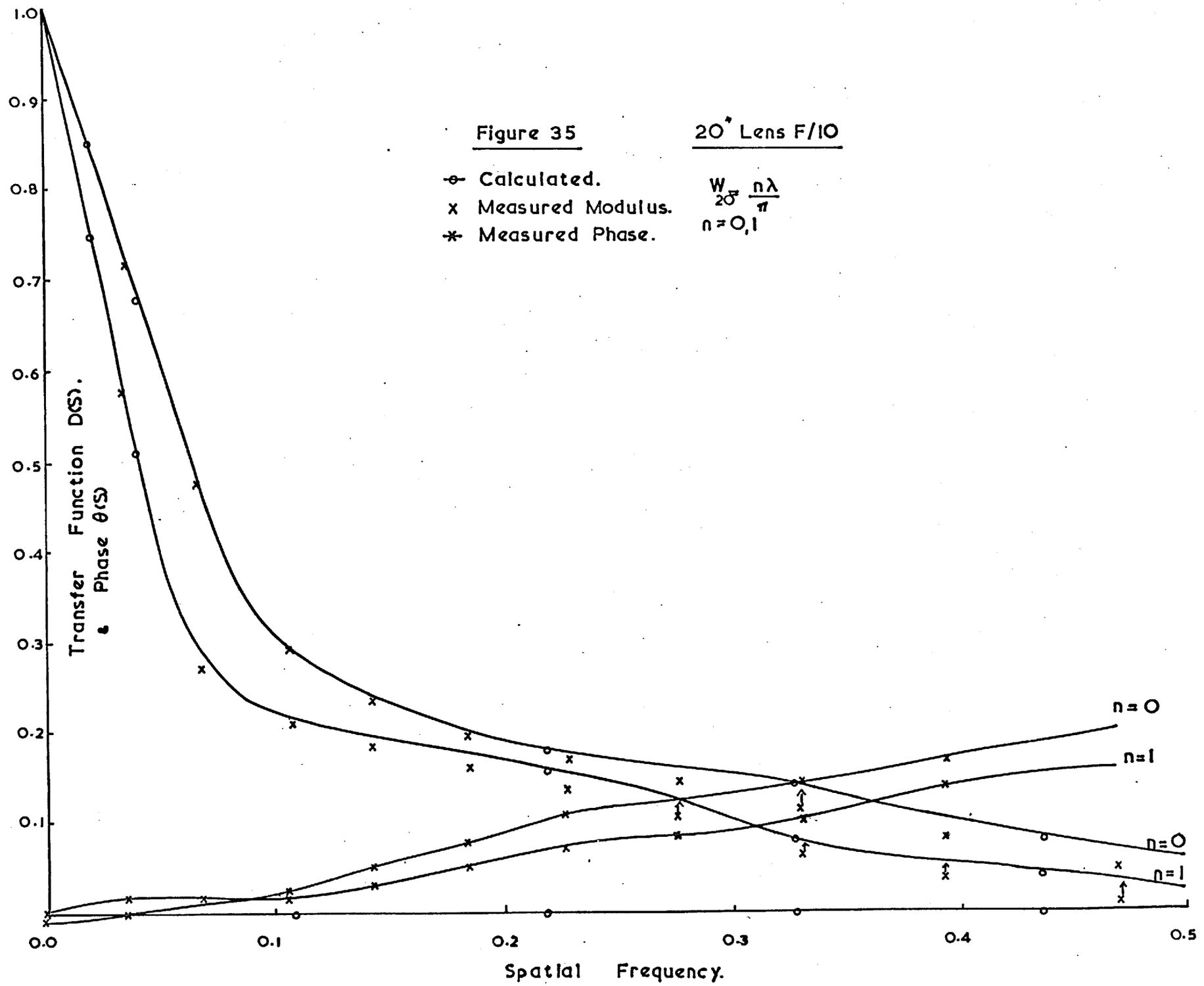
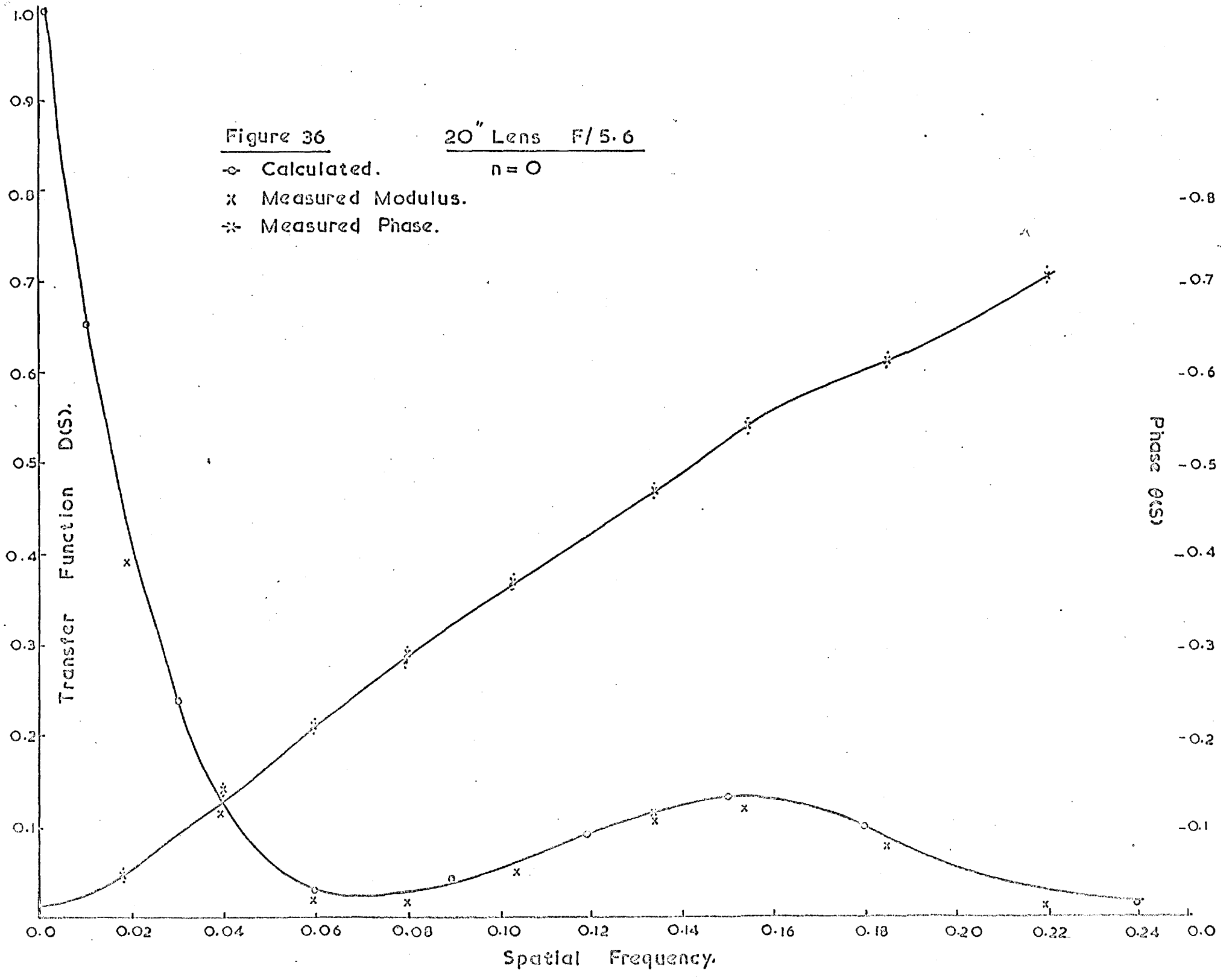

Figure 35
20" Lens F/10
Calculated.
Measured Modulus.
Measured Phase.
$W_{20\sigma} \frac{n\lambda}{\pi}$
n = 0, 1
Transfer Function D(S).
& Phase θ(S)
1.0
0.9
0.8
0.7
0.6
0.5
0.4
0.3
0.2
0.1
0.0
0.1
0.2
0.3
0.4
0.5
Spatial Frequency.
n = 0
n = 1
n = 0
n = 1

Figure 36 — 20" Lens F/5.6 — n = 0

-o- Calculated.

x Measured Modulus.

-*- Measured Phase.



disagreement between theoretical and measured values.

There are several factors which could be responsible for the disagreement. These are

(a) Aberrations present in the system due to optical components other than the test lens.

(b) The presence of on-axis coma in the test lens caused by the decentring or tilting of one or more of its components.

(c) The effect of 'turned edges' in the optical components during manufacture.

(d) The thicknesses and separations of the components being not exactly those described in the specifications.

(e) The refractive indices of the glasses used differing from those specified.

(f) The finite bandwidth of the illuminating light. Each of these factors could cause a reduction in contrast in the image.

Considering firstly factor (a), the maximum aperture at which the decollimator and magnifying system work is F/28. As mentioned in Chapter VI, the observed aberration of the decollimator is about $\lambda/10$ of coma at full aperture (F/14.5). At F/28, this reduces to $\lambda/80$ which will have no effect on the transfer function. It is unlikely, then, that the decollimator is responsible for the disagreement between theory and measurement. Similarly, the state of correction of

the magnifying system is such that no detectable effect would be observed.

Next, let us consider the factor (b). To determine if the tilt or decenting of one or more components of the system under test could be responsible for this disagreement, it is necessary to find the sensitivity of each surface to a tilt or a decentring. If it is assumed that only primary coma is introduced by tilting a surface, the value of $\partial W_{31}/\partial\beta$ where $\partial\beta$ is the angle of tilt must be found. This is done using a computer programme (written by H. Tiziani in connection with work on the decentring of optical systems). For the 20" lens working at F/5.6 these coefficients are listed below :-

SURFACE NUMBER	$(\partial W_{31}/\partial\beta)$ inches/radian
1	0.08040
2	-0.05547
3	0.07755
4	-0.04632
5 (Stop)	0.0
6	0.02024
7	-0.11282
8	0.08328
9	-0.04232

It may be seen that surface 7 (Curvature = 0.131130 in^{-1}) is

the most sensitive to tilt, the value of $\partial W_{31}/\partial\beta$ being equivalent to 1.5λ/minute of arc. Even for the most insensitive surface, the value of $\partial W_{31}/\partial\beta$ is about 0.3λ/minute of arc. Thus, for the former surface, a tilt of one minute of arc would introduce 1.5λ of coma. At this particular surface, the semi-aperture is about 1.5 inches, so that an error in edge location of approximately 0.0005" would introduce 1.5λ of coma. Hence, it is not improbable that there is axial coma present.

To check for the presence of axial coma, the image of a point source on axis as produced by the lens was examined. The intensity distribution in the image is shown in the accompanying photograph. As may be seen, the distribution is assymmetric which indicates the presence of on-axis coma. It is difficult to judge exactly how much coma is present due to the large amount of spherical aberration also present, but something like 1λ of coma appears likely. (This exceeds the Strehl tolerance of about 0.65λ for primary coma). The axis of the star image is at approximately 30° the the vertical axis, so that the effective tilt of the lens components is along this direction.

A further method of investigating this axial coma is as follows. The transfer function is given by

$$D(s) = \frac{1}{A}\iint_S \exp\{iks\ V(x,y,s)\}\,dxdy$$

where $V(x,y,s) = W_x^{I}(x,y) + \frac{1}{3!}\left(\frac{s}{2}\right)^2 W_x^{III}(x,y) + \cdots$ (see Chapter V).



If there are no aberrations present, then $W(x,y) = 0$ and the aberration free transfer function is

$$D_o(s) = \frac{1}{A} \iint_S dxdy = \frac{S}{A}$$

The relative transfer function is thus given by

$$M(s) = \left| \frac{D(s)}{D_o(s)} \right| = \left| \frac{1}{S} \iint_S \exp\{iks\ V(x,y,s)\} dxdy \right|$$

Let us introduce the mean value $\bar{V}$ of V, defined by

$$\bar{V}(s) = \frac{1}{S} \iint_S V(x,y,s)\ dxdy$$

and then write

$$M(s) = \left| \exp\{iks\ \bar{V}(s)\} \iint_S \exp\{iks\ (V-\bar{V})\}\ dxdy \right|$$

Now, if $\{ ks(V-\bar{V}) \} \ll 1$, we may expand $\exp\{iks(V-\bar{V})\}$ in the form

$$\exp\{iks(V-\bar{V})\} = 1 + iks(V-\bar{V}) - \tfrac{1}{2} k^2 s^2 (V-\bar{V})^2$$

so that

$$\frac{1}{S} \iint_S \exp\{iks(V-\bar{V})\} dxdy = \frac{1}{S} \iint_S dxdy + \frac{1}{S} \iint_S iks(V-\bar{V}) dxdy - \frac{1}{S} \iint_S \tfrac{1}{2} k^2 s^2 (V-\bar{V})^2\ dxdy$$

Noting that $\frac{1}{S} \iint_S V dxdy = \bar{V}$, and substituting into the expression for M(s), one obtains

$$M(s) = 1 - \frac{2\pi^2 s^2}{\lambda^2} K(s)$$

where $K(s) = \frac{1}{S}\iint_S \{V(x,y,s)\}^2 dxdy - \{\frac{1}{S}\iint_S V(x,y,s)\, dxdy\}^2$

There is also a phase shift given by

$$\theta(s) = ks\, \bar{V}(s)$$

The above formula for M(s) is, of course, only approximate, but it may be shown that the approximate equality may be converted to an inequality provided the right hand side exceeds zero. Thus

$$M(s) \geqslant 1 - \frac{2\pi^2 s^2}{\lambda^2} K(s)$$

Hopkins (1957) suggested that a useful criterion for image quality would be

$$M(s) \geqslant 0.80$$

This parallels the tolerance theory of Marechal in which the permissible decrease in intensity at the centre of a diffraction pattern due to aberration is 20°/o of the maximum intensity found in a perfect system. If one takes the criterion $M(s) \geqslant 0.80$, then

$$K(s) \leqslant \frac{0.10\lambda^2}{\pi^2 s^2}$$

Now V(x,y,s) may be separated into even and odd parts.

That is

$$V(x,y,s) = V_E + V_o$$

where $V_E = W'_{ox}$ | ..... and $V_o = W'_{Ex}$

Hence $K(s) = \frac{1}{S} \iint_S (V_E+V_o)^2 dxdy - \{ \frac{1}{S} \iint_S (V_E+V_o)\, dxdy\}^2$

or $K(s) = \frac{1}{S} \iint_S V_E^2\, dxdy - \{ \frac{1}{S} \iint_S V_E dxdy\}^2 + \frac{1}{S} \iint_S V_o^2 dxdy$

Here the first two terms arise from odd aberrations such as coma, and the third term arises from even aberrations such as spherical aberration.

To calculate $K(s)$ and $\bar{V}(s)$, integrals of the form

$$H_{k,\ell}(s) = \iint_S x^k y^\ell\, dxdy$$

must be evaluated. For the case of pure primary coma, $K(s)$ is given, for an azimuth ψ relative to the axis of coma, by

$$K(s) = 4H_{2,2}(s)\, W_{31}^2 \cos^2\psi + \{9\, H_{4,0}(s)+6H_{2,2}(s) + H_{o,4}(s)\}\, W_{31}^2 \sin^2\psi$$

Here it has been assumed there is no transverse shift of focus. This is accounted for by the term $\bar{V}(x,y,s)$, which in the present case is given by

$$\bar{V}(s) = C(s)+ \{ 3H_{2,o}(s) + H_{o,2}(s)\}\, W_{31} \sin\psi$$

where $C(s) = \frac{1}{4} s^2 W_{31} \sin\psi$ is a term independent of x and y.

Suppose now that $T_o(s)$ is the contrast transfer function for a perfect system, and that $T(s)$ is the expected theoretical contrast transfer function. If $\delta T(s)$ is the difference between the measured and theoretical transfer functions, then provided $T(s)_{measured} \geqslant 0.65\ T_o(s)$ one may write, with good approximation,

$$\frac{\delta T(s)}{T_o(s)} = \delta M(s) = -2\pi^2 s^2 \delta K(s)$$

Here $\delta K(s)$ is the change in $K(s)$ due to the presence of on-axis coma. That is

$$\delta K(s) = 4H_{2,2}(s)\ W_{31}{}^2 \cos^2\psi + \{9\ H_{4,0}(s) + 6H_{2,2}(s) + H_{0,4}(s)\} \times W_{31}{}^2 \sin^2\psi$$

Hence, using this relation, and the relation

$$\delta K(s) = -\left\{\frac{\delta T(s)}{T_o(s)}\right\} \cdot \frac{1}{2\pi^2 s^2}$$

one may determine the amount of coma required in order that the contrast transfer function is reduced by an amount $\delta T(s)$ for spatial frequency s. Figure 37 shows the ratio $\frac{T(s)\ measured}{T(s)\ theoretical}$ as a function of s for apertures of F/5.6 and

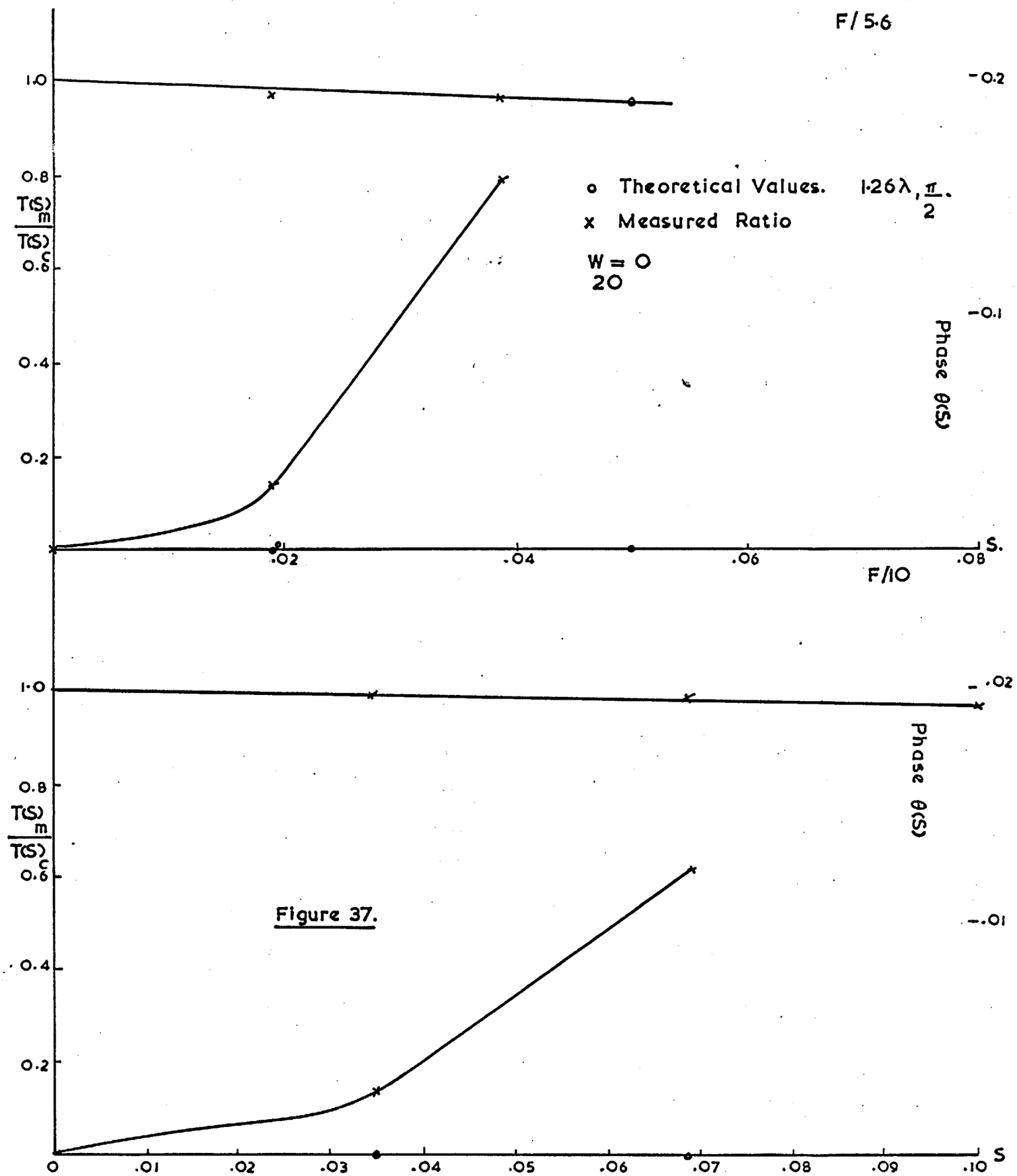

F/5.6
1.0
0.8
$\frac{T(S)_m}{T(S)_c}$
0.6
0.4
0.2
-0.2
-0.1
Phase θ(S)
o Theoretical Values. 1.26λ, π/2.
x Measured Ratio
W = 0
20
.02
.04
.06
.08
S.
F/10
1.0
0.8
$\frac{T(S)_m}{T(S)_c}$
0.6
0.4
0.2
-.02
Phase θ(S)
-.01
0
.01
.02
.03
.04
.05
.06
.07
.08
.09
.10
S

Figure 37.

F/10. At F/5.6, the value of s for which $T^{(s)}_{measured}/T_o(s)=0.65$ is s = 0.04. At this spatial frequency $\delta T(s) = 0.02$. Substituting these values in the above expressions, and evaluating $\delta K(s)$ from the tabulated values of $H_{k,\ell}$, one obtains

$$\delta K(s) = 0.652 = 0.4509\ W_{31}^{\ 2}$$

$$W_{31} = 1.2\lambda.$$

(Here the value $\psi = 30^{\circ}$ has been chosen in evaluating $\delta K(s)$) The value of $W_{31} = 1.2\lambda$ agrees quite well both with the predicted value of W_{31} from the star test, and the order of magnitude axial coma to be expected from the tilting of one or more components of the test lens.

Looking now at the phase term introduced, at s = 0.04, this has the value

$$\theta(s) = 0.175$$

Using the relation obtained above, namely

$$\theta(s) = ks\bar{V}(x,y) = ks\{\ \tfrac{1}{4}\ s^2 W_{31}\sin\psi + [3H_{2,0}(s)+H_{0,2}(s)]\ \cdot\ W_{31}\sin\psi\}\ .$$

and substituting s = 0.04, $\psi = 30^{\circ}$, $\theta(s) = 0.175$, one obtains

$$W_{31} = 1.44\lambda.$$

This value agrees reasonably well with that obtained above.

Hence it may be concluded that the errors in measured values of the modulus and phase of the transfer function are due to the presence of on-axis primary coma.

The factors (c), (d) and (e), mentioned previously, which could lead to differences between measured and theoretical values of the transfer function may be considered together. It is almost certain that the constructional data of the lens as tested are not those laid down by the design parameters of the system. For example, small errors in the separations or thicknesses could lead to significant differences in the performance of the system. Similarly, a change of refractive index (occurring, for example, with age) could produce the same effect. However, in this particular case, it is fairly conclusive that the presence of on-axis coma is producing a greater effect than the other factors mentioned above.

The finite bandwidth of the illuminating light may be introducing some chromatic effects, but this is probably a very small effect. The half-width of the transmission curve of the Wratten filter used is about 150Å , so this factor above will not cause any significant effect. However, it has been assumed throughout the calculations that the principal wavelength is $\lambda = 5461$ Å. This requires that the Wratten filter has a peak transmission at this wavelength. In fact, the peak transmission is at $\lambda = 5480$ Å, so that the values of s obtained using $\lambda = 5461$ Å are erroneous by about $\frac{1}{3}\%$.

This error is completely negligible.

Following the measurements on-axis, and with various amounts of defocussing relative to the paraxial focus, it was decided to test the lens at F/20 choosing a fixed focal plane. This was the best focal plane for the spatial frequency corresponding to 40 lines/mm in the object space. The value of s in this case is $s = 0.873$ which corresponds to setting the scanning slit at an angle $\phi = 48^{\circ}$.

It has been shown by Hopkins (1957) that the position of best focus at a particular spatial frequency s is given approximately by

$$W_{20}/W_{40} = -(1.33 - 1.1s + 0.75^2)\,\lambda$$

where it is assumed that T(s) exceeds 0.8 in value and W_{20}, W_{40} are respectively the defocussing and primary spherical aberration coefficients. For $s = 0.873$ and $W_{40} = 18.219(\mathbf{r})^4$, where $\mathbf{r} = 1$ is the maximum aperture of the system,

$$W_{20} \approx 16.7\mathbf{r}^4\lambda$$

For F/20, $r \simeq 0.28$ and $W_{20} = -0.105\lambda$, dL = 1.83mm. These values are not really valid for the particular spatial frequency chosen, however, since the response at $s = 0.873$ is below 0.8.

At F/10, the reduced spatial frequency corresponding to 40 lines/mm is $s = 0.437$, and $r = 0.56$. Substituting this in

the above formula gives

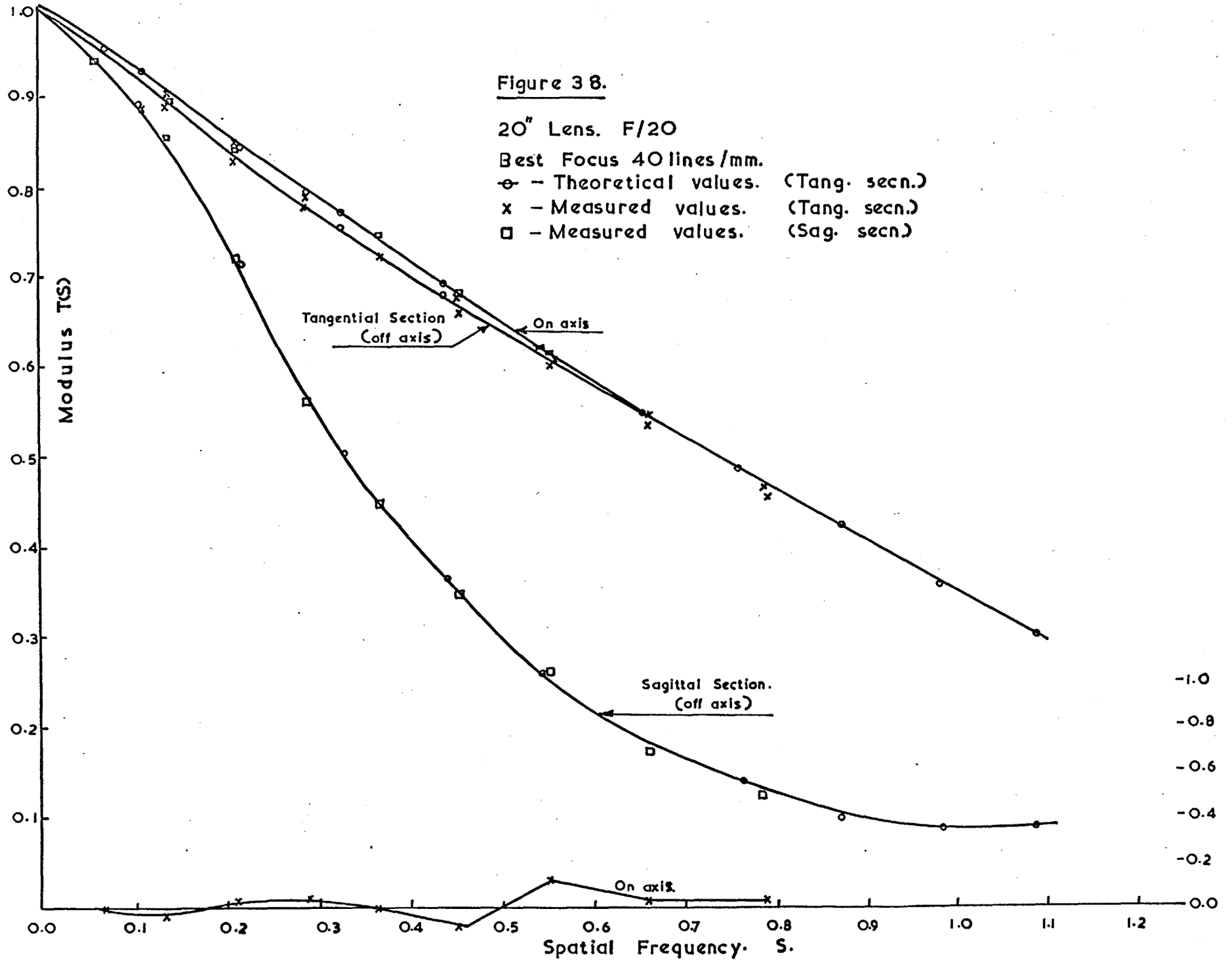
$$W_{20} = -2.12\lambda \ , \quad dL = 0.92 \text{ mm.}$$

Again these values are not valid, since at s = 0.473, T(s) ≈ 0.10.

The position of the test lens was adjusted to give a maximum output signal in the manner described for the paraxial focus at F/20. The final setting practically coincided with the paraxial focal position, contrary to the theoretical value of $W_{20} = -0.105\lambda$ predicted above. Measurements for this focal setting were then obtained, and the results are shown in Figure 38, where curves for the object slit in the sagittal and tangential sections are plotted. For both the sections, there is close agreement of obtained values with those obtained for the paraxial focal setting. This implies that the only contributing aberration is spherical aberration. (If any asymmetric aberration were present at this aperture ratio, measurements in the tangential and sagital sections would give different modulus values). The values of $\theta(s)$ are close to zero for both sections.

These last results also indicate that the instrument is capable of reproducibility with a high degree of accuracy.

The test lens was next moved off-axis by 12°. This necessitated refocussing by an amount $F(\sec\theta.1) = 10.48$ mm. This was achieved by moving the object slit by the specified amount, the correct setting being when a maximum signal output was obtained with the scanning slit at an angle $\phi = 48°$. The


Figure 38.
20" Lens. F/20
Best Focus 40 lines/mm.
-o- – Theoretical values. (Tang. secn.)
x – Measured values. (Tang. secn.)
□ – Measured values. (Sag. secn.)
Modulus T(S)
Tangential Section (off axis)
On axis
Sagittal Section. (off axis)
On axis
Spatial Frequency. S.
1.0
0.9
0.8
0.7
0.6
0.5
0.4
0.3
0.2
0.1
0.0
-1.0
-0.8
-0.6
-0.4
-0.2
0.0
0.1
0.2
0.3
0.4
0.5
0.6
0.7
0.8
0.9
1.0
1.1
1.2

results obtained are shown in Figure 38, where only modulus values have been plotted for the off-axis case. (Phase values are again sensibly zero). As may be seen, there is fairly good agreement with the theoretical values up to the spatial frequency $s = 0.5$, but beyond this errors of up to $7^{o}/o$ occur. The cause of this error is not known precisely, but may be due to the coma arising from centring errors contributing to the aberrations off-axis.

It is worth noting that, on-axis, the aberration function is of the form

$$W(r,\phi) = W_{20}r^2 + W_{40}r^4 + W_{60}r^6$$

where W_{20} = coeff. of longitudinal defocussing
W_{40} = " " primary spherical aberration.
W_{60} = " " secondary spherical aberration.

At the paraxial focus, $W_{20} = 0$ and the only effect is due to spherical aberration. If a finite amount of defocussing is introduced, $W_{20} \neq 0$, and the value of $W(r,\phi)$ changes. By suitably choosing W_{20}, the variance of $W(r,\phi)$ may be reduced - the minimum value obtainable corresponds to the position of 'best focus'.

The above case of the test-lens being adjusted for best focus at 40 lines per millimetre is an example of defocussing to maximise the response at a particular spatial frequency. In this case, however, as the lens is stopped down

to F/20, the aberrations are so small that the defocussing required to obtain best focus at 40 lines/mm is practically zero.

Proceeding along these lines, the lens was tested at F/10 on axis, the focal plane chosen being the best focus at 40 lines/mm. This required a shift of the focal plane of 1.52 mm which corresponds to the value $W_{20} = 3.48\lambda$. This again is contrary to the predicted value of 2.12λ for lower frequencies. Figure 39 shows the resulting curve, and also the curve for $W_{20} = 0$. Also shown are the states of connection of the system for an aperture of F/10. As may be seen, the performance of the system is greatly improved by introducing a defocussing term.

This completes measurements on the 20" lens, and the conclusions to be drawn are as follows :-

(a) The instrument is capable of determining the transfer function with an accuracy of $2^{o}/o$ in both modulus and phase. Measurements are reproducible.

(b) The 20" lens performs as a diffraction limited system at F/40. As the aperture increases, the performance steadily decreases, and at F/5.6 is very poor.

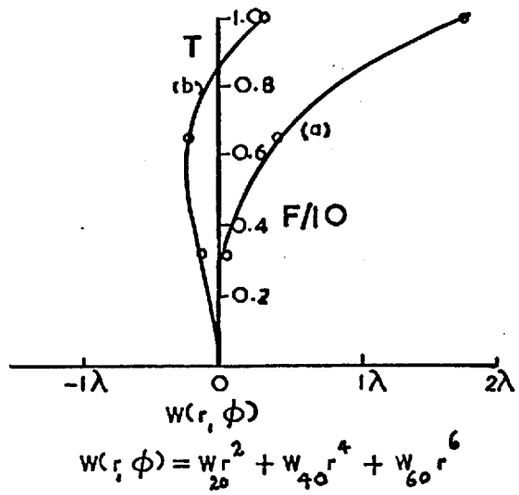
(c) The presence of on-axis coma has been detected, this amounting to about 1λ. For this particular lens, the tolerance on decentring or tilting one of the components is of the order of one minute of arc, which in turn requires a shoulder mounting

Figure 39.

20" Lens F/10

(a) $W_{20} = 0$

(b) Best Focus 80 lines/mm ($s = 0.437$)



$$W(r,\phi) = W_{20} r^2 + W_{40} r^4 + W_{60} r^6$$

accuracy of about one micron. This is a surprisingly close tolerance, and indicates the need for careful consideration of the mounting problem, even in photographic objectives.

(d) the performance of the lens is greatly improved if defocussed (from the paraxial plane) by an appropriate amount.

(3) Measurements on the Plano Convex Lens.

Having considered firstly a compound lens system, it was decided to investigate thoroughly the performance of a simple singlet lens. Of particular interest was the effect of tilting one surface of the lens relative to the other surface.

With this aim in mind, two plano-convex lenses were made very carefully. One of these lenses had its plane surface deliberately tilted relative to the other in order to introduce some on-axis coma. The lenses have the following computed specifications:-

Lens (1)

Focal Length = 18.145197"

Thickness = 0.268"

Clear Aperture = 2.40" F/7.5

C_1 = 0.106519 in^{-1}

C_2 = 0.0

N_e = 1.51738

Lens (2)

Focal Length = 18.145197"

Thickness-Axial = 0.268"

Edge1 = 0.166"

Edge2 = 0.202"

Clear Aperture = 2.40"

C_1 = 0.106519 in^{-1}

C_2 = 0.0

N_e = 1.51738

The computed aberrations of lens (1) were found to be

ON-AXIS		5° OFF-AXIS	
W_{20}	= 0	(W_{11}	= - 0.00005)
W_{40}	= 1.6948	(W_{20}	= 7.4849)
W_{60}	= 0.0072	W_{22}	= 9.2066
		W_{31}	= 1.4120
		W_{33}	= - 0.0210
		W_{40}	= 1.7158
		W_{42}	= 0.0478
		W_{51}	= - 0.0224
		W_{60}	= 0.0025

The aberrations of lens (2) include a coefficient $\delta W_{31} = \frac{\partial W}{\partial \beta}\,\delta\beta$, which arises from the tilt $\delta\beta$ introduced. The value of the term $\partial W/\partial\beta$ is given, at any surface, by

$$\frac{\partial W}{\partial \beta} = Y\Delta(n \cos I) - hy\ \Delta(n)$$

where Δ denotes a difference on refraction, and

Y is incidence height — h is paraxial ray incidence height

n is refractive index — y is reduced height

I is angle of incidence

In this particular case, $Y = 1.20''(=30.48\text{ mm})$, $\Delta(n) = 0.51738$

$I = 0.0661 \approx 3.79^\circ$

$I' = 0.0436 \approx 2.50^\circ$

$hy = Y = 30.48$ mm.

Substituting these values into the expression for $\frac{\partial W}{\partial \beta}$ gives

$$\frac{\partial W}{\partial \beta} = 9.86 \times 10^{-4} \text{ inches/ radian}$$

or

$$\frac{\partial W}{\partial \beta} = 0.87\lambda \text{ / degree.}$$

As may be seen from the lens specifications,

$$\delta\beta = \frac{0.036}{2.4} \text{ radians } \approx 0.9^{\circ} .$$

Hence the coma expected on axis is approximately

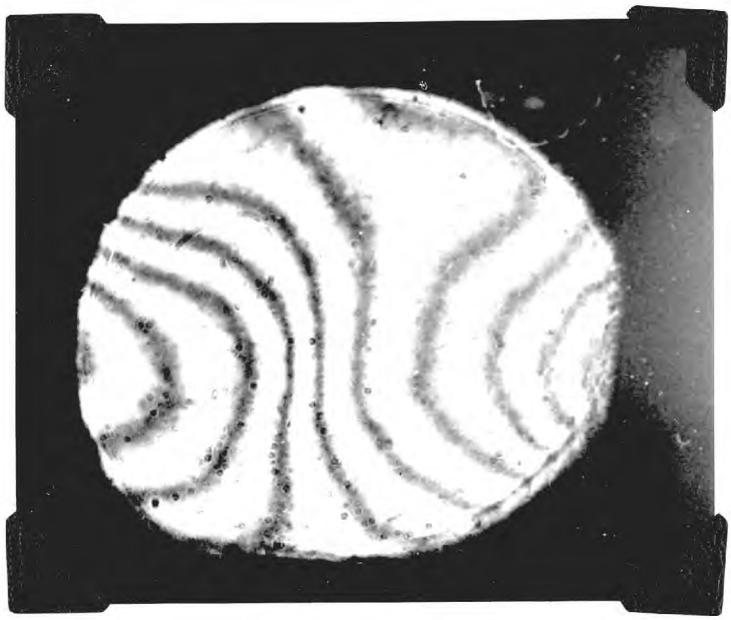
$$W_{31} = 0.8\lambda .$$

Using a wavefront-reversing interferometer designed by Tiziani, which measures comatic aberration in the presence of other aberrations, an interferogram of the lens (2) was obtained and is reproduced in the accompanying photograph. With this interferometer, four times the odd component of wavefront aberration is seen in the fringes, and the even parts of the aberration, such as spherical aberration, are not in evidence. Fitting the polynomial

$$W(r,\phi) = W_{11}\, r + W_{31}\, r^3 + W_{51}\, r^5$$

to the interferogram for the given lens resulted in the following values for the coefficients:

$$W_{11} = \overline{0.65}\lambda \quad W_{31} = \overline{0.58}\lambda \quad W_{51} = 0.24\lambda .$$



Measurements were first made on lens (1), and the results are shown in Figures 40 and 41. Two focal positions have been chosen, namely the paraxial focus and the position of best focus at 25 lines /mm. As may be seen from Figure 40, which shows the on-axis results, the performance of the lens is greatly improved when the best focal plane at 25 lines /mm. is chosen. This is due to the fact that a certain amount of defocussing, W_{20}, has been introduced which partially offsets the effects of spherical aberration. In Figure 41, results are shown for the image formed 5^{o} off-axis. Here the performance is poor both for the paraxial focal plane and for the best focus at 25 lines /mm. The performance of the lens is better in the tangential section than in the sagittal section.

The phase curve in Figure 41 is of particular interest. This is the curve for the sagittal section 5^{o} off-axis, and is interpreted as follows. Due to the presence of coma, there is a phase term in the transfer function which increases steadily with increasing spatial frequency. In addition, there is a reversal of contrast occurring at about s = 0.08. This accounts for the sudden jump in the phase around s = 0.08 followed by an approximately linear variation of phase with spatial frequency.

Also of interest is the fact that below the spatial frequency s = 0.1, the response for the best focal plane

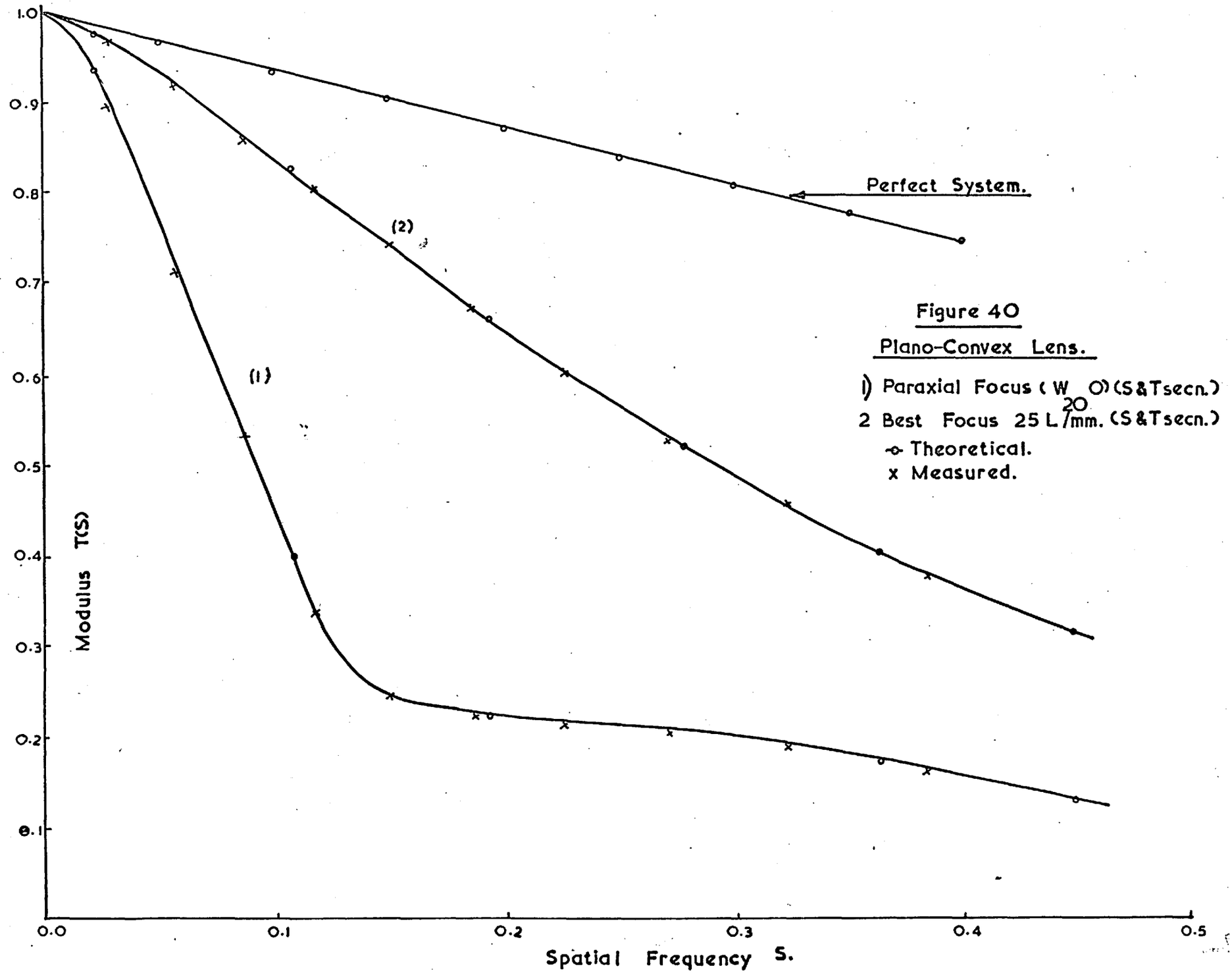


Figure 40

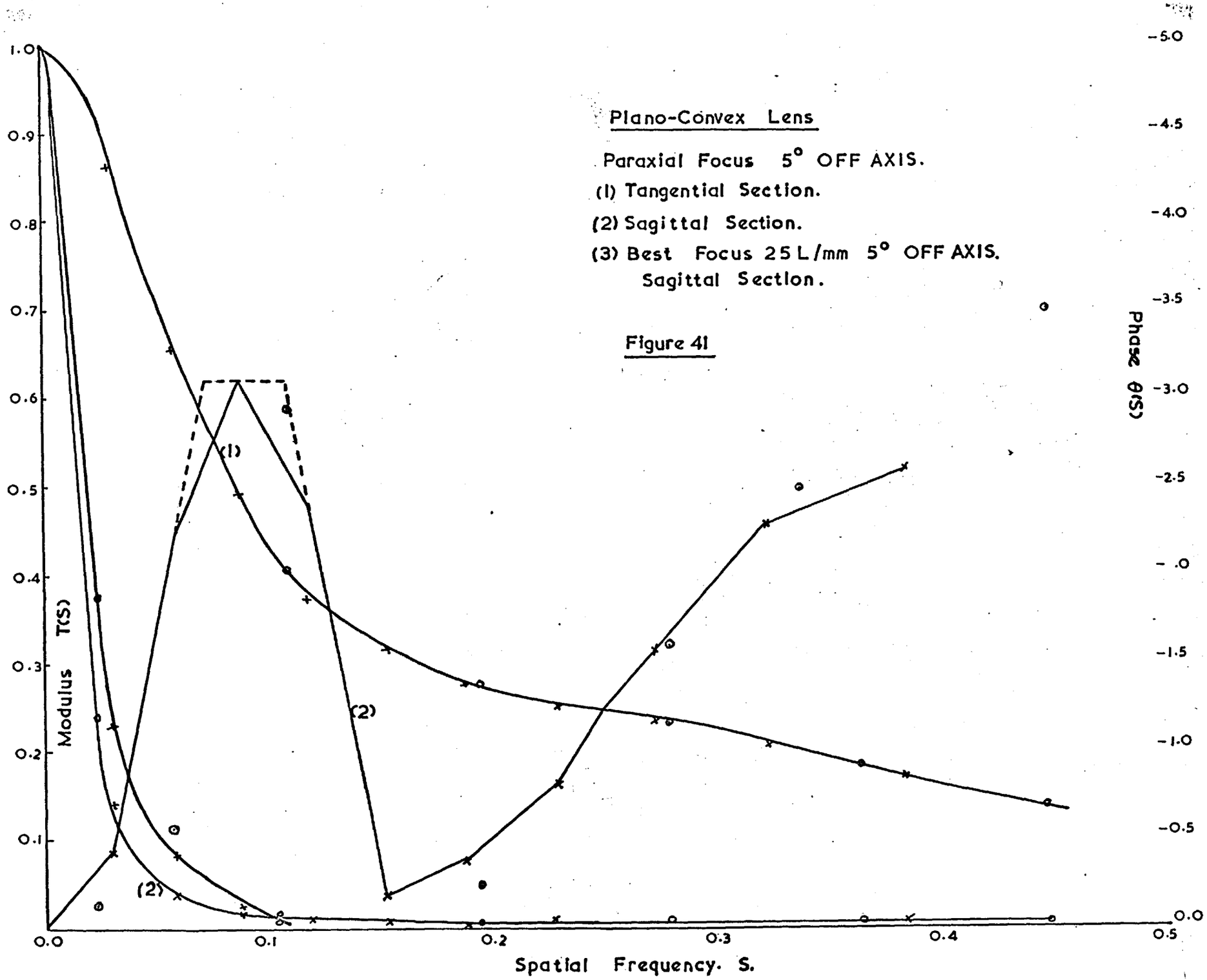
Plano-Convex Lens.

1) Paraxial Focus (W_{20} 0) (S&T secn.)

2 Best Focus 25 L/mm. (S&T secn.)

-o- Theoretical.

x Measured.

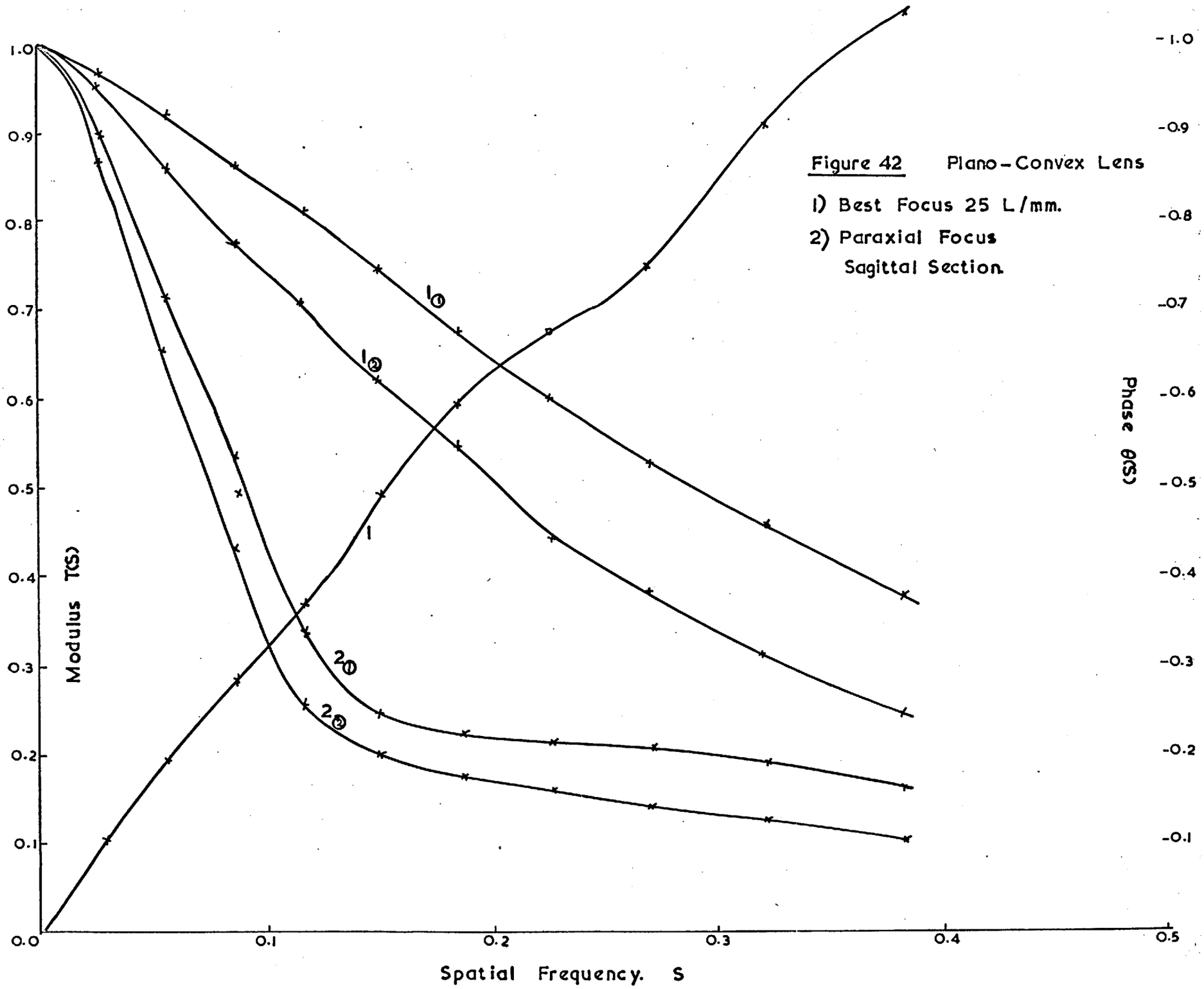

Plano-Convex Lens
Paraxial Focus 5° OFF AXIS.
(1) Tangential Section.
(2) Sagittal Section.
(3) Best Focus 25 L/mm 5° OFF AXIS.
Sagittal Section.
Figure 41
Modulus T(S)
Phase θ(S)
Spatial Frequency. S.
(1)
(2)
(2)
1.0
0.9
0.8
0.7
0.6
0.5
0.4
0.3
0.2
0.1
0.0
0.1
0.2
0.3
0.4
0.5
-5.0
-4.5
-4.0
-3.5
-3.0
-2.5
-.0
-1.5
-1.0
-0.5
0.0

at 25 lines /mm. in the tangential section is better than that for the paraxial focal plane. At higher frequencies, however, the situation is reversed. In fact, the output signal from the scanning slit is so small as to make impossible any accurate determination of contrast attenuation. Hence no values for T(s) above s = 0.1 are plotted in this case. The phase curve is somewhat similar to that obtained for the paraxial focus case (2), and has been omitted from Figure 41 to avoid confusion.

Following measurements with this lens, lens (2) was tested on-axis with the object slit in the sagittal section, both in the paraxial focal plane and the best focal plane at 25 lines /mm. The results are shown in Figure 42, where the corresponding curves for lens (1) are also shown. There is a significant fall in the response, which is due entirely to the presence of the on-axis coma. In addition a phase term has appeared which increases approximately linearly with spatial frequency. Again, only the phase curve for the best focal plane at 25 lines /mm. has been plotted.

In the best focal plane at 25 lines /m.m, the ratio of the transfer functions in Figure 42 has been taken, subject to the condition that $\{T(s)$ measured $/T_o(s)\} \geqslant 0.65$. These values are shown in Figure 43. Also shown in this figure are the theoretical values of T(s) and $\theta(s)$ for

$$W_{31} = 0.63\lambda \qquad \psi = \frac{\pi}{2} \quad .$$


Figure 42 Plano-Convex Lens
1) Best Focus 25 L/mm.
2) Paraxial Focus
Sagittal Section.
Modulus T(S)
Phase θ(S)
Spatial Frequency. S
1.0
0.9
0.8
0.7
0.6
0.5
0.4
0.3
0.2
0.1
0.0
-1.0
-0.9
-0.8
-0.7
-0.6
-0.5
-0.4
-0.3
-0.2
-0.1
0.1
0.2
0.3
0.4
0.5
1①
1②
1
2①
2②

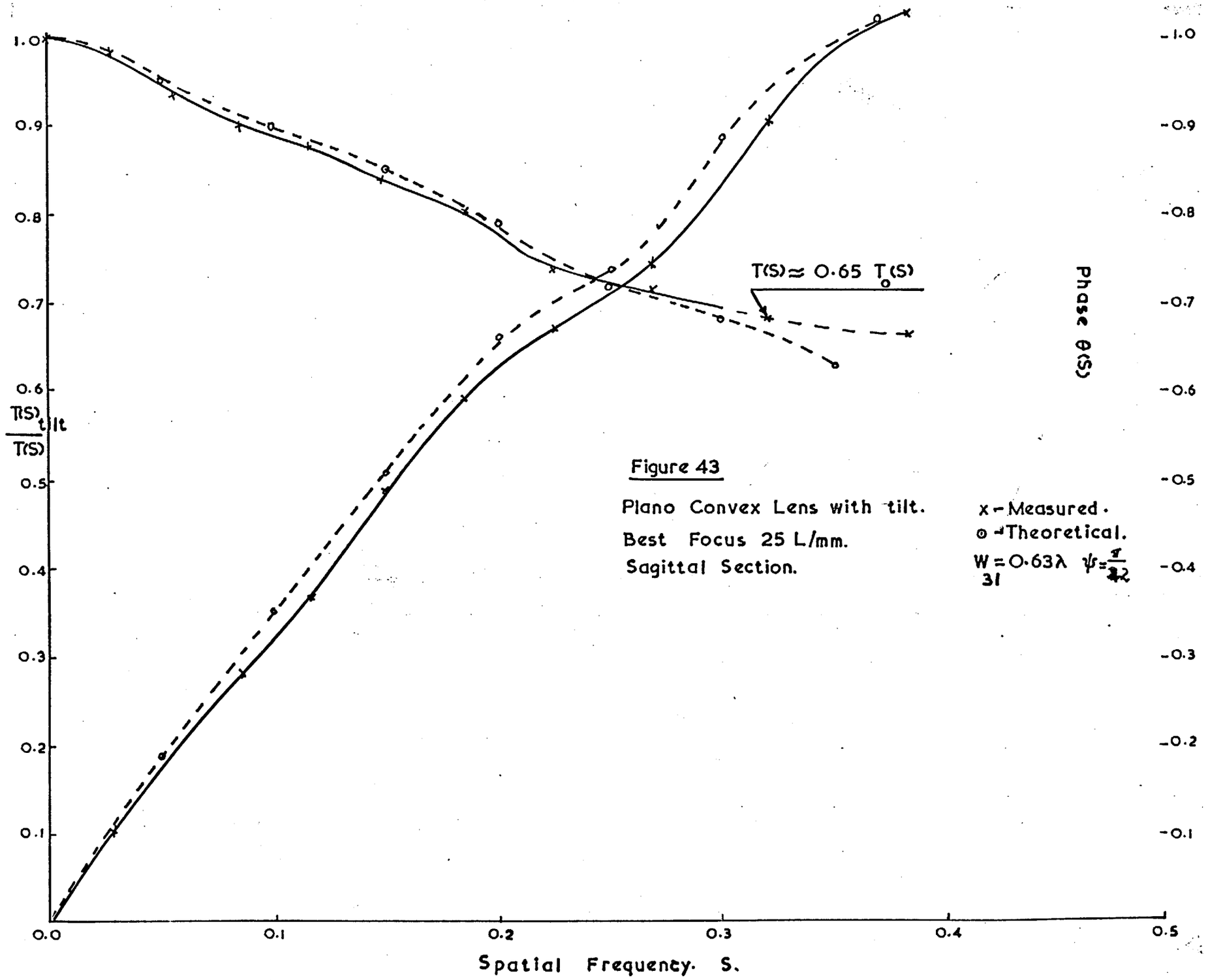


Figure 43

Plano Convex Lens with tilt.
Best Focus 25 L/mm.
Sagittal Section.

x - Measured.
o - Theoretical.
$W_{31} = 0.63\lambda$ $\psi = \frac{\pi}{2}$

There is quite close agreement between the measured ratio, and the theoretical response for $\{W_{31} = 0.63\lambda \quad \psi = \frac{\pi}{2}\}$. Using the tolerance theory of Hopkins in the way done for the 20" lens, one obtains for W_{31}

(Modulus) $W_{31} = 0.5\lambda$ (Phase) $W_{31} = 0.6\lambda$

(Here the spatial frequency chosen is $s = 0.2$ and then $\delta T(s)/T_o(s) = 0.170$). These values are somewhat smaller than those predicted, but some error has been introduced into the prediction by neglecting higher order coma.

It is clear from the above results that the presence of on-axis coma, caused by tilting or decentring a surface, may seriously impair the imaging qualities of an optical system. For this particular singlet lens, a tilt of about 1° has been introduced. However, for a system with many elements, or of larger relative aperture, much smaller tilts may produce effects which are additive. These, in turn, may easily produce a reduction in imaging quality comparable with that observed above. It should also be noted that for a lens with large amounts of aberration present, the effect of the coma introduced by tilting a component would be negligible.

(4) Measurements on 8" Pentac Lens:-

This lens had been obtained in order to compare the measured values with those obtained by other workers. This

lens has the following specifications:-

R in	Thickness	n_d	
3.37	0.627	1.6124	
-3.80	0.128	1.5476	Stop 0.14 in front of R = 67.5
-135.00	0.617		
-3.48	0.128	1.5476	
3.063	0.685		f' = 7.965"
67.50	0.125	1.5476	ℓ_F' = 6.731"
3.146	0.627	1.6124	
-3.146			

At the time of writing, no theoretical values of the transfer function were available, so that the only comparison possible is with other measured values.

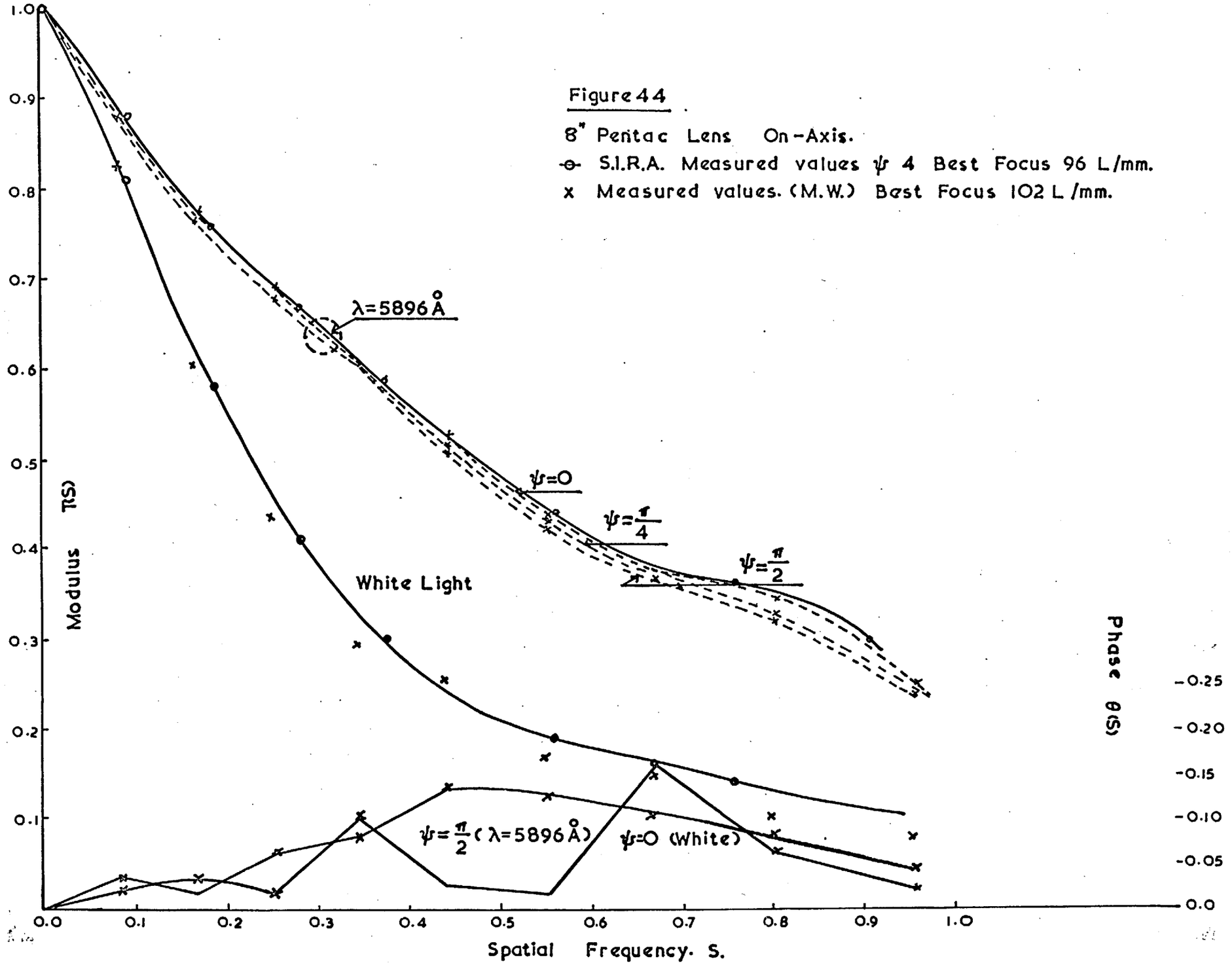
With a focal length of 7.965", the magnification in the instrument is approximately x 20 which means that the image of the object slit has a width of 0.006", a value which far exceeds that required for a maximum signal to noise ratio. This effect was observed during the measurements on this lens; a little difficulty was experienced in determining the true null setting. As a result, errors in setting the parallel plate micrometer and the density wedges of about 0.0005" (=0.0127 mm) and 3° respectively are possible. These errors lead to a possible 2% error in D(s).

The lens was tested in yellow light ($\lambda = 5896\text{A}^{\circ}$) and white light. With the lens in its test position, the magnification was found to be M = 25.992.

Firstly the lens was tested using yellow light. To obtain yellow light, the mercury source and filter were removed and replaced by a white source and yellow filter which has a peak transmission at 5896A°. The lens was tested on-axis in the azimuths 0°, 45°, 90°, and the results are shown in Figure 44 for an aperture ratio of F/8. The focal plane chosen was the best at 102 lines /mm. ($\phi = 45^{\circ}$). The results indicate reasonably good agreement with those obtained elsewhere. The phase results, however, are somewhat erratic, but this may be attributed to the reduction in signal to noise ratio resulting from the use of a slit whose image on the scanning drum had a value far from the optimum.

Next the lens was tested at F/8 using white light with the same focal setting as above, and with the object slit in the tangential section. The results are also plotted on Figure 44, and show an average discrepancy of about 0.06, particularly at higher spatial frequencies. This discrepancy could easily be due to one or more of the following factors -

(a) The spectrum of the white source used is not the same as that used to obtain the comparison curve.


Figure 44
8" Pentac Lens On-Axis.
S.I.R.A. Measured values ψ 4 Best Focus 96 L/mm.
x Measured values. (M.W.) Best Focus 102 L/mm.
λ=5896 Å
ψ=0
ψ=π/4
ψ=π/2
White Light
ψ=π/2 (λ=5896 Å)
ψ=0 (White)
Modulus T(S)
Phase θ(S)
Spatial Frequency. S.
1.0
0.9
0.8
0.7
0.6
0.5
0.4
0.3
0.2
0.1
0.0
-0.25
-0.20
-0.15
-0.10
-0.05
0.0
0.1
0.2
0.3
0.4
0.5
0.6
0.7
0.8
0.9
1.0

(b) The effect of chromatic aberration of the test-lens and other components in the instrument.

(c) The spectral sensitivity of the photomultiplier not being the same as that used to obtain the comparison curve.

The factor (b) causes a spectrum of spread functions to be imaged along the optical axis near to the true image plane. The value of λ for which the corresponding spread function is exactly in the true image plane depends on the amount of chromatic aberration present. Assuming an equal distribution of intensity with wavelength, the wavelength of the light forming the spread function in the true image plane will have a dominating role in determining the spatial frequency at which the lens is tested, since $s = 2F\lambda R$. If this were the only factor affecting the modulus of the transfer function, then a shift of the s-axis in Figure 44 would bring the measured values into coincidence with the comparison curve. This, in fact, proves not the case.

The factor (a) may also cause a disagreement in measurements. For a white source of a particular colour temperature T, there will be a value of λ for which the emitted energy is a maximum, according to the formula

$$dE/d\lambda = A_1 \lambda^{-5} \cdot e^{-A_2/\lambda T}$$

where $A_1 = 2hc^2$, $A_2 = hc/k$, E = energy, λ = wavelength

h = Plank's constant, k = Boltzman's constant,

c = vel. of light.

Hence, if the white source used here has a different energy distribution from that used to obtain the comparison curve, there will be a different λ_{max}. Since the test-lens will have a residual secondary spectrum, its state of correction will vary with wavelength. Hence a variation in observed values of T(s) is to be expected.

It is clear, then, that for comparison of measurements using white light, sources having the same characteristics must be used. Also, any instrument for measuring transfer functions in white light must be free of chromatic aberration to a high degree of correction.

Another possible method of assessing the performance of a lens using white light is to determine the transfer function of the lens at a number of wavelengths spaced at equal intervals around some mean wavelength. Suppose for example that for some spatial frequency s, the moduli $T(s)_n$ are determined for N wavelengths λ_n. Then it may be useful to take the modulus for white light response to be given by

$$T(s)_{white} = \frac{\sum_{n=1}^{N} T(s)_n}{N}$$

This is assuming that the relation between aberration (and therefore change in refractive index Δ_n) is linear with the

change in wavelength λ; that is

$$\Delta n = -k\,\Delta\lambda \quad \text{where } k \text{ is constant.}$$

In fact, for the visible wavelengths, the relation is not linear, it being of the form $n = A + B/\lambda^2 + C/\lambda^4 + \ldots$. It may therefore be more useful to choose weighting factors, different from unity, so that the above expression for $T(s_{white}$ becomes

$$T(s)_{white} = \frac{\sum_{n=1}^{N} g_{\lambda_n} T(s)_n}{N}$$

The value of N, the number of wavelengths chosen, would determine how closely one may determine the true response to white light. Workers in this field have in the past stated that the transfer function is generally less using white light than it is using monochromatic light. The above is one attempt at stating the situation more explicitly. Since a large percentage of lenses are used in white light, it is important to know the imaging quality of the lens under these conditions of illumination.

An added advantage to specifying the white light response in terms of the response at a number of different wavelengths, is that different weighting factors g_{λ_n} may be chosen for any particular use to which the lens is to be put. For example, in aereal photography, one may require the

response of a lens using white light and say a blue filter to be known. Using the approach as suggested above, this may easily be obtained.

In conclusion then, it is important that the transfer function, using white light, be specified in some standard way. This may be done by using a standard colour temperature source when measuring the transfer function, or else by determining the function for a finite number of wavelengths and taking some weighted average. The latter method appears more useful, as it permits the knowledge of the transfer function for any kind of illumination. In addition, the latter method will prove useful to lens designers when considering the effects of residual aberrations on the transfer function.

References

Hopkins, H.H., Proc. Phys. Soc. LXX, 5-B 1957
p. 449-470.

CONCLUSIONS

A new and simple method of measuring optical transfer functions has been devised and is embodied in an instrument with which both the modulus and the phase may be measured to a high degree of accuracy. Minimum numbers of optical and mechanical components are employed to eliminate sources of error. The instrument may be considered as two separate units, namely a source unit and a detector unit, between which any optical system may be placed for testing.

The method employed to measure the transfer functions has the particular advantage over other methods that only one light source, one photodetector, and one amplifier are used, a null-setting of the output signal giving the values of both modulus and phase. This automatically eliminates errors due to fluctuations in light intensity, photodetector sensitivity and amplifier gain.

Initial measurements have been made, using monochromatic light, to confirm known theoretical values of the optical transfer function. Following this, other measurements were made, again with monochromatic light, on several lenses, and the results compared with values calculated from the constructional data. At low apertures, theoretical and experimental values of both modulus and phase agree to better than 2% over a wide range of spatial

frequencies. At higher apertures there is in some cases poor agreement. This has been shown to be due to the presence of on-axis coma arising from the decentring of components in the lenses. Resulting from this is demonstrated the need for the more precise manufacturing of lens components and their mounts if the design performance is to be achieved in practice. Finally, the effect of using white light was examined briefly, and a tentative interpretation of the results has been attempted.

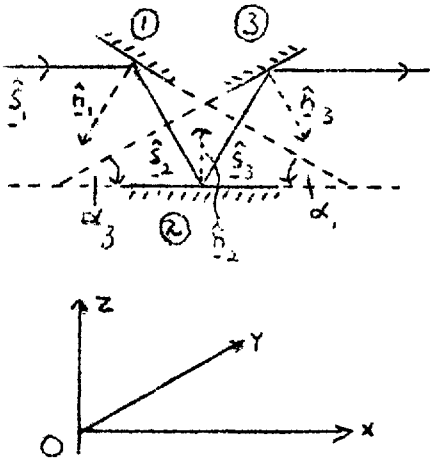
Summarising, an instrument has been built with which a detailed and reliable study of the influence of aberrations on lens performance may be made. The previously established, but by no means satisfactory, criteria of lens performance may be derived from the transfer function curves, but by themselves give incomplete information about a len's performance.

The measurement of transfer functions, particularly for prototypes of new designs, proves extremely useful to both manufacturers and lens designers, and the instrument described above makes this a feasible proposition.

APPENDIX I

Theory of Image Rotating Prism -

An image rotating prism may be considered as a system of three mirrors arranged in the following configuration -



Let rectangular coordinates 0x,y,z be defined, and let $\underline{\hat{i}}, \underline{\hat{j}}, \underline{\hat{k}}$ be unit vectors along these axes respectively. Let $\hat{n}_1$, $\hat{n}_2$, $\hat{n}_3$ be unit normals to the reflecting surfaces ①,②,③, and let $\underline{\hat{s}}$, $\underline{\hat{s}}'$ be ray unit vectors before and after reflection. Then, Snell's Law may be written in the form

$$\underline{\hat{s}}' = \hat{s} + (\cos I' + \cos I)\,\underline{\hat{n}} = \underline{\hat{s}} + 2\cos I'\underline{\hat{n}}.$$

where I and I' are the angles of incidence and reflection. Referring to the above figure

$$\underline{\hat{n}}_1 = -\sin\alpha_1\underline{\hat{i}} - \cos\alpha_1\underline{\hat{k}}$$

$$\underline{\hat{n}}_2 = \underline{\hat{k}}$$

$$\underline{\hat{n}}_3 = \sin\alpha_3\underline{\hat{i}} - \cos\alpha_3\underline{\hat{k}}$$

If $\hat{\underline{s}}_1 = \hat{\underline{i}}$, then applying Snell's law gives

$$\hat{\underline{s}}_1' = \hat{\underline{i}} + 2\cos\,(90^\circ-\alpha_1)\{-\sin\alpha_1\hat{\underline{i}}-\cos\alpha_1\hat{\underline{k}}\}$$

or

$$\hat{\underline{s}}_1' = \cos 2\alpha_1\hat{\underline{i}} - \sin 2\alpha_1\hat{\underline{k}}$$

After reflection from surface ②

$$\hat{\underline{s}}_2' = \cos\,2\alpha_1\hat{\underline{i}} + \sin 2\alpha_1\hat{\underline{k}}$$

After reflection from surface ③

$$\hat{\underline{s}}_3' = \hat{\underline{s}}_3 + 2\cos\,\{\,90^\circ-(2\alpha_1-\alpha_3)\}\,\hat{\underline{n}}_3$$

or

$$\hat{\underline{s}}_3' = \cos(2\alpha_1 - 2\alpha_3)\,\hat{\underline{i}} + \sin(2\alpha_1-2\alpha_3)\,\hat{\underline{k}}$$

If now $\alpha_1 = \alpha_3$, then

$$\hat{\underline{s}}_3' = \hat{\underline{i}}$$

and the ray emerges parallel to its incident direction.
If $\alpha_1 \neq \alpha_3$, the ray emerges at an angle θ to the axis, where

$$\theta = 2(\alpha_1 - \alpha_3) = 2\delta\alpha.$$

Thus for an angular deviation $\delta\alpha$ of one of the reflecting surfaces, the emerging ray is deviated by an angle $2\delta\alpha$.

It may be seen that a similar situation arises if the entering ray is either not parallel to the Ox-axis, or not at the correct height above the Ox-axis when this occurs,

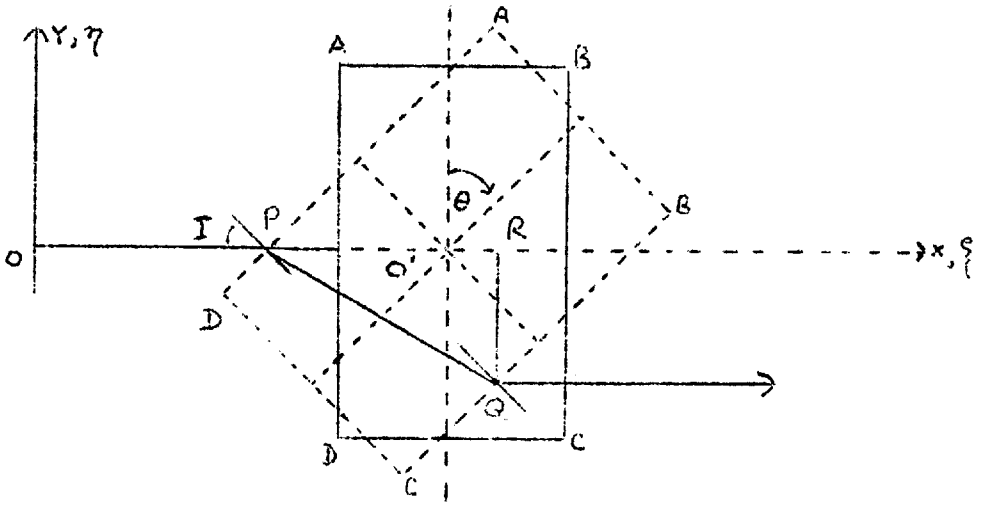
the emerging ray is shifted laterally.

Hence to eliminate any image shift, apart from pure rotation, on rotating the prism (a) the angles α_1 and α_3 must be equal; (b) the axis of rotation of the prism must coincide exactly with the entrance height giving a symmetrical optical path through the prism.

When the prism is rotated through an angle θ, the unit normal vectors will include a θ-dependent term. It may be seen, by comparison with the above analysis, that in this case the emerging rays will have rotated through an angle 2θ.

APPENDIX II

Parallel Plate Micrometer



Let ABCD be a plane parallel glass plate of thickness t and refractive index μ.

Let x, y be rectangular axes, origin 0, and let 0' be the centre of rotation of the glass plate. Suppose the plate is rotated through an angle θ about O'. Consider now a ray OP, parallel to the x-axis, striking the plate at the point P. Let $I_1(=\theta)$ be the angle of incidence. After refraction at this surface, the angle of refraction is given by

$$\sin I_1' = \frac{N_1}{N_1'} \sin I_1 = \frac{1}{\mu} \sin I_1 = \sin I_2$$

After refraction at the second surface

$$\sin I_2' = \frac{N_2}{N_2'} \sin I_2 = \sin I_1$$

That is, the emerging ray is parallel to the incident ray. The lateral shift of the ray is given by

$$RQ = \delta y = PQ \sin (I - I')$$

But $PQ = t/\cos I_1$, so that

$$\delta y = \frac{t}{\cos I'} \{\sin(I - I')\}$$

or

$$\delta y = t \sin I \left\{1 - \frac{\cos I}{\mu \cos I'}\right\}$$

For small angles of incidence I, $\sin I \approx I$, and $\frac{\cos I}{\cos I'} \approx 1$. Hence

$$\delta y \approx tI\left(1 - \frac{1}{\mu}\right)$$

It may thus be seen that for small values of I, the lateral shift of the ray is directly proportional to the angle of rotation of the parallel plate.

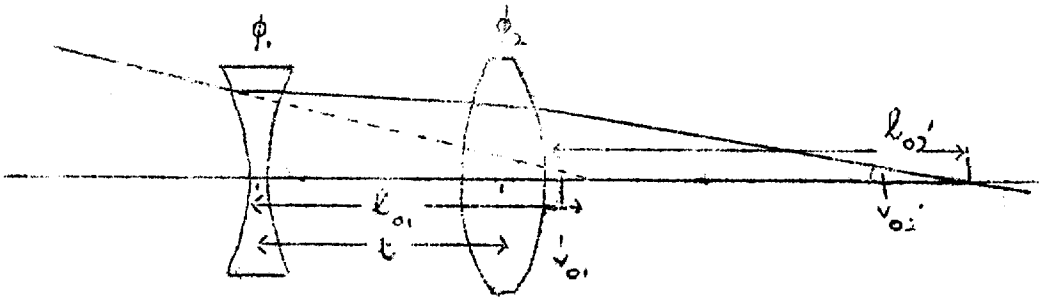
The table below shows the lateral shift expected using a plate 0.25 "thick made of glass having a refractive index of 1.5.

I°	0.0	0.5	1.0	2.0	5.0	10.0	15.0	20.0	25.0	30.0	40.0
$\delta y''$	0.0	.0007	.0015	.0029	.0073	.0147	.0224	.0305	.0392	.0486	0.0651

If these values are plotted graphically, it may be seen that the relation between δy and I is perfectly linear up to about 15°. Above 15°, the term $\left(\frac{\cos I}{\mu \cos I'}\right)$ produces a non-linear effect in the relation, thus rendering calibration more difficult.

APPENDIX III

Design of Magnifying System: Since the system is to work at a low aperture, it is possible to use two singlet lenses in the following configuration -



If ϕ_1 and ϕ_2 are the powers of the separate components, then in the thin lens formulation, the total power ϕ is

$$\phi = \phi + \phi_2 - t\,\phi_1\phi_2$$

Using this relation, and also the relation

$$\text{Magnification } M = (v_{o1}/v_{o2}')$$

One may obtain

$$\ell_{o2}' = M\{(1-t\phi_1)\ell_{o1} - t\}$$

Choosing the values M = 1.913, t = 10", ℓ_{o1} = 11", ℓ_{o2}' = 20" the corresponding powers are

$$\phi_1 = \overline{0.0860}\,, \quad \phi_2 = 0.0448$$

For the system to be free from first order aberrations, we must have

$$(S_I)_1 + (S_I)_2 = 0$$

$$(S_{II})_1 + (S_{II})_2 + (S_I)_2\,\delta q = 0$$

$$(S_{III})_1 + (S_{III})_2 + 2(S_{II})_2\,\delta q + (S_I)_2\,\delta q^2 = -\frac{1}{3}\left\{(S_{IV})_1 + (S_{IE})_2\right\}$$

$$\left\{3(S_{III})_2 + (S_{IV})_2\right\}\delta q + 3(S_{II})_2\,\delta q^2 + (S_I)_2\,\delta q^3 = 0$$

where $S_I \ldots S_{IV}$ are the Seidel aberration coefficients and δq is the shift of the entrance pupil from lens ② . Using the relations

$$(S_{III})_j = \phi_j\, \ell'_{oj} \quad , \qquad (S_{IV})_j = \phi_j\, \ell'_{oj}/N_j$$

these equations may be solved to yield $(S_I)_j$ and $(S_{II})_j$. Having obtained the aberration coefficients required for each component, the shapes S may be determined. The components are then thickened, and the final aberrations calculated.

The values of $(S_I)_j$ and $(S_{II})_j$ depend on the choices of refractive index N. Several changes had to be made in the values of N, and only solutions for the final choices will be

given here.

Lens ①			Lens ②		
N	=	1.5094	N	=	1.5152
ϕ_1	=	$0.\overline{0860}$	ϕ_2	=	0.0448
S_I	=	$0.\overline{333786}$	S_I	=	0.333786
S_{II}	=	2.170606	S_{II}	=	1.167254
S_{III}	=	$8.\overline{666062}$	S_{III}	=	0.447825
S_{IV}	=	$5.\overline{741395}$	S_{IV}	=	0.295555
S_V	=	0	S_V	=	0.

Now, for thin lenses

$$S_I = \frac{1}{8}\phi^3 \ell_o' \{K_1 S^2 + K_2 SP + K_3 P^2 + K_4\}$$

$$S_{II} = \frac{1}{4}\phi^2 \ell_o' \{K_5 S + K_6 P\}$$

where S = Shape of lens

$P = -(v_o + v_o')/\phi y_o$ and y_o is incidence height

$K_1 = (N+2)/N(N-1)^2$ $\qquad$ $K_4 = N^2/(N-1)^2$

$K_2 = 4(N+1)/N(N-1)$ $\qquad$ $K_5 = (N+1)/N(N-1)$

$K_3 = (3N+2)/N$ $\qquad$ $K_6 = (2N+1)/N$

Substituting in these values, one obtains

$$(S_I)_1 = 0.\overline{0160}\ \{\ 8.9601S_1^2+14.5611S_1+14.1606\}$$

$$(S_{II})_1 = 0.\overline{3724}\ \{\ 3.2637S_1+2.9697\}$$

$$(S_I)_2 = 0.0002\ \{\ 8.7404S_2^2+15.\overline{1032}S_2+14.3541\}$$

$$(S_{II})_2 = 0.\overline{0100}\ \{3.2220S_2+3.\overline{1121}\}.$$

These equations may be solved graphically or analytically. Graphically, one obtains curves as shown in Figure A.

It was found that the shapes required to give correct values of S_I did not give the correct values for S_{II} (see curves). Using the differential relations

$$\frac{\partial S_I}{\partial S} = \frac{1}{8}\,\phi^3 \ell_o'\{2K_1S + K_2P\}$$

$$\frac{\partial S_{II}}{\partial S} = -\frac{1}{4}\phi^2 \ell_o'\{K_5\}$$

now values of S were obtained which gave more nearly the aberrations required for each lens. The optimum shapes finally obtained were

$$S_1 = 1.\overline{9997} \qquad S_2 = 4.\overline{0374}$$

These shapes appear to be rather high numerically, but since the powers are small, curvatures will not be too severe.

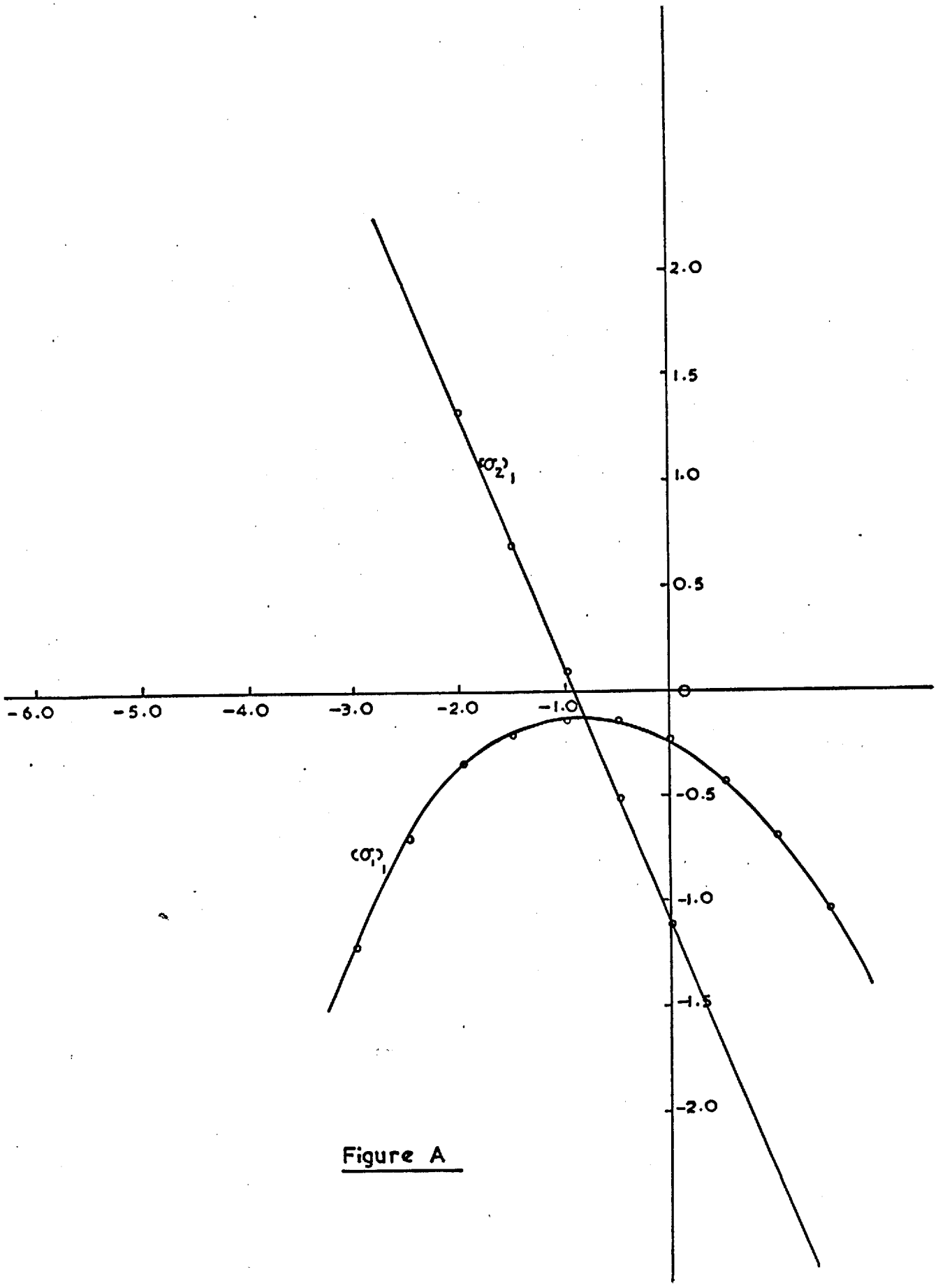


Figure A

The lenses were then thickened, taking axial thicknesses

$$t_1 = 0.100" \qquad t_2 = 0.25"$$

and the final residual aberrations calculated. The final system and its aberration coefficients are as below -

SURFACE NO:	1	2	3	4
RAD. OF CURV. (IN)	11.856	3.951	$8.\overline{998}$	$5.\overline{049}$
THICKNESS	0.100	9.925	0.250	
REFRACTIVE INDEX	1.5094	1.0	1.5152	

$$S_I = 0.0002$$

$$S_{II} = 0.\overline{0866}$$

$$S_{III} = 0.5468$$

$$S_{IV} = 0.\overline{2908}$$

$$S_V = 5.4934$$

Since the maximum aperture at which this system is used is F/28, the residual aberrations are completely negligible.

Acknowledgements.

I wish to thank most sincerely Dr. H.H. Hopkins for initially suggesting this research project, and for the many discussions, suggestions, and criticisms proposed throughout the duration of this work.

Also thanks are due to Mr. A.C. Marchant of the Royal Aircraft Establishment, Farnborough, who has assisted greatly in the running of the computer programmes, and to the Ministry of Aviation for financing this work.

I should further like to express my appreciation to Mr. H. Tiziani who made available the wavefront reversing interferometer used in connection with the measurement of axial coma.